(12) INTERNATIONAL APPLICATION PUBLISHED UNDER THE PATENT COOPERATION TREATY (PCT)

(19) World Intellectual Property Organization
International Bureau

(43) International Publication Date
9 June 2016 (09.06.2016)

WIPO | PCT

(10) International Publication Number
WO 2016/087945 A2

(51) International Patent Classification:
D01D 5/06 (2006.01)

(21) International Application Number:
PCT/IB2015/002467

(22) International Filing Date:
3 December 2015 (03.12.2015)

(25) Filing Language: English

(26) Publication Language: English

(30) Priority Data:
62/086,885 3 December 2014 (03.12.2014) US

(71) Applicant: **KING ABDULLAH UNIVERSITY OF SCIENCE AND TECHNOLOGY** [SA/SA]; 4700 King Abdullah University Of Science And, Technology, Thuwal, 23955-6900 (SA).

(72) Inventors: **ZHOU, Jian**; C/o King Abdullah University Of Science And, Technology, Thuwal, 23955-6900 (SA). **LI, Er, Qiang**; C/o King Abdullah University Of Science And, Technology, Thuwal, 23955-6900 (SA). **LUBINEAU, Gilles**; C/o King Abdullah University Of Science And, Technology, Thuwal, 23955-6900 (SA). **THORODDSEN, Sigurdur, T.**; C/o King Abdullah University Of Science And, Technology, Thuwal, 23955-6900 (SA). **MULLE, Matthieu**; C/o King Abdullah University Of Science And, Technology, Thuwal, 23955-6900 (SA).

(81) Designated States *(unless otherwise indicated, for every kind of national protection available)*: AE, AG, AL, AM, AO, AT, AU, AZ, BA, BB, BG, BH, BN, BR, BW, BY, BZ, CA, CH, CL, CN, CO, CR, CU, CZ, DE, DK, DM, DO, DZ, EC, EE, EG, ES, FI, GB, GD, GE, GH, GM, GT, HN, HR, HU, ID, IL, IN, IR, IS, JP, KE, KG, KN, KP, KR, KZ, LA, LC, LK, LR, LS, LU, LY, MA, MD, ME, MG, MK, MN, MW, MX, MY, MZ, NA, NG, NI, NO, NZ, OM, PA, PE, PG, PH, PL, PT, QA, RO, RS, RU, RW, SA, SC, SD, SE, SG, SK, SL, SM, ST, SV, SY, TH, TJ, TM, TN, TR, TT, TZ, UA, UG, US, UZ, VC, VN, ZA, ZM, ZW.

(84) Designated States *(unless otherwise indicated, for every kind of regional protection available)*: ARIPO (BW, GH, GM, KE, LR, LS, MW, MZ, NA, RW, SD, SL, ST, SZ, TZ, UG, ZM, ZW), Eurasian (AM, AZ, BY, KG, KZ, RU, TJ, TM), European (AL, AT, BE, BG, CH, CY, CZ, DE, DK, EE, ES, FI, FR, GB, GR, HR, HU, IE, IS, IT, LT, LU, LV, MC, MK, MT, NL, NO, PL, PT, RO, RS, SE, SI, SK, SM, TR), OAPI (BF, BJ, CF, CG, CI, CM, GA, GN, GQ, GW, KM, ML, MR, NE, SN, TD, TG).

[Continued on next page]

(54) Title: SEMI-METALLIC, STRONG CONDUCTIVE POLYMER MICROFIBER, METHOD AND FAST RESPONSE RATE ACTUATORS AND HEATING TEXTILES

FIGURE 1

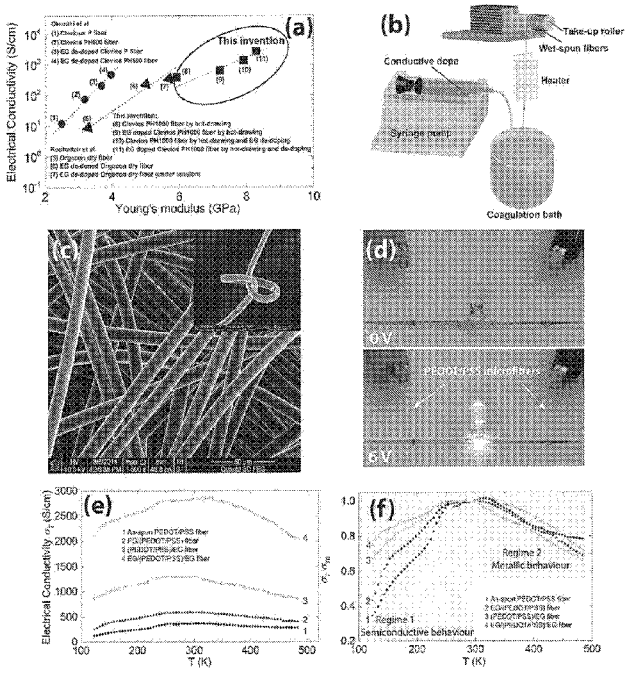

(57) Abstract: A method comprising: providing at least one first composition comprising at least one conjugated polymer and at least one solvent, wet spinning the at least one first composition to form at least one first fiber material, hot-drawing the at least one fiber to form at least one second fiber material. In lead embodiments, high-performance poly(3,4-ethylenedioxy- thiophene)/poly(styrenesulfonate) (PEDOT/PSS) conjugated polymer microfibers were fabricated via wet- spinning followed by hot-drawing. In these lead embodiments, due to the combined effects of the vertical hot-drawing process and doping/de-doping the microfibers with ethylene glycol (EG), a record electrical conductivity of 2804 S · cm^{-1} was achieved. This is believed to be a six-fold improvement over the best previously reported value for PEDOT/PSS fibers (467 S · cm^{-1}) and a twofold improvement over the best values for conductive polymer films treated by EG de-doping (1418 S · cm^{-1}). Moreover, these lead, highly conductive fibers experience a semiconductor-metal transition at 313 K. They also have superior mechanical properties with a Young's modulus up to 8.3 GPa, a tensile strength reaching 409.8 MPa and a large elongation before failure (21%). The most conductive fiber also demonstrates an extraordinary electrical performance during stretching/unstretching: the conductivity increased by 25% before the fiber rupture point with a maximum strain up to 21%. Simple fabrication of the semi-metallic, strong and stretchable wet-spun PEDOT/PSS microfibers can make them available for conductive smart electronics. A dramatic improvement in electrical conductivity is needed to make conductive polymer fibers viable candidates in applications such as flexible electrodes, conductive textiles, and fast-response sensors and actuators.

WO 2016/087945 A2

Published:

— *without international search report and to be republished upon receipt of that report (Rule 48.2(g))*

SEMI-METALLIC, STRONG CONDUCTIVE POLYMER MICROFIBER, METHOD AND FAST RESPONSE RATE ACTUATORS AND HEATING TEXTILES

RELATED APPLICATIONS

This application claims priority to US provisional application serial number 62/086,885 filed December 3, 2014, which is hereby incorporated by reference in its entirety.

BACKGROUND

PART I:

Fiber-shaped conductive materials are attractive for use in applications ranging from simple textiles to complex multimaterial piezoelectric fibres and supercapacitors (a listing of cited references 1-48 is provided hereinbelow for Part I).[1–6] Conjugated polymer fibers, featuring tunable electrical conductivity, have been extensively investigated from both fundamental and application perspectives to understand their electrical and mechanical properties and their practical use in conducting textiles, organic electronics, sensors and actuators.[7–12] The main techniques for processing polymer fibers are dry-spinning, wet-spinning, melt-spinning and electrospinning.[13] In particular, wet-spinning is an important process to produce continuous polymer microfibers by submerging the spinneret in a coagulation bath that causes the fiber to solidify.[13,14]

Among the popular conjugated polymers, polypyrrole (PPy), polyaniline (PANI) and poly(3,4-ethylenedioxythiophene) / poly(styrenesulfonate)(PEDOT/PSS) have been successfully spun into microfibers by the wet-spinning process.[8,9,11,15] PEDOT/PSS has been found to have the good spinnability and its preparation technique can be scaled up to an industrial process.[16] In the past decade, doping and/or de-doping with various polar solvents has been carried out to enhance the conductivity of PEDOT/PSS

films and fibers by two or three orders of magnitude.[9,17–21] Doping PEDOT/PSS involves mixing it with a small amount of secondary dopant (with a high boiling point and < 6 wt%) to change its molecular structure to a more conductive state; de-doping requires partially removing amorphous PSS by washing it with polar solvents. Depending on grade of the employed pristine PEDOT/PSS, as-spun microfibers (without any doping) generally display low electrical conductivity (from 1 to 74 $S \cdot cm^{-1}$).[8,9] Their electrical conductivity could be improved up to 467 $S \cdot cm^{-1}$ by using an ethylene glycol (EG) de-doping process, which partially removes the amorphous and insulating PSS phase.[8] Jalili *et al.*[9] showed that by combining doping and de-doping, the electrical conductivity of PEDOT/PSS microfibers could reach 351 $S \cdot cm^{-1}$. Spinning PEDOT/PSS with functionalized carbon nanotubes into fibers led to limited improvement in conductivity (400 $S \cdot cm^{-1}$).[22,23] To meet the requirements for use as flexible electrodes, conductive textiles and fast-response sensors and actuators, such conductive polymer fibers must have dramatically improved electrical conductivity.

A need exists for improving commercial prospects to find better materials and processing methods which provide improved electronic and mechanical properties and combinations of these and other properties. See, for example, US Patent Nos. 7,132,630; 7,886,617; 8,501,317; WO 2007/099889; and US Pat. Pub. 2008/0099960.

SUMMARY

Embodiments described and/or claimed herein include polymers and compositions, and methods of making and using such polymers and compositions, including devices. The polymers and compositions can be in fiber form or also called a fiber material.

For example, one aspect is for a method comprising: providing at least one first composition comprising at least one conjugated polymer and at least

one solvent, wet spinning the at least one first composition to form at least one first fiber material, and hot-drawing the at least one first fiber material to form at least one second fiber material.

In a preferred embodiment, a method is provided comprising: providing at least one first composition comprising PEDOT/PSS and water, wet spinning the at least one first composition to form at least one first fiber material, hot-drawing the at least one first fiber material to form at least one second fiber material, wherein the method further comprises doping of the first composition and de-doping of the first fiber material.

Other embodiments are the materials provided by these and other methods described herein.

In preferred embodiments and working examples described further hereinbelow, semi-metallic, strong, and stretchable wet-spun PEDOT/PSS conjugated polymer microfibers were fabricated. For some embodiments, the novelty of the fabrication technique lies in a two-step method (wet-spinning followed by immediate hot-drawing) that greatly promotes molecular alignment. When combined with, for example, doping/de-doping by ethylene glycol (EG), it achieves what is believed to be a record electrical conductivity as high as 2804 $S \cdot cm^{-1}$. This is believed to be a six-fold improvement over the best value previously reported for fibers (467 $S \cdot cm^{-1}$) and double the best value reported for PEDOT/PSS films treated with EG (1418 $S \cdot cm^{-1}$).[24] It was also found that these highly conductive fibers display a semiconductor-metal transition at 313 K. They also display superior mechanical properties: for example, the Young's modulus is 8.3±0.4 GPa, the tensile strength is 409.8±13.6 MPa and the elongation at break for these fibers is 21.2±1.4%. These results show that the combined properties of the preferred fibers have been remarkably improved in comparison with previously reported PEDOT/PSS fibers, as shown in Figure 1a. Good thermal stability also can be exhibited.

These and other advantages, found for at least some embodiments, are described more herein.

BRIEF DESCRIPTION OF FIGURES

Figure 1(a)-(f): Wet-spun PEDOT/PSS microfibers and their semi-metallic behaviors. (a) The electrical conductivity and Young's modulus of PEDOT/PSS microfibers. Circle and triangle shapes denote reference values (ref. 8 by Okuzaki et al. and ref. 9 by Rouhallah et al.), square shape denote values in this claimed invention. (b) A schematic of the wet-spinning set-up with the vertical hot-drawing apparatus used in this invention. (c) SEM images of as-spun PEDOT/PSS fibers from a 22 mg/mL PH1000 dispersion. The inset is the SEM image of a knotted fiber. (d) Demonstration of a LED lit by two PEDOT/PSS fibers with diameters of 10 μm at 6 V. (e) Temperature-dependent electrical conductivity and (f) normalized electrical conductivity of an as-spun PEDOT/PSS fiber, an EG/(PEDOT/PSS) fiber, a (PEDOT/PSS)/EG fiber and an EG/(PEDOT/PSS)/EG fiber.

Figure 2(a)-(b): (a) S 2p XPS spectra of as-spun PEDOT/PSS fibers before and after EG de-doping. (b) S 2p XPS spectra of EG doped PEDOT/PSS fibers before and after EG de-doping.

Figure 3(a)-(f): (a), (b), (c) and (d) are AFM phase images of the as-spun PEDOT/PSS fiber, EG/(PEDOT/PSS) fiber, (PEDOT/PSS)/EG fiber and EG/(PEDOT/PSS)/EG fiber, respectively. (e) and (f) HADDAF-STEM images of the as-spun PE-DOT/PSS fiber and EG/(PEDOT/PSS)/EG fiber, respectively. Selected area electron diffraction (SAED) patterns in the insets (e) and (f) indicate random-oriented polycrystalline and preferred-oriented polycrystalline, respectively.

Figure 4(a)-(f): Transmission WAXS characterization of PEDOT/PSS microfibers. 2D WAXS pattern of (a) as-spun PEDOT/PSS fibers, (b) (PEDOT/PSS)/EG fibers, (c) EG/(PEDOT/PSS) fibers and (d) EG/(PEDOT/PSS)/EG fibers. The white markers in (b) show the directions of intensity integration. (e) and (f) Intensity integration in the vertical and horizontal directions of all fibers.

Figure 5: Stretchability of a fiber bundle that was made into a spiral shape. The bundle can be stretched under a large strain and can recover almost to its original shape.

Figure 6(a)-(d): The mechanical behaviors and electrical resistance changes in conjugated polymer fibers upon stretching/unstretching. (a) Representative stress-strain curves of the fibers. (b) Cyclic mechanical tests of as-spun PEDOT/PSS fibers and EG/(PEDOT/PSS)/EG fibers. (c), (d) The resistance change to the cyclic loading of as-spun PEDOT/PSS fibers and EG/(PEDOT/PSS)/EG fibers, respectively. The insert in (c) is a schematic of the response measurement for the fibers.

Figure 7(a)-(b): Correlation between the PEDOT/PSS microstructure and electrical and mechanical properties. (a) Different stages of the molecular level deformation in a PEDOT/PSS fiber upon loading.(b) The grain-level deformation and resistance change mechanism of fibers before and after EG de-doping.

Figure 8: SEM image showing irregular shapes of as-spun PEDOT/PSS microfibers without sufficient drying after winding to the drum collector.

Figure 9: The effect of hot-drawing on the conductivity of the fibers. The draw ratio was controlled to 3.0. The molecular weight of Clevios P < Clevios PH1000.[3]

Figure 10(a)-(d): SEM images of the conductive polymer microfibers. (a) PEDOT/PSS fibers spun from the 11 mg/mL dispersion with hot-drawing, (b) PEDOT/PSS fibers spun from the 22 mg/mL dis-persion without hot-drawing

(c) PEDOT/PSS fibers from the Clevios P dispersion (13 mg/mL). (d) 3 wt% EG doped PEDOT/PSS (EG/(PEDOT/PSS)) fibers spun from the 22 mg/mL dispersion. (a), (b) and (d) are spun from the Clevios PH1000 dispersion, (c) is spun from the Clevios P dispersion.

Figure 11(a)-(d): AFM height images of the conductive polymer microfibers. (a) As-spun PEDOT/PSS fiber, (b) EG/(PEDOT/PSS) fiber, (c) (PEDOT/PSS)/EG fiber and (d) EG/(PEDOT/PSS)/EG fiber. All the images are 1 μm × 1 μm. Root to square (rms) roughness measured from these images are 11.2, 14.1, 21.8 and 18.0 nm for (a), (b), (c) and (d) respectively.

Figure 12: Illustration of Transmission WAXS geometry. The fibers were aligned horizontally into a bundle and placed perpendicularly into a monochromatic x-ray beam. The scattering patterns were collected by a CCD detector at a distance of 10 cm away from sample.

Figure 13(a)-(e): Microstructure of the conductive polymer microfibers. (a), (b) Wide-angle X-ray diffraction of the conductive polymer fibers. (c) and (d) Raman spectra of the conductive polymer fibers. (e) A schematic of the microstructure change of PEDOT chains before and after EG de-doping.

Figure 14(a)-(b): (a) Wide-angle X-ray diffraction pattern of PEDOT/PSS film and EG de-doped PE-DOT/PSS film. (b) Raman spectra of PEDOT/PSS film and EG de-doped PEDOT/PSS film.

Figure 15(a)-(b): SEM images of as-spun PEDOT/PSS fibers after tensile testing show that fibrils are protruding from the cross-sections.

Figure 16: Relative changes in the Young's modulus of the as-spun PEDOT/PSS fiber and EG/(PEDOT/PSS)/EG fiber at maximum strain of each cycle.

Figure 17(a)-(f): Characterization of PEDOT/PSS fibers. (a) SEM image of as-spun PEDOT/PSS fibers. (b) Current density versus voltage curves of four kinds of PEDOT/PSS fibers used in this study, and the break down current densities of copper wire, carbon nanotube fiber and Ag-doped graphene fiber from

literature. (c) and (d) SEM images of an as-spun PEDOT/PSS fiber after electrical failure at different magnifications. (e) and (f) SEM images of an EG/(PEDOT/PSS)/EG fiber after electric failure at different magnifications.

Figure 18(a)-(h): Temperature sensing of single PEDOT/PSS fibers. (a) Temperature-time curves of the as-spun PEDOT/PSS fiber and EG/(PEDOT/PSS)/EG fiber at 7 V cm^{-1} for 25 s. The estimation of the first order response time is shown in the figure. (b) and (c) Temperature variation and current vs. time curves of the as-spun PEDOT/PSS fiber. (d) and (e) Temperature variation and current vs. time curves of the EG/(PEDOT/PSS)/EG fiber. 1 V cm^{-1} increments were made for each step. (f) The dependence of temperature on voltage of four kinds of fibers measured by FBG1.a. (g) Dynamic thermal response of the EG/(PEDOT/PSS)/EG fiber measured by two FBGs at different frequencies. A square wave voltage was applied from 0 to 2.5 V cm^{-1} at frequencies of 0.02, 0.1, 0.5 and 1 Hz. (h) The temperature-time curves under 0.1 Hz of the EG/(PEDOT/PSS)/EG fiber.

Figure 19(a)-(h): A heatable glove using a PEDOT/PSS fiber bundle. (a) A PEDOT/PSS fiber bundle (25 cm long) knitted on the surface of a polyester glove. (b) Optical image of the PEDOT/PSS fiber bundle in polyester glove. (c)-(f) Thermal images showing temperatures of the as-spun PEDOT/PSS fiber bundle on a polyester glove at 0, 0.4, 0.8 and 1.2 V cm^{-1}, respectively. (g) A photo of an assembled circuit with a heatable glove using a 9-V battery. For comparison, the fiber bundle is the as-spun fiber bundle used in (c) to (f) after EG de-doping. (h) The corresponding thermal image in (g) powered by a 9-V battery.

Figure 20(a)-(e): Performance of the as-spun PEDOT/PSS fiber bundle actuator under isotonic conditions. (a) Photograph of a 14-cm-long as-spun PEDOT/PSS fiber bundle (3 mg) carrying a 0.45 g load on its movable end. (b) Illustration of the set-up shows the motion of the actuator by switching the voltage on and off. (c) The evolution of displacement with time at 1.14 V cm^{-1}. Inset images show

the position change of the load by switching the voltage on and off. (d) The corresponding thermal images of the fiber bundle in (a) at different voltages. (e) Readings from video and thermal camera give the displacement and temperature of the fiber bundle as functions of the applied voltage, respectively.

Figure 21(a)-(c): (a) The set-up for isometric measurement of fibers. (b) Actuation stress amplitude to voltage profiles of the as-spun PEDOT/PSS and EG/(PEDOT/PSS)/EG fibers. (c) Dynamic mechanical behavior of as-spun PEDOT/PSS fibers and EG/(PEDOT/PSS)/EG fibers.

Figure 22(a)-(f): Low frequency actuation of single PEDOT/PSS fibers at 0.02 Hz. (a) and (b) Tensile actuation of the as-spun PEDOT/PSS fiber under the applied square wave voltage (0-2.5 V cm^{-1}). (c) and (d) Tensile actuation of the EG/(PEDOT/PSS)/EG fiber under the applied square wave voltage (0-2.5 V cm^{-1}). (e) The enlarged figure in the dash box of (d). (f) Illustration graph of actuation mechanism.

Figure 23(a)-(d): Frequency-dependent actuation of PEDOT/PSS fibers. (a) Tensile actuation of the EG/(PEDOT/PSS)/EG fiber at different frequencies (0.02, 0.1, 0.25, 0.5 and 1 Hz) at a square wave voltage (0-2.5 V cm^{-1}). Inset curves show details of the actuation at different frequencies. (b) Actuation stress amplitude as a function of driven frequency at a square-wave voltage (0-2.5 V cm^{-1}). (c)Tensile actuation of the EG/(PEDOT/PSS)/EG fiber under the applied 1 Hz square-wave voltage (0-2.5 V cm^{-1}) for 10,000 cycles. (d) Detailed information on the tensile actuation given in (c).

Figure 24(a)-(c): Improving the conductivity of PEDOT/PSS fibers. (a) A schematic of the wet-spinning set-up with the vertical hot-drawing apparatus used in this study. The draw ratio was controlled to 3:1. (b) A schematic of strategies to improve the conductivity of PEDOT/PSS fibers. (c) Average electrical conductivity of different PEDOT/PSS fibers by using the strategies in (b).

Figure 25(a)-(b): Temperature sensing by FBGs. (a) Experimental setup for the temperature measurement of the polymer fiber using FBGs. (b) Optical image shows the position of optical fibers and the PEDOT/PSS fiber during the temperature measurement. The distance between two FBGs is 700 mm.
Figure 26: TG curves of the as-spun PEDOT/PSS fiber and the EG/(PEDOT/PSS)/EG fiber. Inset is the TG curve from 20 to 100°C.
Figure 27(a)-(f): SEM images of the conductive polymer microfibers before and after TG analysis (25 to 800°C) in N_2. (a) As-spun PEDOT/PSS fiber, (b) EG/(PEDOT/PSS)/EG fiber, (c) As-spun PEDOT/PSS fiber after TG. (d) EG/(PEDOT/PSS)/EG fiber after TG. (e) and (f) cross section images of the as-spun PEDOT/PSS fiber and the EG/(PEDOT/PSS)/EG fiber after TG.
Figure 28: Actuation stress amplitude of the EG/(PEDOT/PSS)/EG fiber under the applied 1 Hz square wave voltage (0-5V) at different cycle numbers (1, 10, 100, 1000 and 10000).

DETAILED DESCRIPTION

INTRODUCTION

References cited herein can be used by one skilled in the art in the practice of the claimed inventions.

Priority US provisional application serial number 62/086,885 filed December 3, 2014 is hereby incorporated by reference in its entirety including all figures and working examples and associated text linked to the figures and working examples.

One lead aspect provides for a method comprising: providing at least one first composition comprising at least one conjugated polymer and at least one solvent, wet spinning the at least one first composition to form at least one first fiber material, hot-drawing the at least one fiber to form at least one second fiber material. Each of these elements is now described in more detail.

For example, the providing step is not particularly limited as one can, for example, make a first composition or one can purchase a first composition. If one purchases a first composition, one can alter it after purchase. For example, one can dilute a purchased solution.

A fiber material can include, for example, filaments, yarns, and ribbons.

FIRST COMPOSITION

The first composition can comprise at least one conjugated polymer and at least one solvent, each of which is described further hereinbelow.

The first composition can be adapted for wet-spinning as known in the art. See, for example, *Handbook of Conducting Polymers, 3rd Ed.; Conjugated Polymers, Processing and Applications*, Eds. Skotheim and Reynolds, CRC Press, 2007, wherein Chapter 2 (2-1 to 2-72) describes fiber spinning of conjugated polymers.

The conjugated polymer and solvent can be in the form of a dispersion. The conjugated polymer may be in the form of small nano- or micro-sized particles. The solvent can act as a carrier even if the conjugated polymer is not fully soluble in the solvent. In other embodiments, the conjugated polymer may be in the form of a solution, not a dispersion.

In one embodiment, the first composition has a concentration of at least 11 mg/mL, or at least 15 mg/mL of conjugated polymer including in combination, if present, with polymeric dopant. In another embodiment, the first composition has a concentration of at least 22 mg/mL of conjugated polymer including in combination, if present, with polymeric dopant.

CONJUGATED POLYMER

Conjugated polymers are known in the art. See, for example, *Handbook of Conducting Polymers, 3rd Ed.; Conjugated Polymers, Processing and Applications*, Eds. Skotheim and Reynolds, CRC Press, 2007. They can also be

called conducting polymers. The conjugated polymer can have extended conjugation along the backbone as known in the art.

Typical examples of conjugated polymers including polythiophene, polyaniline, polypyrrole, polyphenylene vinylene (PPV), polyacetylene, and the like. The conjugated polymer can be soluble or insoluble.

The conjugated polymer can be doped as known in the art. In one embodiment, the first composition comprises a polymeric dopant for the conjugated polymer. In one embodiment, the first composition comprises a polymeric dopant for the conjugated polymer which is a polyelectrolyte polymer. In one embodiment, the first composition comprises a polymeric dopant for the conjugated polymer which is polystyrene sulfonate (PSS). The polyelectrolyte, such as PSS, can be used in different forms with different forms of counterion including the acid and salt forms.

In one embodiment, the conjugated polymer comprises a polythiophene. In one embodiment, the conjugated polymer comprises a 3,4-di-substituted polythiophene. The substituents at the 3- and 4-positions can be, for example, alkoxy or polyether substituents, and they can be joined together to form a bridge if desired. The bivalent bridging moiety can be, for example, a bivalent alkyleneoxy group such as, for example, ethyleneoxy or propyleneoxy.

In one embodiment, the conjugated polymer comprises PEDOT which is known in the art. See, for example, *PEDOT: Principles and Applications of an Intrinsically Conductive Polymer*, Elschner et al., 2011. The method of making PEDOT is known and use of terms like the monomer, EDOT, and the doped form of the polymer, PEDOT:PSS are known.

SOLVENT

Solvent means a liquid to carry the conjugated polymer in the first composition whether or not a true solution is formed. The solvent can include one or more compounds and can be called also a "solvent system." One

compound can be water. The water can be mixed with one or more organic compounds and organic solvents.

In one embodiment, the first composition is an aqueous dispersion. In one embodiment, the first composition comprises water and at least one polar solvent, including for example at least one protic polar solvent. Aprotic solvents can be used.

Examples of solvents include DMSO, NMP, or an alcohol such as ethanol.

WET-SPINNING

Wet-spinning is known in the art. See, for example, *Handbook of Conducting Polymers, 3rd Ed.; Conjugated Polymers, Processing and Applications*, Eds. Skotheim and Reynolds, CRC Press, 2007, including Chapter 2 (2-1 to 2-72).

For sake of clarity, one embodiment is that the wet-spinning is not an electro-spinning process.

In one embodiment, the wet spinning is carried out with a coagulation bath comprising a mixture of solvents such as, for example, a mixture of two organic solvents such as, for example, a mixture of a C2-C5 ketone and a C2-C5 alcohol, such as for example, a mixture of acetone and isopropyl alcohol. The volume ratio of the two solvents can be, for example, 3:1 to 1:3, or 2:1 to 1:2, or about 1:1.

The spin-dope preferably comprises 1.1 wt.% to 6 wt.%, or 1.1 wt.% to 3.1 wt.%, or 2.2 wt.% to 3.1 wt.%, conjugated polymer based on the total weight of the spin-dope. These relatively low concentrations of conductive polymer in the spin-dope enable the resulting conductive polymer fiber to have for at least some embodiments good spinability, a high conductivity, and a higher modulus.

The extruded conjugated polymer fibers can be spun directly into the coagulation medium without an air gap. The coagulation medium can be contained in a coagulation bath.

The extruded conductive polymer fibers may be spun horizontally, vertically or even under an angle to the vertical direction. In an embodiment, the extruded conductive polymer fibers can be spun directly into the coagulation bath in vertical direction. Extruding conductive polymer fibers in a vertical direction is especially preferred as the density of the spun conductive polymer fibers is higher than the density of the coagulation medium. At start-up of the process, the extruded conductive polymer fibers will go to the bottom of the coagulation bath where the conductive polymer fibers can be picked up and collected through the coagulation bath vertically. The spun conductive polymer fibers enter the coagulation medium directly to coagulate the conductive polymer fibers to increase the strength of the conductive polymer fibers and to ensure that the "wet" conductive polymer fibers are strong enough to support their own weight. The extruded conductive polymer fibers are stretched by gravity forces and are supported by the liquid coagulation medium and are not break up into smaller pieces under their own weight. Vertical spinning can be partially helpful for the electrical conductivity and modulus enhancement and essential for the following step of hot-drawing and temperature control.

FIRST FIBER MATERIAL AND HOT-DRAWING

The first fiber material is in essence an intermediate as it will usually be subjected to hot drawing processes and other processing steps as described herein.

After the wet fiber is taken from the coagulation medium, it can be immediately heated and subjected to a vertical hot-drawing process, as shown in Figure 1b for example. The distance between the collector and the surface of

the coagulation medium is preferably from 0 to 100 cm, more preferably from 20 to 80 cm, even more preferably from 20 to 60 cm, most preferably at 50 cm or so to ensure that the fibers are dried before collecting on the rotating spool and not break during the collection process. Insufficient drying can result in no-circular fibers on the collector. The speed of the rotating spool collector is controlled by a motor, and the conductive polymer fibers are collected at a line speed preferably from 0.5 to 10 m/min, more preferably from 1 to 6 m/min., most preferably from 2 to 4 m/min. The draw ratio is calculated from the fiber collection speed and the wet spinning speed. To obtain conductive polymer fiber having high conductivity and high modulus, hot-drawing was applied to the conductive polymer fiber preferably at a draw ration of 1.0 to 5.0, more preferably from 1.0 to 3.0, most preferably about 3.0.

Hot drawing temperature around the fiber can be controlled by one or more (e.g. two) hot plates with a distance around 4 cm and monitored by, for example, a thermal couple.

In one embodiment, the hot drawing is done at a temperature of 50°C to 140°C, and in another embodiment, the temperature is 50°C to 120°C, and in another embodiment, the temperature is 60°C to 90°C.

SECOND FIBER MATERIAL AND OVERALL FIBER SPINNING PROCESS

The second fiber material can be collected and dried (or dried and collected) as known in the art.

The overall process can be carried out with a draw ratio which is at least 3, or at least 4, or at least 5, or at least 10.

In one embodiment, the second fiber material has a diameter of at least one micron, or at least 2 microns, or at least 3 microns, or at least 5 microns. In another embodiment, the second fiber material has a diameter of at least 10 microns.

The fiber length ranging, for example, from a micrometer to virtually endless. In one embodiment, the fiber length is at least 10 cm, or at least one meter, or at least 10 m, or at least 100 m. In another embodiment, the fiber length is at least 500 m. In another embodiment, the fiber length is at least 1,000 m.

SECONDARY DOPING STEP

In one embodiment, the method further comprises a secondary doping of the first composition. In one embodiment, the doping is carried out with at least one organic solvent such as, for example, an oxygenated solvent such as an alkylene glycol. In one embodiment, the doping is carried out with ethylene glycol. Poly(ethylene glycol) can be used.

The working examples hereinafter further describe embodiments for the doping step.

DE-DOPING STEP

In one embodiment, the method further comprises de-doping of the first fiber material before hot drawing. In one embodiment, the method further comprises doping of the first composition, and the method further comprises de-doping of the first fiber material before hot drawing.

In one embodiment, the de-doping is carried out with at least one organic solvent such as, for example, an oxygenated solvent such as an alkylene glycol. In one embodiment, the de-doping is carried out with ethylene glycol.

The working examples hereinafter further describe embodiments for the de-doping step including coupling of doping and de-doping steps.

FIBERS AND PROPERTIES OF FIBERS

One embodiment is a fiber material prepared by the methods described herein. These include intermediate fibers before all processing steps are

finished as well as final fiber materials including fiber materials which are disposed into articles and devices.

In one embodiment, the fiber material shows a conductivity of at least 300 S · cm^{-1}, or at least 368 S · cm^{-1}or at least 500 S · cm^{-1}. In another embodiment, the fiber material shows a conductivity of at least 2,000 S · cm^{-1} or at least 2,800 S · cm^{-1}.

In one embodiment, the fiber material shows a cross-over temperature of semiconductor-to-metal transition of at least 25°C. In another embodiment, the fiber material shows a cross-over temperature of semiconductor-to-metal transition of at least 40°C.

In one embodiment, the fiber material shows a Young's modulus of at least 5 GPa, a tensile strength of at least 300 MPa, and an elongation at break of at least 10%. In another embodiment, the bundle of fibers shows a Young's modulus of at least 8 GPa, a tensile strength of at least 409 MPa, and an elongation at break of at least 21%.

METHODS OF USE AND APPLICATIONS

The fiber materials can be used in many applications including, for example, actuators, including electromechanical and electrochemical actuators, various sensors including vapor and humidity sensors and strain sensors, resistive heaters and resistive heating textiles, electromagnetic interference shielding, flexible electrodes, and wearable electronics.

Fiber extensional actuators can be prepared which convert electricity or other input energy to mechanical energy at a low voltage and a very high frequency (e.g., up to 10 Hz) in air.

Additional embodiments are provided in the following non-limiting working examples (including Parts I and II).

WORKING EXAMPLES

RESULTS AND DISCUSSION (PART I)

The effect of hot-drawing on the conductivity of as-spun PEDOT/PSS fibers.

Figure 1b shows a schematic of the wet-spinning process (see the Experimental Methods section below for details). A vertical hot-drawing system was set up to process the "wet" fibers as they are pulled out of the acetone/isopropyl alcohol (acetone/IPA) coagulation bath. Optimization of the wet-spinning parameters to achieve the highest reported conductivity of as-spun fibers is described in the Supplemental Working Example Information section. The vertical hot-drawing process helps to align the molecular chains of the fibers in the fiber direction. The draw ratio is calculated from the ratio of the fiber collection speed and the wet-spinning speed (see details in the Supplemental Working Example Information section and Figure 9). Spinning of a pristine PH1000 dispersion (11 mg/mL) by using this system resulted in a discontinuous spinning process producing fibers with lengths up to 20 m at a draw ratio of 3.0. These fibers had an average diameter of 4.9±0.6 μm (Figure 8a). The spinnability of the fiber was dramatically improved by doubling the concentration of the PH1000 dispersion (22 mg/mL), resulting in fibers with lengths up to 100 m, while the diameter increased to 9.8±1.3 μm, as measured in SEM image (Figure 1c). The fibers were found to have remarkably smooth surfaces and they could be easily knotted, demonstrating their excellent flexibility (inset of Figure 1c). The electrical conductivity of the fibers spun from these two concentrations were 361±31 and 368±34 $S \cdot cm^{-1}$, respectively. These results suggest that the initial concentration of the dispersion does not affect the fiber conductivity by much. It is important to point out that no pretreatment was done on these dispersions and that the conductivity values were five times higher than the highest previous values of as-spun PEDOT/PSS fibers (74 $S \cdot cm^{-1}$)[8] and three orders of magnitude higher than that of bulk film (0.7 $S \cdot cm^{-1}$).[17] Fibers without hot-drawing (draw ratio = 1) from the concentrated dispersion (22 mg/mL) were also fabricated and had a diameters of

24.9±1.3 μm (Figure 8b). The conductivity of these fibers without hot-drawing was 188±16 S · cm^{-1}, which was only half of the value of the hot-drawn fibers. To further confirm the effect of the hot-drawing, another source of PEDOT/PSS dispersion (Clevios P, 13 mg/mL) was also spun into much thinner fibers with diameters of 2.9±0.2 μm using the hot-drawing process (Figure 10c). The conductivity of these Clevios P microfibers was 121±11 S · cm^{-1}, which is one order of magnitude higher than that of the earlier reported value (11 S · cm^{-1}).[8] As a result, while not limited by theory, the inventors attributed the improvement in the conductivity of the fibers to the preferential alignment of the molecular chains along the fiber axis induced by the hot-drawing. By using a simple hot-drawing assisted wet-spinning process, the inventors could therefore fabricate fibers with electrical conductivity comparable with that of fibers doped and/or de-doped by organic solvent.

The effect of EG doping and/or de-doping.

To obtain the highest possible electrical conductivity of the conjugated polymer fibers, doping and/or de-doping processes were applied to these fibers, as shown in Table A (Supplemental Working Example Information, hereinafter). First, doping was accomplished by adding 3 wt% EG with respect to the concentrated PH1000 dispersion (22 mg/mL). The average diameter of the fabricated fibers (EG/(PEDOT/PSS) fiber) was 9.7±1.4 μm (Figure 10d) and the conductivity readily improved from 368±34 to 607±60 S · cm^{-1}. While not limited by theory, this conductivity enhancement perhaps was due to the microstructure arrangement of the PEDOT chains. The dipole-dipole interaction of EG with thiophene rings results in a planarization of the PEDOT chains. The quinoid structure becomes the dominating conformation on the chains. Thus, the PEDOT chains transformed from a coil to an expanded coil or linear structure after doping.[9]

The effect of de-doping was studied separately. Specifically, the as-spun fibers produced from the concentrated PH1000 dispersion (22 mg/mL) were de-

doped by directly immersing the fibers in an EG bath for 1 hour and a conductivity of 1304±56 $S \cdot cm^{-1}$ was achieved. While not limited by theory, perhaps the main reason for the conductivity enhancement by de-doping is the partial removal of amorphous PSS.[8]

Earlier research has shown that an effective way of achieving the highest conductivity (1418 $S \cdot cm^{-1}$) of PEDOT/PSS films is to use both doping and de-doping processes together.[24] Here, we achieved a striking increase in the electrical conductivity of the fibers: from 607±60 $S \cdot cm^{-1}$ to 2804±311 $S \cdot cm^{-1}$. This value is six times better than best value for previous reported fibers (467 $S \cdot cm^{-1}$) and twice the best value (1418 $S \cdot cm^{-1}$) of PEDOT/PSS films with EG treatment.[24] Although a conductivity for PEDOT/PSS film ranging from 2400 to 4380 $S \cdot cm^{-1}$ has been achieved by treating the film with sulfuric acid, the use of strong and corrosive acid will cause safety concerns and is undesirable in commercial device fabrication.[18,25] In this work, by assisting the wet-spinning process with hot-drawing and doping/de-doping the fibers with EG, the inventors can achieve a high conductivity that is comparable with the highest values for PEDOT/PSS films. The inventors also demonstrate the electrical properties of our fibers by wiring a light-emitting diode (LED) with two PEDOT/PSS conductive fibers. The fiber resistance was low enough to light the LED at 6 V, as shown in Figure 1d.

The Semi-metallic behavior of the fibers.

Apart from the electrical conductivity at room temperature (RT), a second important factor characterizing electrical transport in conductive fibers is the dependence of conductivity on temperature. Figure 1e shows the temperature-dependent conductivity of an as-spun PEDOT/PSS fiber, an EG/(PEDOT/PSS) fiber, a (PEDOT/PSS)/EG fiber and an EG/(PEDOT/PSS)/EG fiber. All these fibers exhibited two regimes in the conductivity: at low temperature, the conductivity rises with temperature (semiconductive behavior), whereas at high

temperature, the conductivity drops (metallic behavior). The crossover temperature for the semiconductor-metal (S-M) transition is around 313 K (40°C). The insulator-metal (I-M) or S-M transition in conductive polymers or carbon-based fibers has been observed in a wide temperature range in a number of systems, including polyacetylene, polypyrrole, polyaniline, polythiophene derivatives and carbon nanotubes.[3,26–31] Generally, the crossover temperature, T_0, of conductive polymers has been reported to be below room temperature, whereas T_0 of CNT fibers has been reported to vary from 40 K to well above room temperature.[3,31] The conductivity ratio, $\sigma(T)/\sigma(T_0)$, has been chosen to qualify the relative disorder in different samples and for identification of the various regimes.[26] Figure 1f shows that the semiconductive behavior is more pronounced for low conductivity fibers. The typical semiconductive behavior that the fibers displayed at low temperature can be understood as carrier hopping or tunneling between adjacent PEDOT/PSS grains. These points will be addressed in detail in the following. At high temperature, metallic behavior in EG doped and/or de-doped fibers indicates diffusive, intra-chain transport, during which the conductivity is reduced by electron-phonon scattering.

Microstructure characterization.

To understand the electrical properties of the conductive fibers, the inventors studied the surface and inner structural changes of the fibers. The inventors used X-ray photo-electron spectroscopy (XPS) to investigate the as-spun PEDOT/PSS fibers and EG/(PEDOT/PSS) fibers before and after EG de-doping. High-resolution XPS of the S 2p core-level spectra are shown in Figures 2a and b. The S 2p core-level has a signature with two distinct peaks from 162 to 166 eV and from 166 to 171 eV. Each peak involves contributions from a spin-split doublet, S $2p_{3/2}$ and S $2p_{1/2}$, with 1.2 eV energy splitting and a 1:2 intensity ratio.[32] The two peaks from 162 to 166 eV are well separated compared with the peaks from 166 to 171 eV. The S $2p_{3/2}$ components at 163.3

eV and 167.6 eV correspond to sulfur atoms of the PEDOT and the sulfonate fragment of PSS, respectively.[18,33,34] The experimental PEDOT-to-PSS ratio (R_s) was determined by quantitative analysis of the S 2p core-level spectra. In as-spun PEDOT/PSS fiber and EG/(PEDOT/PSS) fiber, the R_s are 0.50 and 0.52, respectively. By EG de-doping, the R_s increased to 0.86 and 1.04 for (PEDOT/PSS)/EG fiber and EG/(PEDOT/PSS)/EG fiber, respectively. This change clearly suggests that PSS is partially removed from fibers by EG de-doping. The fact that the EG/(PEDOT/PSS)/EG fiber also has the highest conductivity (2804 $S \cdot cm^{-1}$) also indicated that the less insulating polymer, PSS, in the fiber will increase the electrical conductivity.

AFM images were taken to probe the changes in the surface microstructures of all fibers. The root mean square (rms) roughnesses measured from height images of as-spun PEDOT/PSS fiber and EG/(PEDOT/PSS) fiber were 11.2 and 14.1 nm, respectively. After de-doping with EG, the roughnesses increased to 21.8 and 18.0 nm, respectively (Figure 11). This trend is in agreement with observations of PEDOT/PSS films with EG de-doping[17] and suggests partial removal of PSS segments in the fibers as indicated by XPS results. In the AFM phase images (Figures 3a and 3b), the EG/(PEDOT/PSS) fiber shows a phase separation between PEDOT and PSS compared with the as-spun PEDOT/PSS fiber, indicating that EG doping can largely reduce electrostatic interactions between PEDOT and PSS.[35] The dark areas can be regarded as the amorphous PSS region, while the bright areas are the conductive PEDOT region. As the thick and insulating PSS acts as barriers for electron transport between PEDOT grains, the conductivity of these fibers is relatively low. Figure 2c and d show that after EG de-doping, the amorphous regions (PSS) of both fibers are largely reduced, resulting in interconnected PEDOT grains with an extremely thin layer of PSS between them. The average size of the grains in the EG/(PEDOT/PSS)/EG fiber (14.8 ±4.4 nm) is much smaller than that in the (PEDOT/PSS)/EG fiber (56.8 ±12.7 nm). The reduction of grain

size indicates that more PSS is removed from the EG/(PEDOT/PSS) fibers after de-doping. This change is also in agreement with the increased R_s (0.86 and 1.04 for the (PEDOT/PSS)/EG fiber and EG/(PEDOT/PSS)/EG fiber, respectively). A crucial point is that doping PEDOT/PSS makes the de-doping step more efficient by reorganizing the initial microstructure of the fiber. As there is a very limited amount of PSS between the conductive PEDOT grains, this leads to an increased number of interconnections with highly conductive PEDOT neighbor grains on the surface of the fibers and makes the electron transport three-dimensional, thereby resulting in the highest conductivity of the fibers considered in this study.

To investigate the inner microstructural changes between the as-spun PEDOT/PSS fiber and the EG/(PEDOT/PSS)/EG fiber, the samples were cut into nanofilms by Focused Ion Beam (FIB) along the fiber axis direction and investigated by High-Angle Annular Dark-Field Scanning Transmission Electron Microscopy (HAADF-STEM). The average thickness of the films was determined to be 56.7 nm from the effective mean free path.[36] Figure 2e shows that the as-spun PEDOT/PSS fiber exhibits no obvious grain structures compared with previous spin-coated PEDOT/PSS nanofilms,[37] indicating that PEDOT/PSS has a very condensed fiber structure. With EG doping/de-doping, PEDOT/PSS aggregates with diameters of 8.5 ± 1.7 nm appear in the film (Figure 2f). Small grains with a size down to 1 nm are also observed between these aggregates, revealing that EG doping/de-doping releases conductive PEDOT from the PEDOT/PSS complex. The selected area electron diffraction (SAED) pattern of the as-spun PEDOT/PSS fibers shows amorphous rings, indicating that the crystallinity of PEDOT is inhibited by a strong electrostatic interaction with the entangled PSS. On the other hand, the SAED pattern of the EG/(PEDOT/PSS)/EG fiber is similar to PEDOT microribbons with a width of 1.8 μm,[38] showing discrete diffraction spots in each Debye ring. These results suggest that after EG doping/de-doping, the PEDOT structure is rearranged

from random-oriented polycrystalline to a preferred-oriented polycrystalline. Thus, interchain charge carrier transport will be significantly improved by the chain alignment so that the EG/(PEDOT/PSS)/EG fiber has the highest conductivity.

To understand the electrical transport in the fibers, the fiber microstructure was investigated by transmission Wide Angle X-ray Scattering (WAXS). The fibers are bundled and aligned perpendicularly to scatter the x-ray beam, as shown in Figure 10. Figure 4 presents the 2D WAXS pattern and the intensity integration plots along the vertical and horizontal directions, presenting the anisotropic structure in the fibers. For the as-spun PEDOT/PSS fibers, three broad peaks are observed in the vertical direction at approximately $q_z = 2.5$, 11.6 and 17.5 nm^{-1}, corresponding to the d-spacing of 2.51, 0.541 and 0.359 nm (Figure 3e), respectively. The (100) peak at $q_z = 2.5$ nm^{-1} is assigned to lamella stacking of alternate orderings of PEDOT and PSS in the plane. The (020) peak at $q_z = 17.5$ nm^{-1} indicates $\pi - \pi$ stacking of PEDOT chains along the vertical direction.[8,35] The broad peak at $q_z = 11.6$ nm^{-1} is attributed to the amorphous halo of randomly distributed PSS.[25,35,39] On the other hand, the integrated plot in the horizontal direction, which shows the microstructure in the transverse fiber direction, has only a PSS peak but no (100) and (020) peaks (Figure 3f). Due to the amorphous nature of PSS, there is no obvious anisotropy with this broad peak ($q_{xy} = 11.6$ nm^{-1}) in both directions. To conclude, the strong scattering anisotropy of PEDOT in as-spun PEDOT/PSS fibers reveals that the PEDOT chains orient preferentially along the fiber direction.

The EG doped fibers have a similar structure as the as-spun fibers but they have better crystallinity. Figure 4c presents the WAXS pattern of EG/(PEDOT/PSS) fibers showing the higher intensity from both $\pi - \pi$ stacking and polymer backbones. The fibers made with 3 wt% EG-doped PEDOT/PSS exhibit narrower peaks at both $q_z = 2.34$ and 17.6 nm^{-1}, indicating that better crystallinity formed in the fibers. The broad hump peak at $q_z = 11.6$ nm^{-1} is

more evident, suggesting that EG weakens the electrostatic interactions between PSS and PEDOT. This improvement is consistent with observations in former AFM phase images (Figure 3a,b), in which the phase segregation of PEDOT and PSS is more evident than that of as-spun PEDOT/PSS fibers. It is worth noting that after de-doping, the $\pi - \pi$ stacking peak of as-spun PEDOT/PSS fibers and EG/(PEDOT/PSS) fibers shifted from q_z = 17.5 and 17.6 nm^{-1} to q_z = 17.9 and 18.0 nm^{-1}, respectively. The above peak shifts correspond to a reduction in the $\pi - \pi$ stacking distances from 3.59 and 3.57 to 3.51 and 3.48 Å, respectively. The shorter distance indicates stronger $\pi - \pi$ interactions between adjacent PEDOT chains, facilitating electron transport in these directions. There is also an intensity reduction on the broad hump peak at q_z and q_{xy} =11.6 nm^{-1}, as manifested by the partial removal of PSS in XPS results (Figure 2a,b). Normal WAXS (Figure 13a,b, Figure 12a and Table B) were also performed and the results are comparable with those of transmission WAXS. The inventors verified again that the most effective way to improve the order of the molecular chains and the crystalinity of the fibers involves stretching the molecular chains by hot-drawing, reducing of the PEDOT and PSS electrostatic interaction by EG doping and reducing the $\pi - \pi$ stacking distance of PEDOT chains by EG de-doping.

Mechanical and electromechanical behaviors.

An important feature of these fibers is that they can be easily shaped into highly flexible structures, which is crucial to successful applications requiring stretchable electronics and functional fabrics. To illustrate this, a bundle of fibers was wound around a thin glass capillary (diameter: 5 mm) to form a helical shape after drying (inset in Figure 5). The spring-like bundle was then manually stretched from 3.5 cm to a final length of 12.5 cm, corresponding to an elongation of 257%. The stretched bundle did not break and could recover its original shape upon release.

Next, the inventors investigated the single fiber mechanical behavior. Figure 6a shows stress-strain curves obtained for fibers subjected to hot-drawing but with various formulations. All fibers display a bi-linear stress-strain curve, which is characteristic of linear strain-hardening behavior. The mechanical properties of these fibers are greatly improved over those of earlier reported PEDOT/PSS fibers.[7–9] First of all, we note that hot-drawing by itself already largely enhances the properties of the fibers. Indeed, as-spun PEDOT/PSS fibers have a tensile strength of 242.5 ± 21.0 MPa and a Young's modulus of 5.9 ± 0.7 GPa, which are already twice the values of as-spun fibers prepared from IPA coagulant in a previous study.[9] Further SEM observation of the cross section of a broken fiber after mechanical testing did not reveal any obvious pores. More importantly, fibrilization at the fracture cross-section was observed (Figure 15), suggesting typical plastic deformation of the fibers.

Our results indicate that doping and/or de-doping the fibers with EG improved the mechanical properties. These fibers had a tensile strength of 409.8 ± 13.6 MPa and a Young's modulus of 8.3 ± 0.4 GPa, which are three and 1.5 times higher than previously reported, respectively.[9] Generally, while not limited by theory, the inventors attribute these improvements to the partial removal of amorphous PSS (Figure 2a,b) and an increase in the crystallinity of PEDOT/PSS fibers as shown in Figure 4. Along with the increase in the Young's modulus, we observe that the plastic behavior was largely reduced after doping and de-doping. First, the yield stress, σ_y, increased from 135 MPa for the as-spun fibers to 187 MPa for the EG/(PEDOT/PSS)/EG fibers, indicating that the plasticity developed at a 38% higher load in the latter. When plasticity was initiated ($> \sigma_y$), it also developed more slowly in the EG/(PEDOT/PSS)/EG fibers compared with the as-spun fibers. Indeed, this typical bi-linear be-havior can be matched as a first approximation by a simple Prandtl-Reuss elasto-plastic model.[40] In this model, the classical linear

hardening parameter, H, ranges from 0 for materials with perfect plasticity to $+\infty$ for perfectly elastic behaviors and it can be expressed as:

$$(1) \quad H = \frac{\sigma_m - \sigma_y}{D}$$

where σ_m is the final tensile stress and D is the plastic strain, as shown in Figure 4a. H takes here the values 819, 1039, 1216 and 1315 MPa for the as-spun fibers, the EG/(PEDOT/PSS) fibers, the (PEDOT/PSS)/EG fibers and the EG/(PEDOT/PSS)/EG fibers, respectively. The increases in the Young's modulus (E), the yield stress (σ_y) and the linear hardening parameter (H) are consistent with removal of the PSS phase. Indeed, the PEDOT/PSS fiber is in fact a composite between a soft and plastic phase (PSS) with a much stiffer and less plastic phase (PEDOT). Removal of PSS tends to increase the elastic properties while decreasing the plastic properties. Note that the mechanical tests in this work were performed at room temperature and 60% relative humidity (RH). It is expected that the values reported here for tensile strength and Young's modulus would further increase by reducing the RH level.[41,42] The inventors also found that the fibers that display the best mechanical properties (i.e., EG/(PEDOT/PSS)/EG fibers), are also those that exhibit the highest electrical conductivity. Thus, the mechanical properties and electrical conductivity are improved in a correlated manner as the degree of chain alignment is increased, as shown in Figure 1a.

The superior mechanical and electrical properties motivated the inventors to further investigate the degradation of the mechanical and electrical properties by stretching/unstretching. First, the inventors performed cyclic loading/unloading tests (Figure 6b). These are consistent with the monotonic loading test in the sense that the former confirms the envelope of the cyclic curve, excluding any effect of the cycling on the envelope curve. To track any development of degradation within the fibers while increasing the loading, the

inventors followed a classical damage mechanics approach.[43] The relative Young's modulus change, E_i/E_0, of as-spun PEDOT/PSS fibers and EG/(PEDOT/PSS)/EG fibers is plotted as a function of the maximum strain at each cycle (Figure 16), where E_0 and E_i are the initial and current Young's modulus, respectively. For the as-spun PEDOT/PSS fibers, the inventors observe a 20% decrease in the Young's modulus at low strain levels (< 4%). Beyond this point, the modulus increases slightly. This behavior in the low strain regime is attributed to the large amount of amorphous PSS in PEDOT/PSS fibers. At larger strains (> 4%), the PEDOT crystalline region rotates the chain molecules into the fiber loading direction and the modulus increases again. In contrast, the Young's modulus of EG/(PEDOT/PSS)/EG fiber remains almost constant until the strain level increases over 4%. While not limited by theory, this can be explained by the fact of that partial removal of PSS can lead to an earlier rotation of the PEDOT crystalline region in comparison with the as-spun PEDOT/PSS fiber.

The relative resistance change ($\Delta R/R_0$) was also monitored under cyclic loading/unloading with progressive extension of the as-spun PEDOT/PSS fiber and EG/(PEDOT/PSS)/EG fiber (Figure 6c,d). As expected, the resistance of the sample increases with increasing strain. The resistance in a bulk material with a circular cross section is given by:

$$(2)\quad R = l/\pi r^2\sigma$$

where C is the electrical conductivity, and l and r are the length and the radius of the fiber, respectively. To determine the intrinsic conductivity change, the pure geometric factor was calculated and subtracted from the measured resistance. The relationship between the relative resistance change and the conductivity change can be expressed by:

$$(3)\quad \Delta R/R_0 = -\Delta\sigma/\sigma + \Delta l/l - 2\,\Delta r/r$$

For small changes $\Delta l/l = \varepsilon_l$ and $\Delta r/r = -\nu\varepsilon_l$, where ε_l is the strain in the fiber direction, and ν is the Poisson's ratio. substituting these values in equation (3) gives

(4) $\Delta R/R_0 = - \Delta\sigma/\sigma + \varepsilon_l(1 + 2\nu)$

where $F = \varepsilon_l(1 + 2\nu)$ comes only from the change in the cross-section of the fibers, whereas the first part on the right-side term, $\Delta\sigma/\sigma$, reflects changes in the conductivity of the material that can also be dependent on the strain.

For the as-spun PEDOT/PSS fibers, the relative resistance change is 0.23 at 13% strain level. Assuming $\nu = 0.34$,[44] one can calculate $F= 0.22$ and $\Delta\sigma/\sigma \approx 0$. Therefore, the variation in resistance can be mostly attributed to the change in the geometry of the sample. However, it is important to highlight that the EG/(PEDOT/PSS)/EG fiber exhibits a much lower variation in resistance. At the same strain level of 13%, the resistance change is only 0.05, which is almost 3.5 times lower than that of the as-spun fiber. With the previous values, one finds that $\Delta\sigma/\sigma = 0.17$, suggesting an increase in the conductivity of the fiber.

Correlation between the microstructure and the electrical and mechanical properties.

The morphology, microstructure and electromechanical analyses of the fibers provide some insight into the correlation between the PEDOT/PSS microstructure and the electrical and mechanical behaviors. While not limited by theory, the stages of the molecular level deformation of PEDOT/PSS fiber are proposed in Figure 7a. PEDOT/PSS is a semi-crystalline complex, in which PEDOT is a conductive nanocrystal and PSS is an amorphous insulator.[35] The plastic deformation starts by lengthening amorphous PSS chains. At larger strains, the PEDOT crystalline region rotates the molecule chains into the fiber's loading direction. Further deformation results in crystalline regions separating into differ-ent blocks. This rearrangement improve the dispersion of the PEDOT nanocrystals in the fiber and the molecule chains tend to align with

respect to the loading direction, leading to an enhancement of the Young's modulus. As the weakest part is the interface between amorphous and crystalline regions in PEDOT/PSS, deformation at the last stage may result in damage to the interfaces and rupture of the fiber.[45]

To address the mechanism that leads to electrical conductivity changes in the fibers, a schematic deformation of PEDOT/PSS grains in fibers before and after EG de-doping is displayed in Figure 7b. A key point is that as-spun PEDOT/PSS fibers contain large amounts of amorphous PSS as insulators. Upon stretching, the PSS-rich shell around the PEDOT-rich core is elongated, so that the electron hopping distance between neighbor PEDOT/PSS grains in the fiber direction increases. This change results in a larger $\Delta R/R_0$. In EG/(PEDOT/PSS)/EG fibers, the PSS insulator is partially removed by EG de-doping, reducing the distance between PEDOT-rich cores and thereby creating conductive pathways. As a result, the $\Delta R/R_0$ for EG/(PEDOT/PSS)/EG fiber is dramatically reduced compared with that of as-spun PEDOT/PSS fibers under the same strain. Oh et al.[46] have shown that using PEDOT/PSS in electrodes and electrical circuits presents a number of challenges, especially that the conductivity decreases at large strains (> 2%). However, our conductive fibers show an extraordinary electrical performance during stretching/unstretching: the conductivity increased by 25% (as calculated from Equation (4)) before the fiber rupture point with the maximum strain up to 21%.

In conclusion, in the working examples, the inventors systematically studied the effects of hot-drawing and EG doping/de-doping on the conductivity of wet-spun PEDOT/PSS microfibers. Specifically, hot-drawing can improve the conductivity from 187 to 368 $S \cdot cm^{-1}$, and EG doping these fibers (3 wt%) further improves the conductivity from 368 to 607 $S \cdot cm^{-1}$. Finally, with EG de-doping the EG doped fibers, the conductivity value reaches as high as 2804 $S \cdot cm^{-1}$, the highest value in conjugated polymer fibers. All the fibers in this study display a semiconductor-metal transition around 313 K. The results also

show a clear correlation between the microstructure and the electrical and mechanical properties. In particular, the inventors found a maximum Young's modulus of 8.3 GPa for the most conductive fiber, which corresponds an increase of 41% over as-spun PEDOT/PSS fibers. The enhanced properties resulted from microstructural refinement, which was achieved by (1) preferred alignment of PEDOT molecule chains through hot-drawing, (2) reduction in the electrostatic interaction of PEDOT and PSS by EG doping and (3) partial removal of amorphous PSS from the fibers by EG de-doping. The fibers with enhanced properties also show superior stretchability and are able to retain high stiffness with an obvious increase in electrical conductivity (25%) at strain levels as high as 21%. These results can provide a foundation for performance maximization of conjugated polymer microfibers and pave the way for stretchable electronics in the form of fiber structures.

EXPERIMENTAL METHODS (PART I)

Materials. The PEDOT/PSS aqueous dispersion (Clevios^{TM}P and PH1000) was purchased from HC Starck, Inc. Ethylene glycol (EG), Isopropyl alcohol (IPA), and acetone were purchased from Sigma-Aldrich.

Preparation of highly spinable inks. PEDOT/PSS inks: 10 mL of water was evaporated from 20 mL of the PH1000 dispersion (11 mg mL^{-1}) at 50°C to increase the viscosity of the ink. Then 0.3 g of EG was mixed into the concentrated PH1000 dispersion (22 mg mL^{-1}) by a magnetic stirrer for two hours to enhance the electrical conductivity.[17,47] Then it was homogenized at 20,000 rpm for 5 mins using a T18 homogenizer (IKA) and followed by 20 mins bath sonication using a Brason 8510 sonicator (250 W, Thomas Scientific) at room temperature. Finally, the dispersion was degassed in a vacuum oven at room temperature (21°C) before wet-spinning.

Wet-spinning of PEDOT/PSS fibers. The spinning formulation was loaded into a 5 mL glass syringe and spun into a coagulation bath though a metal needle

with an inner diameter from 100 to 220 μm. The flow rate of the ink was controlled between 2 to 50 μL min^{-1} by using a syringe pump. The fibers were collected vertically onto a 50 mm winding spool, which gives a line speed of 2 to 4 m min^{-1}. The air temperature along the path of the fiber was controlled by two vertically located hot-plates (see Figure 1b) and was monitored by a thermocouple. After wet-spinning, de-doping of the as-spun fibers was carried out by immersing them in a EG bath for 1 hour and the fibers were then dried in air at 160°C for 1 hour. Herein, as-spun PEDOT/PSS fiber, EG/(PEDOT/PSS) fiber, (PEDOT/PSS)/EG fiber and EG/(PEDOT/PSS)/EG fiber represent pristine PEDOT/PSS fiber, 3 wt% EG doped PEDOT/PSS fiber, EG de-doped PEDOT/PSS fiber and EG de-doped 3 wt% EG doped PEDOT/PSS fiber, respectively.

Characterizations. Electrical resistance of the fibers was measured by using an Agilent 1252B multimeter. The electrodes on the fiber were made by connecting a copper wire to the fiber surface with silver epoxy. The distance between two contacts was about 10 mm. The temperature-dependent DC electrical conductivity was measured by the two probe method in a temperature controllable chamber, in which highly pure N_2 was purged at a flow rate of 200 mL min^{-1} to protect the sample and measurement electronics from the humid air. The electrical conductivity measurements of the specimens were carried out in the temperature range from -150 to 220°C with a heating rate of 5°C min^{-1}. At least three measurements were conducted for each type of fiber.

Scanning electron microscopy (SEM) was performed using a Quanta 3D (FEI Company). TEM samples were prepared by focused ion beam (FIB) cutting with help from the same SEM machine. The conductive fibers were first fixed on the SEM holder with silver epoxy. The samples were tilted 52° and cuts were made along the fiber axis direction. The ion beam source was a field-emission

FIB with a Pt ion emitter, an ion beam voltage of 30 kV and a beam current of 0.47 nA.

X-ray photoelectron spectroscopy (XPS) analyses were carried out with a Kratos Axis Ultra DLD spectrometer equipped with a monochromatic Al Kα X-ray source (hν = 1486.6 eV) operating at 150 W, a multichannel plate and delay line detector under a vacuum of 1×10^{-9} mbar. All spectra were recorded using an aperture slot of 300 × 700 μm. The survey and high-resolution spectra were collected at fixed analyzer pass energies of 160 eV and 20 eV, respectively. The XPS peaks were analyzed using a Shirley-type background and a nonlinear least-squares fitting of the experimental data based on a mixed Gauss/Lorentz peak shape. XPS quantification was performed by applying the appropriate relative sensitivity factors (RSFs) to the integrated peak areas.

Atomic Force Microscopy (AFM) images of conductive polymer fibers were taken using an Agilent 5400 (Agilent Technologies) microscope in the tapping mode over a window of 1 μm × 1 μm. The fibers were fixed on glass slides with a thin layer of epoxy adhesive.

TEM images of conductive polymer fibers were taken by using a Titan G2 80-300 CT (FEI Company) at an accelerating voltage of 300 kV equipped with a field-emission electron source. The PEDOT/PSS thin films cut from fibers by FIB were analyzed with High-Angle Annular Dark-field Scanning Transmission Electron Microscopy (HAADF-STEM) observation modes at a dose of 187 e Å−2. The HAADF-STEM micrographs were recorded with an analog detector (E. A. Fischione, Inc). The entire image acquisition as well as processing of the data was accomplished by using the GMS v1.8.3 microscopy suite software (Gatan, Inc).

Transmission Wide-angle X-ray Scattering (WAXS) measurements were performed on the D-line, Cornell High Energy Synchrotron Source (CHESS) at Cornell University. The fibers were aligned vertically into a bundle and placed perpendicularly into a monochromatic x-ray beam with the wavelength of 0.115

nm. The scattering patterns were collected by a CCD detector (Medoptics) with a pixel size of 46.9 μm at a distance 100 mm away from sample. The exposure time was 10 s. To present the anisotropic scattering, the plots were integrated along the horizontal and vertical directions in the ±5° region by the Fit2d program.[48]

Normal WAXD tests were performed from 2 to 35° in a continuous mode using a Bruker D8 Advance powder X-ray diffractometer, with Cu-Kα radiation (λ =1.54 Å) at 40 kV and 40 mA. To generate peaks with relatively high intensity, a slow increment at 0.02° and a slow scan speed at 12 sec/step was applied, and the percentage of crystallinity was determined by the Diffract.EVA software (Bruker). Raman spectra were collected using a LabRAM Aramis Raman spectrometer (Horiba, Ltd.) on casted films and fibers using a 632 nm laser.

The mechanical behavior of the fibers was measured by an 5966 Instron universal testing machine at a strain rate of 5% min^{-1}. The tests were performed inside an enclosure to protect the fibers from environmental disturbances. 2 cm long fibers were prepared and fixed on a paper card. The tensile strength, Young's modulus and elongation were calculated, and the values were collected from at least 10 tests for each formulation. The electrical resistance change of the fibers was monitored using an U1252B digital multimeter. A cyclic loading/unloading program was applied to the fiber with an incremental extension of 0.2 mm at each cycle and then releasing to a load of 1 mN. The resistance data were captured every 1 s during the test. Two ends of the samples were connected with copper wires and painted with silver epoxy, followed by sealing the silver epoxy area by epoxy glue.

Listing of References 1-48 (PART I):

(1) Cherenack, K et al., Woven Electronic Fibers with Sensing and Display Functions for Smart Textiles. *Adv. Mater.* **2010**, *22*, 5178.

(2) Abouraddy, et al.. Towards Multimaterial Multifunctional Fibres That See, Hear, Sense and Communicate. *Nat. Mater.* **2007**, *6*, 336–347.

(3) Behabtu, N. et al. Strong, Light, Multifunctional Fibers of Carbon Nanotubes with Ultrahigh Conductivity. *Science* **2013**, *339*, 182–186.

(4) Egusa, S. et al., Multimaterial Piezoelectric Fibres. *Nat. Mater.* **2010**, *9*, 643–648.

(5) Kou, L. et al., Coaxial Wet-spun Yarn Supercapacitors for High-Energy Density and Safe Wearable Electronics. *Nat. Commun.* **2014, DOI: 10.1038/ncomms4754.**

(6) Yang, Z. B.; Deng, J.; Chen, X. L.; Ren, J.; Peng, H. S. A Highly Stretchable, Fiber-Shaped Supercapacitor. *Angew. Chem. Int. Ed. Engl.* **2013**, *52*, 13453–13457.

(7) Okuzaki, H.; Ishihara, M. Spinning and Characterization of Conducting microfibers. *Macro- mol. Rapid. Commun.* **2003**, *24*, 261–264.

(8) Okuzaki, H.; Harashina, Y.; Yan, H. Highly Conductive PEDOT/PSS Microfibers Fabricated by Wet-spinning and Dip-treatment in Ethylene Glycol. *Europ. Polym. J.* **2009**, *45*, 256–261.

(9) Jalili, R.; Razal, J. M.; Innis, P. C.; Wallace, G. G. One-Step Wet-Spinning Process of Poly(3,4-ethylenedioxythiophene):Poly(styrenesulfonate) Fibers and the Origin of Higher Electrical Conductivity. *Adv. Funct. Mat.* **2011**, *21*, 3363–3370.

(10) Fanous, J.; Schweizer, M.; Schawaller, D.; Buchmeiser, M. R. Crystalline and Conductive Poly(3-hexylthiophene) Fibers. *Macromol. Mater. Eng.* **2012**, *297*, 123–127.

(11) Foroughi, J.; Spinks, G. M.; Wallace, G. G. A Reactive Wet Spinning Approach to Polypyrrole Fibres. *J. Mater. Chem.* **2011**, *21*, 6421–6426.

(12) Plesse, C.; Vidal, F.; Teyssie, D.; Chevrot, C. Conducting Polymer Artificial Muscle Fibres: toward an Open Air Linear Actuation. *Chem. Commun.* 2010, 46, 2910–2912.

(13) Jiang, H.; Adams, W.; Eby, R. *Materials Science and Technology*, 1st ed.; WILEY-VCH, 2006; pp 597–652.

(14) Xu, X. Z.; Uddin, A. J.; Aoki, K.; Gotoh, Y.; Saito, T.; Yumura, M. Fabrication of High Strength PVA/SWCNT Composite Fibers by Gel Spinning. *Carbon* 2010, 48, 1977–1984.

(15) Pomfret, S. J.; Adams, P. N.; Comfort, N. P.; Monkman, A. P. Electrical and Mechanical Properties of Polyaniline Fibres Produced by a One-step Wet Spinning Process. *Polymer* 2000, 41, 2265–2269.

(16) Miura, H.; Fukuyama, Y.; Sunda, T.; Lin, B.; Zhou, J.; Takizawa, J.; Ohmori, A.; Kimura, M. Foldable Textile Electronic Devices Using All-organic Conductive Fibers. *Adv. Eng. Mater.* 2014, 16, 550–555.

(17) Zhou, J.; Lubineau, G. Improving the Electrical Conductivity in Polycarbonate Nanocomposites Using Highly Conductive PEDOT/PSS Coated MWCNTs. ACS. *Appl. Mater. Interfaces.* 2013, 5, 6189–6200.

(18) Xia, Y.; Sun, K.; Ouyang, J. Solution-Processed Metallic Conducting Polymer Films as Transparent Electrode of Optoelectronic Devices. *Adv. Mater.* 2012, 24, 2436–2440.

(19) Ouyang, J.; Xu, Q.; Chu, C.; Yang, Y.; Li, G.; Shinar, J. On the Mechanism of Conductivity Enhancement in Poly (3,4-ethylenedioxythiophene): poly(styrene sulfonate) Film through Solvent Treatment. *Polymer* 2004, 45, 8443–8450.

(20) Fan, B. H.; Mei, X. G.; Ouyang, J. Y. Significant Conductivity Enhancement of Conductive Poly(3,4-ethylenedioxythiophene): Poly(styrenesulfonate) Films by Adding Anionic Surfactants into Polymer Solution. *Macromolecules* 2008, 41, 5971–5973.

(21) Xia, Y.; Ouyang, J. Significant Different Conductivities of the Two Grades of Poly(3,4-ethylenedioxythiophene):Poly(styrenesulfonate), Clevios P and Clevios PH1000, Arising from Different Molecular Weights. *ACS. Appl. Mater. Interfaces.* **2012**, *4*, 4131–4140.

(22) Jalili, R.; Razal, J. M.; Wallace, G. G. Exploiting High Quality PEDOT:PSS-SWNT Compos- ite Formulations for Wet-spinning Multifunctional Fibers. *J. Mater. Chem.* **2012**, *22*, 25174–25182.

(23) Jalili, R.; Razal, J. M.; Wallace, G. G. Wet-spinning of PEDOT: PSS/Functionalized-SWNTs Composite: a Facile Route Toward Production of Strong and Highly Conducting Multifunctional Fibers. *Sci. Rep.* **2013**, *3*, 1–7.

(24) Kim, Y. H.; Sachse, C.; Machala, M. L.; May, C.; Muller-Meskamp, L.; Leo, K. Highly Conductive PEDOT:PSS Electrode with Optimized Solvent and Thermal Post-Treatment for ITO-Free Organic Solar Cells. *Adv. Funct. Mater.* **2011**, *21*, 1076–1081.

(25) Kim, N.; Kee, S.; Lee, S.; Lee, B.; Kahng, Y.; ; Jo, Y.; Kim, B.; Lee, K. Highly Conductive PEDOT:PSS Nanofibrils Induced by Solution-Processed Crystallization. *Adv. Mater.* **2014**, *26*, 2268–2272.

(26) Heeger, A.; Sariciftci, N.; Namdas, E. *Semiconducting and Metallic Polymers*, 1st ed.; Oxford University Press: Oxford, New York, 2010; pp 1–278.

(27) Wessling, B. In *Handbook of Conducting Polymers*, 3rd ed.; Skotheim, T., Reynolds, J., Eds.; CRC press: Boca Raton, London and New York, 2007; Vol. 2; pp 1049–1122.

(28) Epstein, A. In *Handbook of conducting polymers*, 3rd ed.; Skotheim, T., Reynolds, J., Eds.; CRC press: Boca Raton, London and New York, 2007; Vol. 1; pp 595–667.

(29) Lee, K.; Cho, S.; Park, S. H.; Heeger, A. J.; Lee, C. W.; Lee, S. H. Metallic Transport in Polyaniline. *Nature* **2006**, *441*, 65–68.

(30) Dhoot, A. S.; Yuen, J. D.; Heeney, M.; McCulloch, I.; Moses, D.; Heeger, A. J. Beyond the Metal-insulator Transition in Polymer Electrolyte Gated Polymer Field-effect Transistors. *Proc. Natl. Acad. Sci.* 2006, 103, 11834–11837.

(31) Lekawa-Raus, A.; Patmore, J.; Kurzepa, L.; Bulmer, J.; Koziol, K. Electrical Properties of Carbon Nanotube Based Fibers and Their Future Use in Electrical Wiring. *Adv. Funct. Mater.* 2014, 24, 3661–3682.

(32) Schaarschmidt, A.; Farah, A.; Aby, A.; AS, H. Influence of Nonadiabatic Annealing on the Morphology and Molecular Structure of PEDOT-PSS Films. *J. Phys. Chem. B.* 2009, 113, 9352–9355.

(33) Kim, G.; Shao, L.; Zhang, K.; Pipe, K. Engineered Doping of Organic Semiconductors for Enhanced Thermoelectric Efficiency. *Nat. Mater.* 2013, 12, 719–723.

(34) Vardeny, Z.; Korovyanko, O. In *Handbook of Conducting Polymers*, 3rd ed.; Skotheim, T., Reynolds, J., Eds.; CRC press: Boca Raton, London and New York, 2007; Vol. 1; pp 907–940.

(35) Takano, T.; Masunaga, H.; Fujiwara, A.; Okuzaki, H.; Sasaki, T. PEDOT Nanocrystal in Highly Conductive PEDOT:PSS Polymer Films. *Macromolecules* 2012, 45, 3859–3865.

(36) Williams, D.; Carter, C. *Transmission Electron Microscopy: A Textbook for Materials Science*, 2nd ed.; Springer: Boca Raton, London and New York, 2009; pp 79–100.

(37) Lang, U.; Müller, E.; Naujoks, N.; Dual, J. Microscopical Investigations of PEDOT:PSS Thin Films. *Adv. Funct. Mater.* 2009, 19, 1215–1220.

(38) Cho, B.; Park, K.; Baek, J.; Oh, H.; YK, L.; Sung, M. Single-Crystal Poly(3,4-ethylenedioxythiophene) Nanowires with Ultrahigh Conductivity. *Nano Lett* 2014, 14, 3321–3327.

(39) Kim, N.; Lee, B. H.; Choi, D.; Kim, G.; Kim, H.; Kim, J. R.; Lee, J.; Kahng, Y. H.; Lee, K. Role of Interchain Coupling in the Metallic State of Conducting Polymers. *Phys. Rev. Lett.* 2012, 109.

(40) Ladevèze, P.; Pelle, J. *Mastering Calculations in Linear and Nonlinear Mechanics*; Springer New York 1986.

(41) Okuzaki, H.; Suzuki, H.; Ito, T. Electromechanical Properties of Poly(3,4-ethylenedioxythiophene)/Poly(4-styrene sulfonate) Films. *J. Phys. Chem. B.* 2009, 113, 11378–11383.

(42) Zhou, J.; Fukawa, T.; Shirai, H.; Kimura, M. Anisotropic Motion of Electroactive Papers Coated with PEDOT/PSS. *Macromolecular. Mater. Eng.* 2010, 295, 671–675.

(43) Kachanov, L. *Introduction to Continuum Damage Mechanics*, 2nd ed.; Springer Science and Business Media, 1986.

(44) Lang, U.; Naujoks, N.; Dual, J. Mechanical Characterization of PEDOT:PSS Thin Films. *Synth. Met.* 2009, 159, 473–479.

(45) Roesler, J.; Harders, H.; Baeker, M. *Mechanical Behaviour of Engineering Materials*, 1st ed.; Springer: Berlin, Heidelberg and New York, 2007; pp 281–284.

(46) Oh, J.; Shin, M.; Lee, J.; Ahn, J.; Baik, H.; Jeong, U. Effect of PEDOT Nanofibril Networks on the Conductivity, Flexibility, and Coatability of PEDOT:PSS Films. *ACS. Appl Mater. Interfaces.* 2014, 6, 6954–6961.

(47) Zhou, J.; Ventura, I.; Lubineau, G. Probing the Role of PEDOT/PSS-coated MWCNTs in the Thermal and Mechanical Properties of Polycarbonate Nanocomposites. *Ind. Eng. Chem. Res.* 2014, 53, 3539–3549.

(48) Hammersley, A. P. *ESRF Internal Report*, ESRF98HA01T, FIT2D V9.129 Reference Manual V3.1; 1998.

SUPPLEMENTAL WORKING EXAMPLE INFORMATION (PART I):

A. Optimization of wet-spinning parameters

Research has showed that fiber spinnability can be greatly affected by various physical parameters, such as composition of the coagulation bath, the ink concentration and viscosity, the spinning speed and nozzle diameter. (See

Reference S-1 and Reference S-2). Among these parameters, viscosity and spinning speed can play important roles in obtaining continuous fibers.

Spinning Dope Formulation:

Pristine PH1000 dispersion (11 mg/mL) can form fibers over a wide range of spin speeds from 0.3 to 150 μL/min. However, fibers can easily break in the coagulation bath or in the air due to the low viscosity of the dispersion. Higher concentrations of PH1000 dispersion (22 mg/mL) greatly improve the stability of the wet-spinning process due to the easier entanglement of the polymer chains. To improve the conductivity of the fibers, EG was mixed with the PH1000 dispersion (22 mg/mL) (this process was called EG doping). We found that 3 wt% of EG was the optimized concentration for doping concentrated PH1000 dispersion (22 mg/ml), and the final conductivity was as high as 607.0 ±60.2 $S \cdot cm^{-1}$.

Fiber hot-drawing:

After the "wet" fiber was taken from the coagulation bath, it was immediately heated and subjected to a vertical drawing process, as shown in Figure 1b. The temperature around the fiber was controlled by two hot plates and monitored by a thermal couple. The draw ratio was calculated from the fiber collection speed and the wet-spinning speed. Fibers collected without hot drawing and with a draw ratio of 3.0 were first investigated. The distance between the collector and the surface of the coagulation bath was fixed at 50 cm to ensure that the fibers were dried before collecting on the rotating spool. Insufficient drying resulted in non-circular fibers on the collector, as shown in Figure 8. The effect of hot-drawing on fiber conductivity is shown in Figure 9.

Coagulation bath:

By fixing the dispersion concentration at 22 mg/ml, and keeping the same collection speed, two kinds of coagulation baths were tried. Conductivity of the fibers was 231 ± 12 $S \cdot cm^{-1}$ from the acetone bath, while the conductivity increased to 368±34 $S \cdot cm^{-1}$ by using an acetone/IPA (volume ratio 1:1) bath. Research has shown that the conductivity of PEDOT/PSS films can be enhanced from 0.30 to 468 $S \cdot cm^{-1}$ by IPA dip-treatment for 10 min. (See Reference S-4). As the continuous wet-spinning process ends up with a dip time of 10 s for the fibers in the bath, the conductivity enhancement should be minimal. However, introducing IPA could greatly reduce the number of pores inside the fibers, which would result in better mechanical properties. (See Reference S-5, Reference S-6). Thus, in this study, a mixture of acetone/IPA (volume ratio 1:1) was used as the cogulation bath to maximized the fiber quality.

Spinnability:

Spinnability of the inks was monitored in an acetone/IPA (volume ratio 1:1) tank by a high speed camera. Commercial Clevios PH1000 ink after homogenization and sonication was first spun through a 50 μm glass nozzle. The concentration of prepared PH1000 ink (11 mg/mL) was relatively smaller compared with earlier studies, e.g., Clevios P (13 mg/mL), PH500 (11 mg/mL) and even Orgacon dry inks (15-30 mg/mL). See Reference S-5, Reference S-7, Reference S-8. It is noted that PH1000 ink in the current study had a wide range of spin speeds from 0.3 to 150 μL/min.

B. Morphology of conductive polymer fibers (SEM, AFM)

Table A: Summary of the electrical conductivity of EG doped and/or de-doped PEDOT/PSS fibers prepared from concentrated Clevios PH1000 (22 mg ml^{-1}).

Doped and/or de-doped PEDOT/PSS fiber type	Diameter (μm)	Conductivity (S cm^{-1})
EG/(PEDOT/PSS) fiber	9.7±1.4	607±60
(PEDOT/PSS)/EG fiber	8.6±0.8	1304±56
EG/(PEDOT/PSS)/EG fiber	8.4±0.7	2804±311

C. Microstructure characterization (XRD and Raman) of PE-DOT/PSS fibers

To understand the electrical transport in the fibers, microstructure characterization of the fibers was carried out by normal XRD and Raman spectroscopy. Figures 13a and 13b present the XRD patterns of PEDOT/PSS fibers with or without EG doping and/or de-doping. For the as-spun PEDOT/PSS fiber, the XRD patterns show four characteristic peaks at 2θ values of 4.7°, 14.0°, 17.5° and 26.3° that correspond to lattice spacings (d) of 18.7, 6.3, 5.1 and 3.4 Å, respectively as calculated using Brag's Law. See Reference S-9. Three peaks of interest at 2θ = 4.7, 14.0 and 26.3 ◦ correspond to the lamella stacking distance, $d_{(100)}$, of alternate orderings of PEDOT and PSS in the plane, its second-order reflection with the stack distance, $d_{(200)}$, and the interchain planar π –π stacking distance $d_{(010)}$ of PEDOT, respectively. See Reference S-10, Reference S-11 In fact, the as-spun fiber has the same π –π stacking distance as the EG de-doped PEDOT/PSS films ($d_{(010)}$= 3.4 Å),and the EG de-doped Clevios P and Clevios PH500 fibers ($d_{(010)}$= 3.4 Å),8 which indicates that wets-pinning of the fibers incorporating hot-drawing prompts alignment of the molecular chains, thus reducing the π –π stacking distance of the PEDOT chains from 3.5 to 3.4 Å. After de-doping these as-spun fibers with

EG, one of the high-angle peaks at $2\theta = 17.7°$ indicating amorphous halo of PSS chains almost disappeared, while the intensity of second-order lamella stacking at $2\theta = 14°$ increased noticeably. This change can be attributed to the partial removal of amorphous PSS in these fibers by EG de-doping. Another peak representing the interchain planar $\pi - \pi$ stacking distance, $d_{(010)}$, of PEDOT, became broader and centered at $2\theta = 27°$ (corresponding to the lattice spacing $d_{(010)} = 3.3$ Å). It is necessary to note the lack of a distinct shift in the characteristic peak of lamella stacking at $2\theta = 4.7°$ after de-doping of as-spun fibers (Figure 13a), indicating no obvious planarization of alternating PEDOT and PSS polymer chains. By incorporating both doping and de-doping of EG, the $d_{(100)}$ peak shifted from 4.7 to 4.1°. The $d_{(010)}$ peak shifted from 26.3 to 28.0°, corresponding to a further reduction of $\pi - \pi$ stacking distance from 3.4 to 3.2 Å. It is important to note that the intensity of the $d_{(010)}$ peak obviously increased after EG de-doping, suggesting that the crystallinity had increased in the fibers. The corresponding lattice distance and percentage of crystalinity for all samples are listed in Table A. Figure 13a, b and Table A indicate that the most effective way to increase the order of the molecular chains and percentage of crystalinity of the fibers involves partially stretching the molecular chains by hot-drawing, planarization of the thiophene rings on PEDOT by EG doping and reduction of the $\pi - \pi$ stacking distance of PEDOT chains by EG de-doping.

Figures 13c, d show the Raman spectra of PEDOT/PSS fibers. The strong peak at 1421 cm^{-1} is assigned to the $C_\alpha = C_\beta$ symmetric stretching of the thiophene ring in PEDOT chains in as-spun PEDOT/PSS fibers. See Reference S-5, See Reference S-12. Note that the position of the peak is 16 cm^{-1} lower than pristine PEDOT/PSS films (Figure 14b) and 5 cm^{-1} lower than other PEDOT/PSS fibers. This suggests that the quinoid structure of the thiophene rings dominate in our conductive PEDOT/PSS fibers (368 $S \cdot cm^{-1}$) over benzoid structures. This peak did not show an obvious shift after doping with 3 wt% EG. However, after de-doping the as-spun PEDOT/PSS fiber and the

EG/(PEDOT/PSS) fiber, the peak shifted from 1421 to 1415 and 1411 cm^{-1}, respectively. The peak shift to 1411 cm^{-1} indicated the most preferred quinoid structure and resulted in the record conductivity of 2804±311 S cm^{-1}. Figure 13e shows a schematic microstructure of the change of the fibers before and after de-doping as manifested by XRD and Raman results. Though it is beyond the scope of this study to quantify the ratio between the quinoid and benzoid structures in the fibers, we could still remark that a more favorable quinoid structure in the fiber leads to planarization of the conductive PEDOT chains, resulting in the reduction of $\pi-\pi$ stacking distance. As a result, the electrical transport in the most conductive fibers becomes three-dimensional, because the electrons diffuse to a neighboring chain prior to traveling between defects on a single chain. See Reference S-13. This reduces electron pathways on the chains and results in high conductivity of the fibers.

Table B: 2θ and d-spacing values of different PEDOT/PSS fibers and films extracted from Figure 13a,b and Figure 14.

Sample	$2\theta(°)/d_{(100)}$(Å)	$2\theta(°)/d_{(200)}$(Å)	$2\theta(°)/d_{(010)}$(Å)	Crystallinity(%)
As-spun PEDOT/PSS fibers	4.71/18.70	14.00/6.30	26.33/3.38	27.8
EG/(PEDOT/PSS) fibers	4.73/18.60	14.22/6.21	26.32/3.38	27.4
(PEDOT/PSS)/EG fibers	4.47/19.75	13.7/6.45	27.00/3.30	38.2
EG/(PEDOT/PSS)/EG fibers	4.20/22.3	13.60/6.50	27.02/3.30	39.8
PEDOT/PSS film	4.22/20.88	13.73/6.45	25.74/3.46	11.0
(PEDOT/PSS)/EG film	3.64/24.25	13.73/6.44	26.36/3.38	19.0

D. Mechanical Property Evaluation

See Figures 15 and 16.

References S-1 to S-13 for Supplemental Working Example Information (PART I):

(S-1) Hwang, K. S.; Lin, C. A.; Lin, C. H. *Journal of Applied Polymer Science* 1994, 52, 1181–1189.

(S-2) Fujiwara, H.; Shibayama, M.; Chen, J. H.; Nomura, S. *Journal of Applied Polymer Science* 1989, 37.

(S-3) Xia, Y.; Ouyang, J. *ACS Appl Mater Interfaces* 2012, 4, 4131–4140.

(S-4) Alemu, D.; Wei, H.; Ho, K.; Chu, C. *Energ Environ Sci* 2012, 5, 9662–9671.

(S-5) Jalili, R.; Razal, J. M.; Innis, P. C.; Wallace, G. G. *Advanced Functional Materials* 2011, 21, 3363-3370.

(S-6) Jalili, R.; Razal, J. M.; Wallace, G. G. *Journal of Materials Chemistry* 2012, 22, 25174–25182.

(S-7) Okuzaki, H.; Ishihara, M. *Macromolecular Rapid Communications* 2003, 24, 261–264.

(S-8) Okuzaki, H.; Harashina, Y.; Yan, H. *European Polymer Journal* 2009, 45, 256–261.

(S-9) Guinebretiere, R. *X-ray Diffraction by Polycrystalline Materials*, 1st ed.; ISTE: London andNewport Beach, 2007; pp 24–26.

(S-10) Kim, N.; Lee, B. H.; Choi, D.; Kim, G.; Kim, H.; Kim, J. R.; Lee, J.; Kahng, Y. H.; Lee, K. *Physical Review Letters* 2012, 109.

(S-11) Kim, N.; Kee, S.; Lee, S.; Lee, B.; Kahng, Y.; ; Jo, Y.; Kim, B.; Lee, K. *Adv Mater* 2014, 26, 2268-2272.

(S-12) Zhou, J.; Lubineau, G. *ACS Appl Mater Interfaces* 2013, 5, 6189–6200.

(S-13) Heeger, A.; Sariciftci, N.; Namdas, E. *Semiconducting and Metallic Polymers*, 1st ed.; Oxford University Press: Oxford, New York, 2010; pp 1–278.

ADDITIONAL EMBODIMENTS (PART II):

High-ampacity conductive polymer microfibers as fast response wearable heaters and electromechanical actuators

Additional embodiments are provided hereinbelow for Part II including further working examples which supplement Part I. Conductive fibers with

enhanced physical properties and functionalities are needed for a diversity of electronic devices. Here, we report very high performance in the thermal and mechanical response of poly(3,4-ethylenedioxythiophene)/poly(styrenesulfonate) (PEDOT/PSS) microfibers when subjected to an electrical current. These fibers were made by combining hot-drawing assisted wetspinning process with ethylene glycol doping/de-doping can work at a high current density as high as 1.8×10^4 A cm^{-2}, which is comparable to that of carbon nanotube fibers. Their electrothermal response was investigated using optical sensors and verified to be as fast as 63 °C s^{-1} and is comparable with that of metallic heating elements (20-50 °C s^{-1}). We investigated the electromechanical actuation resulted from the reversible sorption/desorption of moisture controlled by electro-induced heating. Results revealed an improvement of several orders of magnitudes compared to other linear conductive polymer-based actuators in air. Specifically, the fibers we designed here have a rapid stress generation rate (> 40 MPa s^{-1}) and a wide operating frequency range (up to 40 Hz). These fibers have several characteristics including fast response, low-driven voltage, good repeatability, long cycle life and high energy efficiency, favoring their use as heating elements on wearable textiles and as artificial muscles for robotics.

Introduction

For Part II, additional introduction is provided. Electroactive materials that convert electrical energy to thermal or mechanical energy have great potentials for many applications, including heating components for wearable textiles and artificial muscles for robots (for Part II, a new listing of references is provided, A1-A64).(A1–4) Among these electroactive materials, conductive polymers are very promising for these types of applications because they can be easily shaped into low-voltage driven actuators and sensors.(A5–7) One of the

most widely used conductive polymers, poly(3,4-ethylenedioxythiophene)/poly(styrenesulfonate) (PEDOT/PSS), is ideal for such applications because it is lightweight, and has good processibility, tunable electrical conductivity, suitable mechanical properties and good thermal stability.(A8–12)

Previous works have attempted to design electroactive materials based on PEDOT/PSS. The conversion of electrical energy into thermal energy has been realized using PEDOT/PSS microfilms or silver nanowire/PEDOT/PSS transparent nanofilms as heaters, although the heaters had slow response times (15-80 s).(A13-14) Meanwhile, the conversion of electrical energy into mechanical energy has been widely investigated in PEDOT/PSS film or papers. The well-known actuation mechanism is strongly related to the highly hygroscopic nature of PEDOT/PSS. When PEDOT/PSS is subjected to an electrical current, Joule heating induces the desorption of water, which subsequently results in a volume contraction. Actuation in PEDOT/PSS-based devices thus results from an electro-thermal-mechanical coupling, a multiphysics nature that facilitates various actuation stimuli.(A13, A15–19) For example, a (PEDOT/PSS)/elastomer bilayer actuator was developed to achieve a bending motion under multiple control stimuli, such as electrical current, heat and humidity changes.(A20) To date, most research on PEDOT/PSS-based electroactive materials has focused on two-dimensional films or coated papers.(A13, A16, A17, A19) Therefore, opportunities to design PEDOT/PSS fibers or wires for specific applications, such as functional textiles, or to increase their sensitivity in general remain outstanding.

In a previous study, we investigated the electromechanical actuation properties of low conductivity (PEDOT/PSS)/polyvinyl alcohol fibers, which can generate a maximum actuation stress of 11 MPa at 8 V.(A21) However, they feature a low response time (80 s), which leads to a slow stress generation rate (0.14 MPa s^{-1}) and a narrow operating frequency window (< 1 Hz). Other

conductive polymer fiber-based actuators have also been developed, where their actuations are controlled by oxidation-reduction reactions in liquid. These materials can produce large actuation strain but have limited cyclability and the technique requires complicated counter electrode, electrolyte and device packaging.(A6, A22)

A direct consequence of low efficiency in converting electrical energy to thermal or mechanical energy is an increase in power consumption. Although it has been shown that short-time application of high voltages does not harm the polymer, long term operation results in electrical failure of the materials. (A23) Small size microactuators should also feature enhanced response rate and be powered with coin batteries.(A5) In addition, increasing the conductivity of the material can improve response rate and permit the use at low voltage power sources. In our previous study, we fabricated highly conductive polymer microfibers by combining hot-drawing assisted wet-spinning process with chemical treatment (ethylene glycol doping/de-doping).(A24) Results showed that the performance of these fibers was superior to that of other conductive polymer fibers, with conductivity ranging from 368 to 2804 S cm^{-1} and Young's modulus values as high as 8.3 GPa.(A25, A26) These improvements favored these fibers for use as actuators. For instance, their high conductivity allows them to withstand high current density for long periods of time before electrical failure, and their high Young's modulus imparts good structural stability to the systems based on these fibers.

Here, we demonstrate fast electrothermal and electromechanical responses of a new generation of PEDOT/PSS fibers made by combining hot-drawing-assisted wet-spinning process and chemical treatment. By increasing the conductivity of the fibers, current density can be considerably increased a maximum current density of 1.8×10^4 A cm^{-2}, which is two orders of magnitude of copper wires and comparable to carbon nanotube fibers, indicating their high potential for used as interconnects in a electrical circuit. Within the operating

range before electrical failure, the electrothermal response was investigated systematically using fiber Bragg gratings (FBGs). The single conductive polymer fiber shows rapid electrothermal responsiveness and high reversibility at low voltages. Based on these features, the fiber bundle was demonstrated as wearable heaters on a glove. The fibers also showed remarkable electromechanical behavior induced by Joule heating and featured in fast response, long cycle life and excellent repeatability. Additionally, we show that bundles of novel fibers could be used as actuators, which can lift a load much heavier than itself. The availability of these fibers with high conductivity, high ampacity, and rapid electrothermal and electromechanical responsiveness could facilitate the development of, for example, electronic interconnects, wearable heating textiles and artificial muscles.

Experimental (Part II)

Materials

The PEDOT/PSS aqueous dispersion (CleviosTM PH1000) was purchased from HC Starck, Inc. Ethylene glycol (EG), isotropyl alcohol (IPA) and acetone were purchased from Sigma-Aldrich.

Preparation of PEDOT/PSS fibers

Fiber preparation strategies are systematically illustrated in Fig. 24. The as-spun fiber was wet-spun from a 22 mg mL^{-1} dispersion (using Clevios PH1000) followed by a vertical hot-drawing process (Fig. 24a). Both doping and dedoping methods were used to enhance the conductivity of the fibers (Fig. 24b). Doped dispersion was prepared by adding 3 wt% EG in a PEDOT/PSS dispersion (22 mg ml^{-1}). The spinning formulation (with or without EG doping) was loaded into a 5 mL syringe and spun into a coagulation bath though a needle with an inner diameter of 220 mm. The flow rate of the dispersion was

controlled at 10 mL min^{-1} by using a syringe pump. Wet fibers were pulled out from 1:1 volume ratio of acetone to IPA coagulation bath, where the volume ratio of acetone and IPA is 1 to 1. The fibers were collected vertically onto a 50 mm winding spool, which gives a line speed of 2 to 4 m min^{-1}. The temperature along the path of the fiber was set to 90°C by two vertically hot-plates and was monitored by a thermocouple.(A24) After wet-spinning, dedoping of as-spun and EG-doped fibers was performed by immersing them in a pure EG bath for 1 h and the fibers were then dried in air at 160°C for 1 h. In this study, the as-spun PEDOT/PSS fibers, EG/(PEDOT/PSS) fibers, (PEDOT/PSS)/EG fibers and EG/(PEDOT/PSS)/EG fibers represent the pristine PEDOT/PSS fibers, 3 wt% EG doped PEDOT/PSS fibers, EG de-doped PEDOT/PSS fibers and EG de-doped 3 wt% EG doped PEDOT/PSS fibers, respectively.

General characterizations

Thermogravimetric analysis (TGA) was performed to measure the water absorbed in the fibers using a TG 209 F1 instrument (NETZSCH Company) under a nitrogen purge. Samples were heated from 25 to 800 °C at a heating rate of 10 °C min^{-1}.

Characterization of properties and demonstration for applications as heating elements

To assess the potential of these fibers for applications as heating elements, their electrothermal response needed to be accurately calculated. We followed a previous report based on fiber Bragg gratings (FBG) to make temperature measurements for single PEDOT/PSS fibers subjected to electrical stimulus; FBGs have been proven to be suitably efficient both experimentally and numerically.(A27) Measurements were performed inside a chamber to avoid environmental disturbances, and the experimental set-up is sketched in Fig. 25. Conductive polymer fibers were prepared and fixed on a paper card.

The relationships between temperature and voltage and between temperature and frequency at a certain voltage were investigated by applying electrical fields to the fiber using a 382280 DC power supply (EXETECH instruments) and an 81150A pulse function generator (Agilent Technology). Each end of the fibers were connected with copper wires, painted with silver epoxy and sealed with an epoxy glue. The effective length of the fibers between the silver paste was 2.0 ± 0.1 cm. Next, the fibers were positioned along the optical fiber containing a 5-mm long FBG and fixed with tape. The temperature of the optical fiber was monitored by an FBG (FBG1.a) connected to the first channel (CH1). An FBG reflects a part of the incident light signal that is represented by a spectrum of reflected wavelength, which peaks in correspondence with the Bragg wavelength, λ_B.(A28) When the FBG is only subjected to temperature changes, ΔT, the peak shifts proportionally. The Bragg wavelength variation, $\Delta\lambda_B/\lambda_B$, can be expressed as(A29):

$$\Delta\lambda_B / \lambda_B = K_T \Delta T \qquad (1)$$

where, K_T , is the thermo-optic coefficient related to the temperature sensitivity of the FBG. This sensitivity was calibrated by immersing it with a thermocouple in a beaker filled with water, and the sensitivity of the FBG was determined to be 9.9 pm $°C^{-1}$.(A27) We used 5-mm long FBGs written on SMF28e standard fibers, and the coating was removed. The Bragg wavelength of the sensor was 1530 nm at room temperature. The radiation/convection heat transfer was also estimated by measuring the temperature at about 700 mm away from the PEDOT/PSS fibers by using another FBG (FBG2.a), which was connected to the second channel (CH2) (Fig. 27b). Note that evaluating long distance (non-contact) heat transfer is of interest for some heating applications in which the heater is not directly in contact with the system to be heated. Due to the limitation of the instrument (the data acquisition rate is 2 Hz), frequencies in

temperature change higher than 2 Hz were not measured in this study. Current flow in the fibers was monitored using a U1252B digital multimeter that captured every 1 s throughout the test. All tests were conducted three times in air. The FBG signal and current changes were collected through USB communication with the computer. Knitted fabric was used to create a heatable glove, where a PEDOT/PSS fiber bundle was interlaced onto a nonconductive polyester glove. The voltage was supplied by using a 382280 DC power supply (EXETECH instruments) or a 9-V battery. Thermal images of the glove were taken by an SC7000 thermographic camera (FLIR Systems, Inc).

Characterization of properties and demonstration for application as actuators

To test the suitability of the fibers as actuators, the following tests were conducted. Demonstration of a PEDOT/PSS fiber bundle actuator was performed under an isotonic measurement, where a load was attached to the movable end of the bundle to eliminate bulking. Displacement at the movable end was measured with a video camera, and thermal images of the fiber bundle during the actuation test were taken with an SC7000 thermographic camera. Single-fiber actuation test was performed under isometric conditions (the length of the fiber remained to be constant during the duration of the test). All tests were performed by applying a preload of 0.5 mN, which kept the fibers straight. Two types of tests are performed by applying either a constant voltage or a harmonic voltage variation with prescribed frequency. In both cases, the force generated by the fiber was monitored, where sampling rate depend on frequency. The data acquisition rate was every 100 ms at 0.02, 0.1, 0.25 and 0.5 Hz; every 20 ms for 1, 2 and 5 Hz; every 2 ms for 10, 20 and 40 Hz. All tests were performed at room temperature (21 °C) with a relative humidity of 60%. The actuation stress values were determined by normalizing the measured load to the fiber cross-sectional area measured before the test. Dynamic mechanical

analysis (DMA) was performed on arrays made from 15 fibers of approximately 6 mm in length on a Q800 instrument (TA Instruments) in tension mode. DMA measurements were performed between 25 and 120 °C, at 1 Hz and at a heating rate of 3 °C min^{-1} in air.

RESULTS AND DISCUSSION

High current density of PEDOT/PSS fibers

Before any deeper investigation into the electrothermal and electromechanical behavior, we need to determine the maximum current density (denoted as j_b) that each formulation could sustain before reaching electrically induced failure. By gradually increasing the applied voltage on the fibers, heat induced by Joule heating finally result in the fiber breakage. The current carrying capacity is defined here as a maximum current density at which two ends of the fiber fixed on a paper card and show a constant resistance during the experiment. The method for measuring resistance is described earlier by a two-probe method. If the temperature increase in the fiber, caused by an increase in electrical resistance, does not stabilize then at a certain temperature, the fiber breaks.

Fig. 17a shows the SEM image of as-spun PEDOT/PSS fibers fabricated from a hot-drawing-assisted wet-spinning process. The length of the fibers could be several hundred meters with an average diameter of around 10 mm and remarkably smooth surfaces (Fig. 27a). Fig. 17b and Table 1 show that the j_b is relatively small for the as-spun PEDOT/PSS fibers (5.6 x 10^3A cm^{-2}). By EG doping, j_b increased to 7.1 x 10^3 A cm^{-2}. After a combination of the EG-doping and de-doping, j_b increased considerably (about 330%) up to 1.8 x 10^4 A cm^{-2}; this value is two orders of magnitude higher than that of copper wire (1.6 x10^2 A cm^{-2}) and even higher than that of carbon nanotube fibers and Ag-doped graphene fibers, as shown in Fig. 17b.(A30–33)

The SEM images in Fig. 17c and d show that a slight increase in the diameter at the tip and short nodules form in the failure surface of an as-spun PEDOT/PSS fiber. Similarly, the SEM images in Fig. 17e and f shows that the diameter is twice that of the original and fibrils have formed at the tip in the failure cross section of an EG/(PEDOT/PSS)/EG fiber. The failure mechanism was revealed by pure thermal heating by TG analysis in a N_2 atmosphere (Fig. 26). This technique shows that weight loss up to 120 °C can be ascribed to 12 and 8 wt% loss of water in as-spun PEDOT/PSS fibers and EG/(PEDOT/PSS)/EG fibers, respectively. Differences in water loss indicate that PSS phases are partially removed due to EG de-doping. The first decomposition of PEDOT/PSS fibers is from 265 °C to 320 °C. The weight loss of about 30 wt%, which is attributed to the decomposition of PSS as the sulfonate groups disassociate from styrene.(A34) Next, a weight loss of about 10 wt% occurs between 350 and 600 °C, which is caused by the rupture of the polymer backbone.(A11, A34). It is interesting to see that both as-spun PEDOT/PSS and EG/(PEDOT/PSS)/EG fibers remain fibrous structures after heating from 25 to 800 °C (Fig. 27c and 27d). Energy dispersive x-ray spectroscopy quantification showed that carbon to oxygen and carbon to sulfur atomic ratios increased considerably in the fiber due to degradation (Table S1), and nanofibrils were also observed on both the surface and cross section of EG/(PEDOT/PSS)/EG fibers after degradation; However, no nanofibrils are observed for as-spun PEDOT/PSS fibers after degradation (Fig. 27c). Electrically induced failure of structures are expected to cause these types of morphological changes, and differences in changes indicated that these two polymer fibers have different microstructures.

In fact, the weakest part of the fibers is the amorphous nonconductive PSS interface that connects PEDOT/PSS grains. The decomposition temperature of PSS phases is low enough to cause an electrical current that results in over-heating followed by failure of the material (Fig. 26). The

relatively small current density of as-spun fiber can be ascribed to the presence of large amounts of PSS between PEDOT/PSS grains, in which the amorphous nature of PSS is the source of electrical failure. On the other hand, amorphous regions (PSS) of EG/(PEDOT/PSS)/EG fibers are partially removed due to EG de-doping, resulting in interconnected PEDOT grains with extremely thin layers of PSS between them.(A24, A35) Hence, these thin layers will become fibrils from the over-heating of PSS phases induced by the electrical current. The combination of high current density and high conductivity of PEDOT/PSS fibers makes them promising candidates in the mini circuits, which need small electrical interconnects.

Electrothermal response

Chemical treatment through EG doping/de-doping not only improves the maximum current density, but also increase the conductivity of PEDOT/PSS fibers (Fig. 24). The resistance of 2-cm-long fibers in the electrothermal response study were 8.4, 5.2, 2, 1.1 kW, corresponding to the electrical conductivities of 315.8, 520.7, 1722.4 and 3131.6 S cm^{-1} for as-spun PEDOT/PSS, EG/(PEDOT/PSS), (PEDOT/PSS)/EG and EG/(PEDOT/PSS)/EG fibers, respectively. All properties of PEDOT/PSS fibers investigated in this study are listed in Table 1.

Fig. 18a shows the changes in the temperature-time curves of the fibers when a voltage of 7 V cm^{-1} was applied for 25 s. The first-order response time, Δt, of as-spun PEDOT/PSS fiber and EG/(PEDOT/PSS)/EG fiber were estimated to be 2 and 1.2 s, respectively. The maximum heating rate estimated from Fig. 18a for the EG/(PEDOT/PSS)/EG fiber was about 63 °C s^{-1}. We also tested the thermal response of these fibers by increasing the voltage by increments of 1 V cm^{-1} within the operating range, as indicated in Fig. 17b. Taking the as-spun PEDOT/PSS fiber and the EG/(PEDOT/PSS)/EG fiber as

examples, curves of temperature variation to current were plotted with respect to time in Fig. 18b-e. Results are given for both FBGs in contact with the polymer fiber (FBG1.a) and for the one located at 700 mm from the polymer fiber (FBG2.a), as show in Fig. 25b. Each target temperature plateau at different voltage was achieved within 2.5 s and the first order response time, Δt, was estimated to be 1 s. The reachable temperature measured by both FBG1.a and FBG2.a increased clearly when the resistance dropped from 8.4 to 1.1 kW. To reach a target temperate of 75 °C, only 7 V cm^{-1} was required for EG/(PEDOT/PSS)/EG fibers, less than half of the 18 V cm^{-1} that was needed for the as-spun PEDOT/PSS fiber. Note that distance affected the change in temperature, as detected by the FBG2.a, indicating that the PEDOT/PSS fiber under an electrical current can create a temperature field nearby via radiation and convection.(A27) The temperature of each conductive polymer fiber is proportional to the square of the voltage applied to the fiber, proving that the coupling between electrical and thermal behaviors was generated by the Joule effect, which produces the body heat source in the PEDOT/PSS fiber (Fig. 18f). The temperature of the fiber is determined by storage of the electrical power and release of the energy through heat transfer (radiation and convection) to air. The conduction mechanism was considered to be negligible due to the loose contact of PEDOT/PSS fibers to FBGs. The temperature of the fiber, the heat flux dissipated by the fiber and the relative fraction of the radiated and convective heat flux can be extracted by a non-phenomenological model that we developed previously.(A27) The stable and fast heating/cooling property of the fibers was confirmed by analyzing the dynamic thermal response of the EG/(PEDOT/PSS)/EG fiber using repetitive on-off cycles with a square-wave voltage (0-2.5 V cm^{-1}) at different frequencies (Fig. 18g). The amplitude of the temperature change stayed nearly constant at each frequency, indicating that the thermal response is stable and repeatable for long-term use; however, from one frequency to another, the temperature variation differs, showing that higher

frequency cause less temperature variation. This indicates that either maximum Joule heat was not generated or that its transmission to the temperature sensor was not completed before the start of the next cycle. In detail, when the curve at 0.1 Hz was enlarged, as shown in Fig. 18h, it clearly shows a reversible heating/cooling process. The first order response time during both heating and cooling was about 1 s. The fast cooling rate of the PEDOT/PSS fiber was associated with the small diameter of the fiber and fast water absorption to reduce the temperature of the fiber. The water absorption will start with the fixation of H_2O molecules on the highly hygroscopic SO_3H groups in PSS. Then the weakened hydrogen bonds in SO_3H will react with water via reversible reactions during the cooling/heating processes below. (A9, A55, A56) The superior dynamic thermal response of the fiber is extremely crucial for fast thermal response applications, which need reliable repeatability.

$$H_2O + PSS(HSO_3) \xrightarrow{\text{cooling}} H_3O^+PSS(SO_3)^{-\square} \quad (2)$$

$$H_3O^+PSS(SO_3)^{-\square} \xrightarrow{\text{heating}} H_2O + PSS(HSO_3) \quad (3)$$

Table 2 compares the performance of various electrically driven heaters prepared by different methods. The first-order response time of PEDOT/PSS fibers is comparable with tungsten wires or copper interconnects, which need several hundred mini-seconds to several seconds.(A36, A37) Moreover, these fibers have the fastest response rate (63 °C s^{-1}) compared with other types of heaters. Nanomaterial-based heaters, such as silver nanowires (AgNWs), carbon nanotubes (CNTs) and graphene, generally need a long response time for heating because substrates hinder the measured heating rate as compared to a free-standing arrangement. Some other PEDOT based heaters, such as PEDOT/PSS film and PEDOT nanofiber mat, have a response time several times longer than our PEDOT/PSS fibers due to their low conductivities.(A13, A54) To summarize, the merit of PEDOT/PSS fibers as heaters lies in (1) very

fast response which is comparable with metal wires; (2) low density, high conductivity, high flexibility, stretchability and better tolerance to frequent bending and contact as compared to carbon fibers and metallic wires(A57); and (3) good spinnability for directly co-spinning with nonconductive polyester fibers from different nozzles, which can be easily twisted and woven into textiles for the application of wearable heaters.

As we know that the temperature range required for wearable applications is much lower than the maximum temperature generated by the fiber (90 °C) and the initial thermal degradation temperature of the fiber (265 °C), the thermal stability of the PEDOT/PSS fiber is estimated to be appropriate for wearable heating textiles. Fig. 19 demonstrates the application of PEDOT/PSS fibers as heating elements on a glove. A textile-based electrode was fabricated by knitting a PEDOT/PSS fiber bundle (25 cm long) onto the surface of a polyester glove, as show in Fig. 19a and 19b. Fibers were adequately strong to avoid damage during knitting or from repeated exposure to tensile and bending strains on the hand. This is due to the excellent stretchability of PEDOT/PSS fibers (16 to 21%) compared with metallic wires or carbon nanotube fibers (1 to 8%).(A24, A31, A58) The representative thermal images that taken at 0, 0.4, 0.8 and 1.2 V cm^{-1} at steady state show a clear temperature increase from 28 to 52 °C for the as-spun PEDOT/PSS fiber bundle (Fig. 19c to f). The temperature distribution of the coiled fiber bundle at each applied voltage was predominately homogeneous. The bundle produces heat not only along the paths where the fiber bundle extend but also into the spaces between adjacent segments, especially at high voltages. A heat field generated by the fiber bundle at 1.2 V cm^{-1} becomes apparent, further proving that the non-contact heating mechanism (radiation and convection) is integral to the heat flux in the nearby environment. To approach the practical use of these fibers as heating elements, the as-spun PEDOT/PSS fiber bundle used in Fig. 19g was EG de-doped to enhance electrical conductivity.(A24) Now, the fiber bundle on the glove can be

powered by a 9-V battery (corresponding to an electrical field of 0.36 V cm^{-1}) and can reach a maximum temperature of 36 °C (Fig. 19g and h), which is a comfortable temperature range for hands (between 33 and 38 °C).(A44, A57) Smaller power sources, such as coin batteries, could also be used, but the location of the electrodes, the conductivity and the arrangement of the fiber bundle on the glove would need to be engineered.

Electromechanical response

We applied voltages to a similar fiber bundle as that used in the heatable gloves and found that it displayed linear electromechanical motion. The preliminary actuation performance of the fibers presented as a bundle actuator containing 118 fibers with 14 cm in length under isotonic conditions, as show in Fig. 20a and b. Applying voltage to the fiber bundle enables it to lift up a 0.45 g load, which is 150 times of the fiber bundle (3 mg). Using a video camera, we measured the displacement, ΔL, and found that it took about 6 s to reach a maximum displacement of 530 mm with a first order response of 2 s when applying a voltage of 1.14 V cm^{-1} (Fig. 20c). This value corresponds to an actuation strain of 0.4%, which is appropriate for use as heating elements on gloves because by switching the voltage on and off, would not be noticeable to the wearer; however, this would be a limitation especially for applications that need large actuation strokes. Here, we show that aligning polymer chains to increase electronic conductivity and Young's modulus leads to low power consumption, long cycle life and good repeatability but lower actuation strains in the direction of the alignment. Actuation strain can be increased by amplifiers such as level systems or by improving the relative humidity around the actuator.(A13, A59) In addition, we took the thermal images of the fiber bundle at different voltages, and as show in Fig. 20d, thensile actuation is correlated with and depends on the temperature of the fiber bundle. The evolution of displacement with voltage is plotted together with the temperature of the fiber

bundle (Fig. 20e); the displacement clearly increased with temperature until reaching saturation after 40 °C.

By measuring the tensile actuation of single fibers, we learned more about what affects their actuation performance (Fig. 21a). A 2-cm fiber weighing 2.2 mg was clamped and preloaded with a force of 0.5 mN to keep it tight and straight. Actuation stress was then measured as the voltage, V, was increased while the extension was held constant. Actuation stress evolved in three regimes as the applied voltage increased for both as-spun PEDOT/PSS and EG/(PEDOT/PSS)/EG fibers, as shown in Fig. 21b. In the first regime ($0 < V < V_p$), actuation stress increases with voltage such that the maximum actuation stress amplitudes, Δs, at peak voltage, V_p, were 14 MPa ($V_p = 6$ V cm^{-1}) and 22 MPa ($V_p = 2.5$ V cm^{-1}) for as-spun PEDOT/PSS and EG/(PEDOT/PSS)/EG fibers, respectively. These values are close to those generated by PEDOT/PSS films or papers(A13, A15) and are also comparable with the performance of polypyrrole-based actuators (27 MPa) driven by moisture gradients.(A60) Note that the peak temperature, T_p, of the fiber at the maximum $\Delta\sigma$ for both fibers was about 30 °C. In the second regime ($V_p < V < V_t$), the mechanical response of the fibers lies in a state of equilibrium. The $\Delta\sigma$ remains almost constant when the voltage is increased. We propose that at relatively higher voltage levels, the fibers may start to soften and expand. In the third regime ($V > V_t$), the temperature increases over 40 °C and 60 °C for as-spun PEDOT/PSS fiber and EG/(PEDOT/PSS)/EG fiber, respectively (Fig. 18f). The actuation stress drops when voltages are higher thanV_t (11 and 6 V cm^{-1} for as-spun PEDOT/PSS and EG/(PEDOT/PSS)/EG fibers, respectively). We ascribe V_t and T_t as the turning voltage and temperature for actuation, respectively. DMA analysis was performed to explain the evolution of $\Delta\sigma$ with temperature. We found that at first the storage modulus increased with temperature up to T_p, which was due to the desorption of water from the fibers, but then it decreased due to the softening and expansion of amorphous PSS

phases at higher temperatures (Fig. 21c). As a result, reduced actuation stress was caused by softening of the amorphous PSS phase in the fiber at higher temperatures ($T > T_t$), and the thermal expansion of the fibers is compensation for the contraction of the fibers induced by the electrical current. Our result agrees with the results of PEDOT/PSS film or paper actuation at higher temperatures, where the actuation stress reduces due to thermal expansion of PEDOT/PSS.(A13, A15)

Knowing that the actuation stress can be generated and maximized in the first regime ($0 < V < V_p$), we applied a cyclic current loading to the fiber to investigate the repeatability of the actuator in this regime. The actuation stress, voltage and current of the fibers at 0.02 Hz and a square wave voltage of 2.5 V cm^{-1} are shown in Fig. 22a-d. Using EG/(PEDOT/PSS)/EG fibers as an example, when the current passing through the fiber is 3.5 mA and the temperature is raised from 21 to 29 °C (Fig. 18f). Under the isometric condition, the fiber charges the actuation force as elastic energy and then releases this energy by contracting reversibly from maximum tension to near zero. Fig. 22e, the response time is estimated about 0.5 s. The fiber shows a repeatable generation of the actuation stress with fast rates of 40 MPa s^{-1}, a value that is comparable to the peak capacity of natural and other artificial muscles (30 MPa s^{-1});(A23, A61) and an actuation mechanism similar to that of PEDOT/PSS films or papers.(A13, A15) When an electrical field is applied to the sample, electrical energy is converted to thermal energy, causing temperature to increase on the fiber (Fig. 20d). Then the water vapor absorbed by the fiber desorped to a certain level due to Joule heating, the volume of the fiber changed (Fig. 22f). Superior and reversible electrothermal heating of the PEDOT/PSS fibers, caused a reversible electro-induced actuation simplifying the actuation mechanism: an electro-thermal-mechanical energy transfer in PEDOT/PSS fibers.

Square-wave voltages at different frequencies were applied to further investigate the high frequency performance of PEDOT/PSS fiber actuators. Inset curves in Fig. 23a show that the actuation amplitude remains almost constant below 1 Hz. As actuation frequency increased, we observed a reduced actuation stress amplitude after 1 Hz between the on and off states. We suggest that neither actuated or relaxed states achieved stability because duration of the step voltage was insufficient (Fig. 23a and b). Actuation was appreciable up to 40 Hz for EG/(PEDOT/PSS)/EG fibers, and the long-term reliability of actuator performance was evaluated by repetitive cycling of this fiber actuator up to 10,000 cycles at 1 Hz. No obvious decline in the actuation amplitude presented with more than 10,000 cycles (Fig. 23c and Fig. 28), which is likely because the fiber actuator worked in the elastic region and because of the superior Young's modulus over PEDOT/PSS films.(A13) The performance of conductive polymer-based linear actuators from the literature is summarized and compared with this study in Table 3. Though the PEDOT/PSS have been shown before in the film or fiber structure as actuators, the novelty of the current work lines in clearly understanding the electrothermal and electromechanical response of a pure single conductive polymer fiber. To summarise, our fiber actuators have several merits including the following: (1) they are capable of working directly in air at a low-driven voltage; (2) continuous fiber can be readily bundled for use as large force linear actuators. Assembly of these fibers in air is much easier than other conductive polymer film actuators; (3) they have a fast response rate (up to 40 MPa s^{-1}); (4) wide frequency operating window (0.02 to 40 Hz); and (5) excellent repeatability and long cycle life of the actuator due to their improved Young's modulus compared with films.

Finally, Figure 26 shows that the first stage of weight loss up to 200 °C is from the loss of water. The decomposition of PSS starts from 265 °C ends at 320 °C with a weight loss of 25 wt%. This is due to the decomposition of PSS as the sulfonate groups disassociate from styrene.(A63) This decomposition is

followed by another decomposition of PEDOT in the range between 350 and 600 °C with a weight loss of 10 wt%, which is due to the rupture of the polymer back bone.(A63, A64) It is worth noting that the residual is over 40 % around 800 °C.

In summary, in Part II, we systematically studied the current density, electrothermal and electromechanical responses of highly conductive PEDOT/PSS fibers. We construct these fibers by a combination of thermomechanical (hot-drawing-assisted wetspinning) and chemical treatment (EG doping/de-doping). We found that high-performance PEDOT/PSS fibers can carry high current density that is comparable with carbon nanotube fibers, making them promising candidates for use as interconnects in circuits. These fibers could also be used as heating elements in wearable textiles because they enable rapid heating at low operation voltages and show excellent heating repeatability. Moreover, the unique electromechanical response of PEDOT/PSS fibers surpasses other conductive polymer based actuators working in air. They feature with low-driven voltage, fast response time (< 0.5 s), a wide frequency window (up to 40 Hz), excellent repeatability (10,000 cycles) and controllability in air. We demonstrated that a PEDOT/PSS fiber bundle can be used as a glove heater powered by a 9-V battery. The fiber bundle can also be used as a linear actuator to lift a load that is 150 times of its own weight. Our results provide the basis bear the potential of these fibers to be implemented in wearable heating textiles and in microelectromechanical systems that need actuators.

References A1-A64

A1 T. Mirfakhrai, J. D. W. Madden and R. H. Baughman, *Mater. Today.*, 2007, 10, 30–38.

A2 M. A. C. Stuart, W. T. S. Huck, J. Genzer, M. Muller, C. Ober, M. Stamm, G. B. Sukhorukov, I. Szleifer, V. V. Tsukruk, M. Urban, F. Winnik, S. Zauscher, I. Luzinov and S. Minko, *Nat. Mater.*, 2010, 9, 101–113.

A3 J. Z. Li, W. J. Ma, L. Song, Z. G. Niu, L. Cai, Q. S. Zeng, X. X. Zhang, H. B. Dong, D. Zhao, W. Y. Zhou and S. S. Xie, *Nano. Lett.*, 2011, 11, 4636–4641.

A4 O. Kim, T. J. Shin and M. J. Park, *Nat. Commun.*, 2013, 4, year.

A5 E. Smela, *Adv. Mater.*, 2003, 15, 481–494.

A6 W. Lu, E. Smela, P. Adams, G. Zuccarello and B. R. Mattes, *Chem. Mater.*, 2004, 16, 1615–1621.

A7 H. Okuzaki and K. Funasaka, *Macromolecules*, 2000, 33, 8307–8311.

A8 S. Kirchmeyer, K. Reuter and J. Simpson, in *Poly(3,4-Ethylene-dioxythiophene) Scientific Importance, Remarkable Properties, and Applications*, ed. T. Skotheim and J. Reynolds, CRC press, Boca Raton, London and NewYork, 3rd edn, 2007, vol. 1, pp. 79–100.

A9 J. Zhou, D. Anjum, L. Chen, X. Xu, I. Ventura, L. Jiang and G. Lubineau, *J. Mater. Chem. C.*, 2014, 2, 9903–9910.

A10 J. Zhou and G. Lubineau, ACS. *Appl. Mater. Interfaces.*, 2013, 5, 6189–6200.

A11 J. Zhou, I. Ventura and G. Lubineau, *Ind. Eng. Chem. Res.*, 2014, 53, 3539–3549.

A12 I. Aguilar Ventura, J. Zhou and G. Lubineau, *Composite. Sci. Technology.*, 2015, 117, 342–350.

A13 H. Okuzaki, H. Suzuki and T. Ito, *J. Phys. Chem. B.*, 2009, 113, 11378–11383.

A14 S. L. Ji, W. W. He, K. Wang, Y. X. Ran and C. H. Ye, *Small*, 2014, 10, 4951–4960.

A15 J. Zhou, T. Fukawa, H. Shirai and M. Kimura, *Macromolecular. Mater. Eng.*, 2010, 295, 671–675.

A16 J. Zhou and M. Kimura, Sen-i. *Gakkaishi.*, 2011, 67, 125–131.

A17 J. Zhou, T. Fukawa and M. Kimura, *Polym. J.*, 2011, 43, 849–854.

A18 J. Zhou, Q. Gao, T. Fukawa, H. Shirai and M. Kimura, *Nanotechnology*, 2011, 22, year.

A19 Y. C. Li, R. Tanigawa and H. Okuzaki, *Smart. Mater. Struct.*, 2014, 23, year.

A20 S. Taccola, F. Greco, E. Sinibaldi, A. Mondini, B. Mazzolai and V. Mattoli, *Adv. Mater.*, 2015, 27, 1668–1675.

A21 H. Miura, Y. Fukuyama, T. Sunda, B. Lin, J. Zhou, J. Takizawa, A. Ohmori and M. Kimura, *Adv. Eng. Mater.*, 2014, 16, 550–555.

A22 C. Plesse, F. Vidal, D. Teyssie and C. Chevrot, *Chem. Commun.*, 2010, 46, 2910–2912.

A23 M. D. Lima, N. Li, M. J. de Andrade, S. L. Fang, J. Oh, G. M. Spinks, M. E. Kozlov, C. S. Haines, D. Suh, J. Foroughi, S. J. Kim, Y. S. Chen, T. Ware, M. K. Shin, L. D. Machado, A. F. Fonseca, J. D. W. Madden, W. E. Voit, D. S. Galvao and R. H. Baughman, *Science*, 2012, 338, 928–932.

A24 J. Zhou, E. Q. Li, R. Li, X. Xu, I. Aguilar Ventura, A. Moussawi, D. Anjum, M. N. Hedhili, D. Smilgies, G. Lubineau and S. T. Thoroddsen, J. *Mater. Chem. C.*, 2015, 3, 2528–2538.

A25 H. Okuzaki, Y. Harashina and H. Yan, *Europ. Polym. J.*, 2009, 45, 256–261.

A26 R. Jalili, J. M. Razal, P. C. Innis and G. G. Wallace, *Adv. Funct. Mat.*, 2011, 21, 3363–3370.

A27 J. Zhou, Y. Zhang, M. Mulle and G. Lubineau, Meas. *Sci. Technol.*, 2015, 26, 085003.

A28 K. O. Hill and G. Meltz, J. *Lightwave. Technol.*, 1997, 15, 1263–1276.

A29 Y. J. Rao, Opt. Laser. Eng., 1999, 31, 297–324.

A30 X. Wang, N. Behabtu, C. C. Young, D. E. Tsentalovich, M. Pasquali and J. Kono, *Adv. Funct. Mater.*, 2014, 24, 3241–3249.

A31 N. Behabtu, C. C. Young, D. E. Tsentalovich, O. Kleinerman, X.Wang, A.W. K. Ma, E. A. Bengio, R. F. terWaarbeek, J. J. de Jong, R. E. Hoogerwerf, S. B. Fairchild, J. B. Ferguson, B. Maruyama, J. Kono, Y. Talmon, Y. Cohen, M. J. Otto and M. Pasquali, *Science*, 2013, 339, 182–186.

A32 Z. Xu, Z. Liu, H. Y. Sun and C. Gao, *Adv. Mater.*, 2013, 25, 3249–3253.

A33 F. C. Meng, X. H. Zhang, R. Li, J. N. Zhao, X. H. Xuan, X. H.Wang, J. Y. Zou and Q.W. Li, *Adv. Mater.*, 2014, 26, 2480–2485.

A34 D. Antiohos, G. Folkes, P. Sherrell, S. Ashraf, G.Wallace, P. Aitchison, A. Harris, J. Chen and A. Minett, *J Mater Chem*, 2011, 21, 15987–15994.

A35 J. Zhou, D. H. Anjum, E. Q. Li, G. Lubineau and S. T. Thoroddsen, *Macromolecules*, 2015, 48, 5688–5696.

A36 P. Liu, L. Liu, Y. Wei, K. Liu, Z. Chen, K. L. Jiang, Q. Q. Li and S. S. Fan, *Adv. Mater.*, 2009, 21, 3563–3566.

A37 A. H. Hussain, E. B. Lizardo, G. A. T. Sevilla, J. M. Nassar and M. M. Hussain, *Adv. Healthcare. Mater.*, 2015, 4, 665–673.

A38 K. D. M. Rao and G. U. Kulkarni, *Nanoscale*, 2014, 6, 5645–5651.

A39 S. Hong, H. Lee, J. Lee, J. Kwon, S. Han, Y. D. Suh, H. Cho, J. Shin, J. Yeo and S. H. Ko, *Adv. Mater.*, 2015, xx, DOI: 10.1002/adma.201500917.

A40 S. Choi, J. Park, W. Hyun, J. Kim, J. Kim, Y. B. Lee, C. Song, H. J. Hwang, J. H. Kim, T. Hyeon and D. H. Kim, *ACS. Nano.*, 2015, 9, 6626–6633.

A41 J. P. Li, J. J. Liang, X. Jian, W. Hu, J. Li and Q. B. Pei, *Macromol. Mater. Eng.*, 2014, 299, 1403–1409.

A42 R. Gupta, K. D. M. Rao, K. Srivastava, A. Kumar, S. Kiruthika and G. U. Kulkarni, ACS. *Appl. Mater. Interfaces.*, 2014, 6, 13688–13696.

A43 G. Kim, L. Shao, K. Zhang and K. Pipe, Nat. Mater., 2013, 12, 719–723.

A44 P. C. Hsu, X. G. Liu, C. Liu, X. Xie, H. R. Lee, A. J. Welch, T. Zhao and Y. Cui, *Nano. Lett.*, 2015, 15, 365–371.

A45 P. Ilanchezhiyan, A. S. Zakirov, G. M. Kumar, S. U. Yuldashev, H. D. Cho, T. W. Kang and A. T. Mamadalimov, *RSC. Adv.*, 2015, 5, 10697–10702.

A46 T. J. Kang, T. Kim, S. M. Seo, Y. J. Park and Y. H. Kim, *Carbon*, 2011, 49, 1087–1093.

A47 Y. H. Yoon, J. W. Song, D. Kim, J. Kim, J. K. Park, S. K. Oh and C. S. Han, *Adv. Mater.*, 2007, 19, 4284–4287.

A48 D. Jung, D. Kim, K. H. Lee, L. J. Overzet and G. S. Lee, *Sensor. Actuat. A. Phys.*, 2013, 199, 176–180.

A49 J. Yan and Y. G. Jeong, *Sensor. Actuat. A. Phys.*, 2015, 86, 72–79.

A50 J. J. Bae, S. C. Lim, G. H. Han, Y. W. Jo, D. L. Doung, E. S. Kim, S. J. Chae, T. Q. Huy, N. V. Luan and Y. H. Lee, *Adv. Funct. Mater.*, 2012, 22, 4819–4826.

A51 K. Y. Shin, J. Y. Hong, S. Lee and J. Jang, *J. Mater. Chem.*, 2012, 22, 23404–23410.

A52 S. Maity, A. Chatterjee, B. Singh and A. P. Singh, J. *Textile. Institute.*, 2014, 105, 887–893.

A53 K. Opwis, D. Knittel and J. S. Gutmann, *Synthetic Metals*, 2012, 162, 1912–1918.

A54 A. Laforgue, *J. Material. Chem.*, 2010, 20, 8233–8235.

A55 M. De Jong, L. Van IJzendoorn and M. de Voigt, *Appl. Phys. Lett.*, 2000, 77, 2255.

A56 S. Dupont, F. Novoa, E. Voroshazi and R. Dauskardt, *Adv. Funct. Mater.*, 2014, 24, 1325–1332.

A57 F.Wang, C. Gao, K. Kuklane and I. Holmer, Int. *J. Occup. Saf. Ergon.*, 2010, 16, 387–404.

A58 W. B. Lu, M. Zu, J. H. Byun, B. S. Kim and T. W. Chou, *Adv. Mater.*, 2012, 24, 1805–1833.

A59 H. Okuzaki and T. Kunugi, *J. Polym. Sci. Pol. Phys.*, 1998, 36, 1591–1594.

A60 M. M. Ma, L. Guo, D. G. Anderson and R. Langer, *Science*, 2013, 339, 186–189.

A61 C. S. Haines, M. D. Lima, N. Li, G. M. Spinks, J. Foroughi, J. D. W. Madden, S. H. Kim, S. L. Fang, M. J. de Andrade, F. Goktepe, O. Goktepe, S. M. Mirvakili, S. Naficy, X. Lepro, J. Y. Oh, M. E. Kozlov, S. J. Kim, X. R. Xu,

B. J. Swedlove, G. G.Wallace and R. H. Baughman, *Science*, 2014, 343, 868–872.

A62 H. Okuzaki, T. Kuwabara, K. Funasaka and T. Saido, *Adv. Funct. Mater.*, 2013, 23, 4400–4407.

A63 D. Antiohos, G. Folkes, P. Sherrell, S. Ashraf, G.Wallace, P. Aitchison, A. Harris, J. Chen and A. Minett, *J Mater Chem*, 2011, 21, 15987–15994.

A64 J. Zhou, I. Ventura and G. Lubineau, *Ind Eng Chem Res*, 2014, 53, 3539–3549.

TABLES FOR PART II:

Table 1 Properties of PEDOT/PSS fibers for the study of electrothermal response.

Samples	Diameter (D, μm)	Current density (j_b, A cm^{-2})	Resistance (R, kΩ)	Conductivity (σ, S cm^{-1})	Young's modulus (E, GPa)
As-spun PEDOT/PSS fiber	9.8±1.3	5.6×10^3	8.4	315.8	5.9±0.7
EG/(PEDOT/PSS) fiber	9.7±1.4	7.1×10^3	5.2	520.7	7.3±0.5
(PEDOT/PSS)EG/ fiber	8.6±0.8	1.3×10^4	2.0	1722.4	7.7±0.5
EG/(PEDOT/PSS)/EG fiber	8.4±0.7	1.8×10^4	1.1	3131.6	8.3±0.4

Table 2 Comparisons on the performance of electrically driven heaters from the related literature. σ is electrical conductivity, R_s is sheet resistance and R is the resistance.

Heater type	Preparation method	Electrical properties	First order response (s)	Max. heating rate (°C s^{-1})	Voltage (V)	Refs.
Tungsten wire	-	σ: 1.9× 10^5 S cm^{-1}	0.1-0.5	-	-	36
Copper interconnects	Lithography	σ: 5.9× 10^5 S cm^{-1}	1-2	20	0.3-1	37
Gold microwire network	Sacrificial templating	R_s: 3.1-5.4 Ω sq^{-1}	15-50	50	2-15	38
AgNW/PDMS	Vacuum filtration	R_s: 30 Ω sq^{-1}	30	2	2-10	39
AgNW/SBS	Ligand exchange	σ: 3.5 × 10^3 S cm^{-1}	10-25	3	0.5-1	40
AgNW/polyacrylate	Drop casting	R_s: 10-60 Ω sq^{-1}	>15	9	5-11	41
Ag/Crackle precursor	Metal sputtering	R_s: 2-6 Ω sq^{-1}	6-20	10	1-5	42
AgNW/CNT/PET film	Spray/roll-to-roll coating	R_s: 10-1000 Ω sq^{-1}	15	6	15	43
AgNW coated cloth	Dip coating	-	50	0.6	0.6-1.2	44
SWCNT coated cloth	Dip coating	-	100	0.3	8-16	44
SWCNT functionalized fabrics	Dip coating	R: 2.5-200 kΩ	30-40	3	10-40	45
SWCNT coated glass	Dip coating	R: 22.6-54.6 kΩ	18-30	1	10-60	46
SWCNT coated glass or PET	Filtration and transfer	R_s: 0.25-3.5 kΩ sq^{-1}	25	3	6-12	47
MWCNT coated glass	Pulling from CNT forest	R_s: 172-756 Ω sq^{-1}	18-25	5	0-40	48
MWCNT/PDMS	Spin-coating and casting	R_s: 1-100 kΩ sq^{-1}	20-40	10	1-100	49
Graphene coated glass	Layer-by-layer transfer	R_s: 403 Ω sq^{-1}	50-100	2	6-30	50
Graphite nanoplatelet/polyimide	Screen printing	R_s: 10-150 Ω sq^{-1}	70-100	2	2-14	51
Polypyrrole coated textile	Chemical polymerization	R_s: 1000 Ω sq^{-1}	> 60	1	5-30	52
PEDOT/PTSA coated textile	Chemical polymerization	R_s: 12.8-127.9 Ω sq^{-1}	> 60	1	6-24	53
PEDOT/PSS microfilm	Casting	σ: 150 S cm^{-1}	15	3	2-16	13
PEDOT nanofiber mat	Electrospinning/deposition	σ: 60 S cm^{-1}	15	3	10	54
AgNW/(PEDOT/PSS)/PET	Blade coating	R_s: 3-4 Ω sq^{-1}	50-80	2	1.5-6	14
PEDOT/PSS fibers	Wet-spinning/hot-drawing	σ: 360-2804 S cm^{-1}	1.2-2	63	2-36	This study

Table 3 Comparisons of the performance of linear, conductive polymer actuators that work in air.

Materials	Driven voltage (V)	Maximum actuation stress (MPa)	Maximum actuation strain (%)	Response time (s)	Maximum frequency (Hz)	References
$PPy(BF_4)_{0.33}(H_2O)_{0.25}$ film	0-3	8.9	1	50	-	[illegible]
PEDOT/PSS film	0-10	17	2.4-4.5	20	-	13
PEDOT semi-IPN hollow fiber	0-1	<1	3	80	-	22
PEDOT/PSS/PVA blended fiber	0-8	11	0.12	50	1	21
As-spun PEDOT/PSS fiber	0-20	13	~0.4	0.5	2	This study
EG/(PEDOT/PSS) fiber	0-16	16	~0.4	0.5	5	This study
(PEDOT/PSS)EG/ fiber	0-8	19	~0.4	0.5	10	This study
EG/(PEDOT/PSS)/EG fiber	0-5	22	~0.4	0.5	40	This study

Table S1 Relative element quantification in the fibers by the energy dispersive x-ray spectroscopy (EDS).

	Element atomic ratio (At %)			
Sample	C	O	S	Na
As-spun PEDOT/PSS fibers	75.67	12.67	11.02	0.64
EG/(PEDOT/PSS)/EG fibers	76.19	13.88	9.14	0.79
As-spun PEDOT/PSS fibers-800°C	89.70	6.61	2.43	1.27
EG/(PEDOT/PSS)/EG fibers-800°C	88.48	7.02	2.41	2.10%

WHAT IS CLAIMED IS:

1. A method comprising: providing at least one first composition comprising at least one conjugated polymer and at least one solvent, wet spinning the at least one first composition to form at least one first fiber material, hot-drawing the at least one first fiber material to form at least one second fiber material.

2. The method of claim 1, wherein the method further comprises doping of the first composition.

3. The method of any one of claims 1-2, wherein the method further comprises de-doping of the first fiber material before hot drawing.

4. The method of any one of claims 1-3, wherein the method further comprises doping of the first composition and de-doping of the first fiber material before hot drawing.

5. The method of any one of claims 2-4, wherein the doping is carried out with at least one organic solvent.

6. The method of any one of claims 2-5, wherein the doping is carried out with ethylene glycol.

7. The method of any one of claims 3-6, wherein the de-doping is carried out with at least one organic solvent.

8. The method of any one of claims 3-7, wherein the de-doping is carried out with ethylene glycol.

9. The method of any one of claims 1-8, wherein the conjugated polymer comprises a polythiophene.

10. The method of any one of claims 1-9, wherein the conjugated polymer comprises a 3,4-di-substituted polythiophene.

11. The method of any one of claims 1-10, wherein the conjugated polymer comprises PEDOT.

12. The method of any one of claims 1-11, wherein the first composition comprises a polymeric dopant for the conjugated polymer.

13. The method of any one of claims 1-12, wherein the first composition comprises a polymeric dopant for the conjugated polymer which is a polyelectrolyte polymer.

14. The method of any one of claims 1-13, wherein the first composition comprises a polymeric dopant for the conjugated polymer which is polystyrene sulfonate (PSS).

15. The method of any one of claims 1-14, wherein the first composition is an aqueous dispersion.

16. The method of any one of claims 1-15, wherein the first composition comprises water and at least one protic polar solvent.

17. The method of any one of claims 1-16, wherein the first composition has a concentration of at least 15 mg/mL of conjugated polymer including in combination, if present, with polymeric dopant.

18. The method of any one of claims 1-17, wherein the first composition has a concentration of at least 20 mg/mL of conjugated polymer including in combination, if present, with polymeric dopant.

19. The method of any one of claims 1-18, wherein the wet spinning is carried out with a coagulation bath comprising acetone and isopropyl alcohol.

20. The method of any one of claims 1-19, wherein the hot drawing is done at a temperature of 50°C to 140°C.

21. The method of any one of claims 1-20, wherein the average fiber diameter is about 3 microns to about 150 microns.

22. The method of any one of claims 1-21, wherein the process is carried out with a draw ratio which is at least 3.

23. The method of any one of claims 1-22, wherein the second fiber material has a diameter of at least 3 microns.

24. The method of any one of claims 1-23, wherein the second fiber material has a diameter of at least 10 microns.

25. The method of any one of claims 1-24, wherein the fiber length is at least 100 m.

26. The method of any one of claims 1-25, wherein the fiber length is at least 500 m.

27. A method comprising: providing at least one first composition comprising PEDOT:PSS and water, wet spinning the at least one first composition to form at least one first fiber material, hot-drawing the at least one first fiber material to form at least one second fiber material, wherein the method further comprises doping of the first composition and de-doping of the first fiber material before hot-drawing.

28. A fiber material prepared by the method of any one of claims 1-27.

29. The fiber material of claim 28, wherein the fiber material shows a conductivity of at least 300 $S \cdot cm^{-1}$.

30. The fiber material of any one of claims 28-29, wherein the fiber material shows a conductivity of at least 2,000 $S \cdot cm^{-1}$.

31. The fiber material of any one of claims 28-30, wherein the fiber material shows a cross-over temperature of semiconductor-to-metal transition of at least 25°C.

32. The fiber material of any one of claims 28-31, wherein the fiber material shows a cross-over temperature of semiconductor-to-metal transition of at least 40°C.

33. The fiber material of any one of claims 28-32, wherein the fiber material shows a Young's modulus of at least 5 GPa, a tensile strength of at least 300 MPa, and an elongation at break of at least 10%.

34. The fiber material of any one of claims 28-33, wherein the fiber material shows a Young's modulus of at least 8 GPa, a tensile strength of at least 409 MPa, and an elongation at break of at least 21%.

FIGURE 1

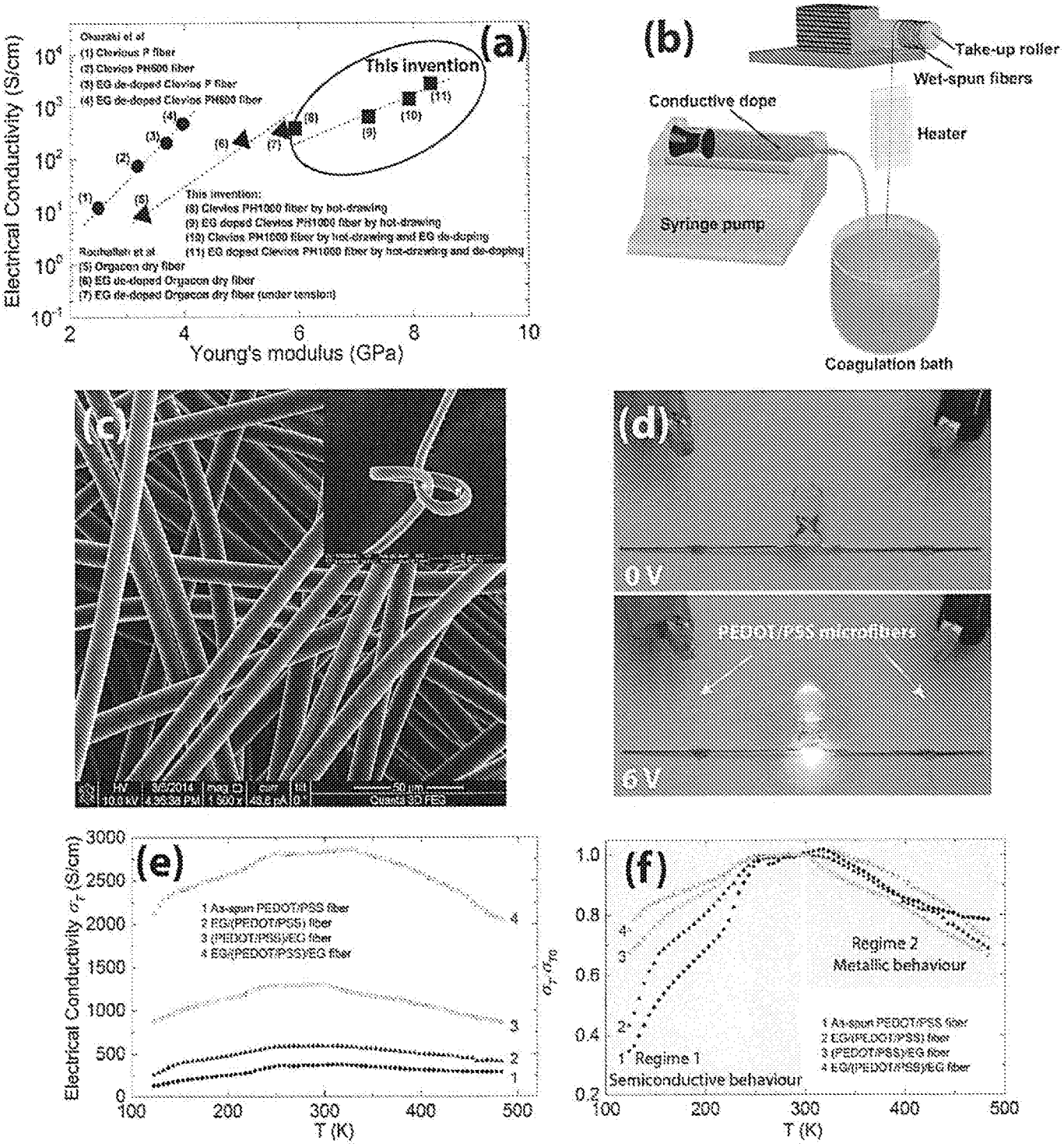
(a)
Electrical Conductivity (S/cm)
Young's modulus (GPa)
This invention
Okuzaki et al
(1) Clevious P fiber
(2) Clevios PH500 fiber
(3) EG de-doped Clevios P fiber
(4) EG de-doped Clevios PH500 fiber
Rochefallet et al
(5) Orgacon dry fiber
(6) EG de-doped Orgacon dry fiber
(7) EG de-doped Orgacon dry fiber (under tension)
This invention:
(8) Clevios PH1000 fiber by hot-drawing
(9) EG doped Clevios PH1000 fiber by hot-drawing
(10) Clevios PH1000 fiber by hot-drawing and EG de-duping
(11) EG doped Clevios PH1000 fiber by hot-drawing and de-doping
(b)
Take-up roller
Wet-spun fibers
Conductive dope
Heater
Syringe pump
Coagulation bath
(c)
(d)
0 V
PEDOT/PSS microfibre
6 V
(e)
Electrical Conductivity σ_T (S/cm)
T (K)
1 As-spun PEDOT/PSS fiber
2 EG/(PEDOT/PSS) fiber
3 (PEDOT/PSS)/EG fiber
4 EG/(PEDOT/PSS)/EG fiber
(f)
σ_T/σ_{T0}
Regime 1
Semiconductive behaviour
Regime 2
Metallic behaviour
T (K)

FIGURE 2

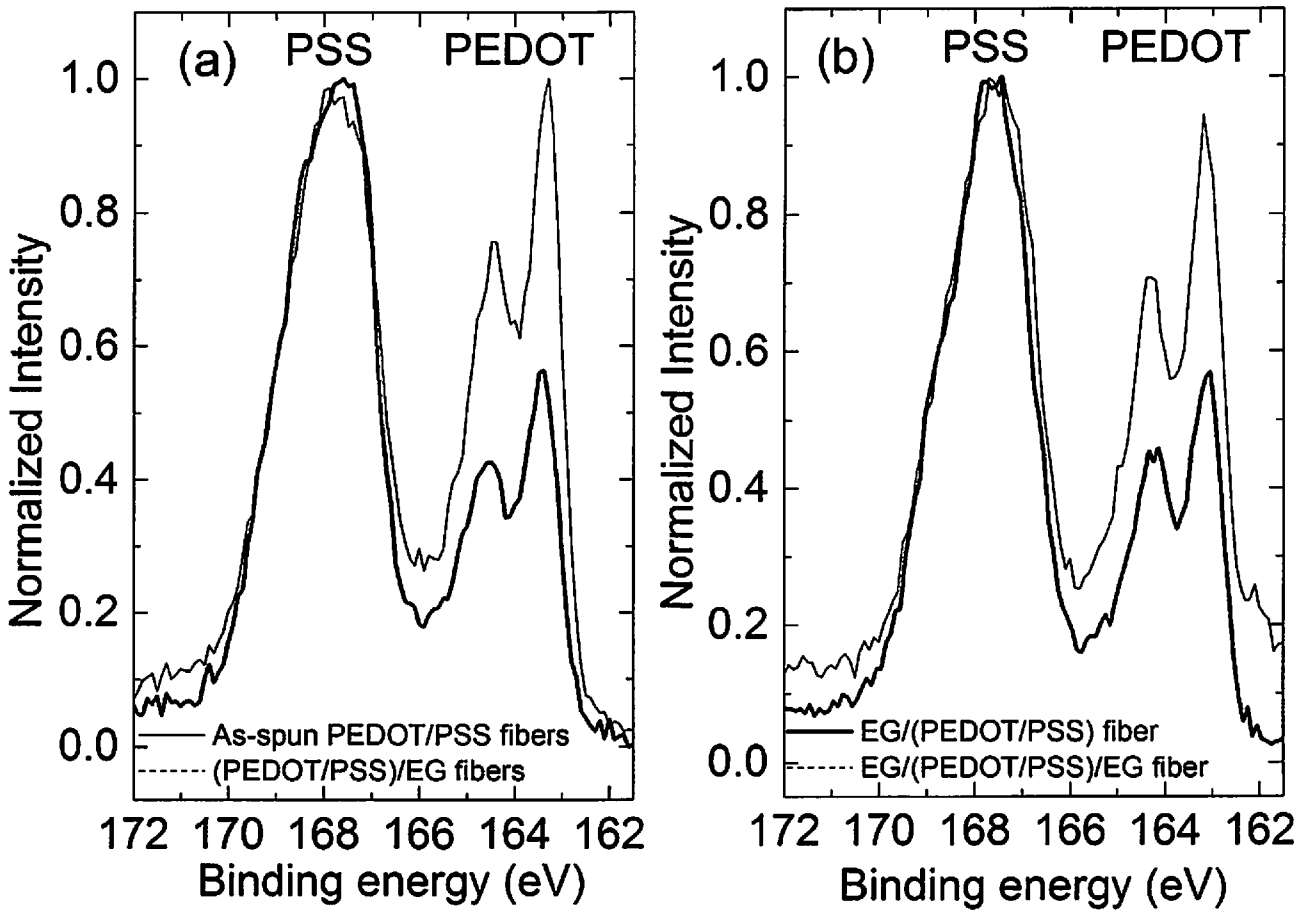
(a)
PSS
PEDOT
Normalized Intensity
1.0
0.8
0.6
0.4
0.2
0.0
As-spun PEDOT/PSS fibers
(PEDOT/PSS)/EG fibers
172 170 168 166 164 162
Binding energy (eV)
(b)
PSS
PEDOT
Normalized Intensity
1.0
0.8
0.6
0.4
0.2
0.0
EG/(PEDOT/PSS) fiber
EG/(PEDOT/PSS)/EG fiber
172 170 168 166 164 162
Binding energy (eV)

FIGURE 3

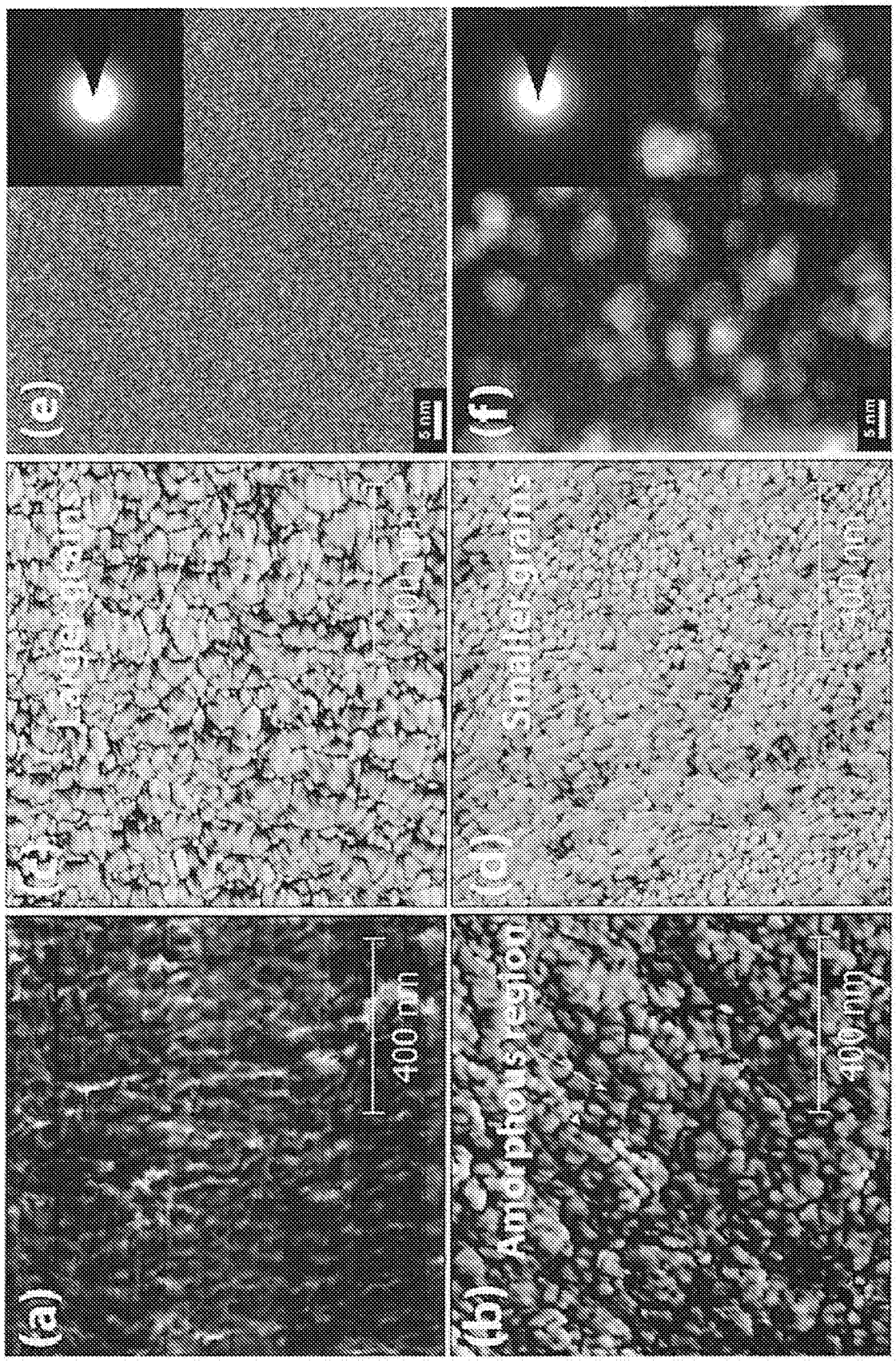
(a)
400 nm
(b) Amorphous region
400 nm
(c) Small grains
400 nm
(d) Small grains
400 nm
(e)
5 nm
(f)
5 nm

FIGURE 4

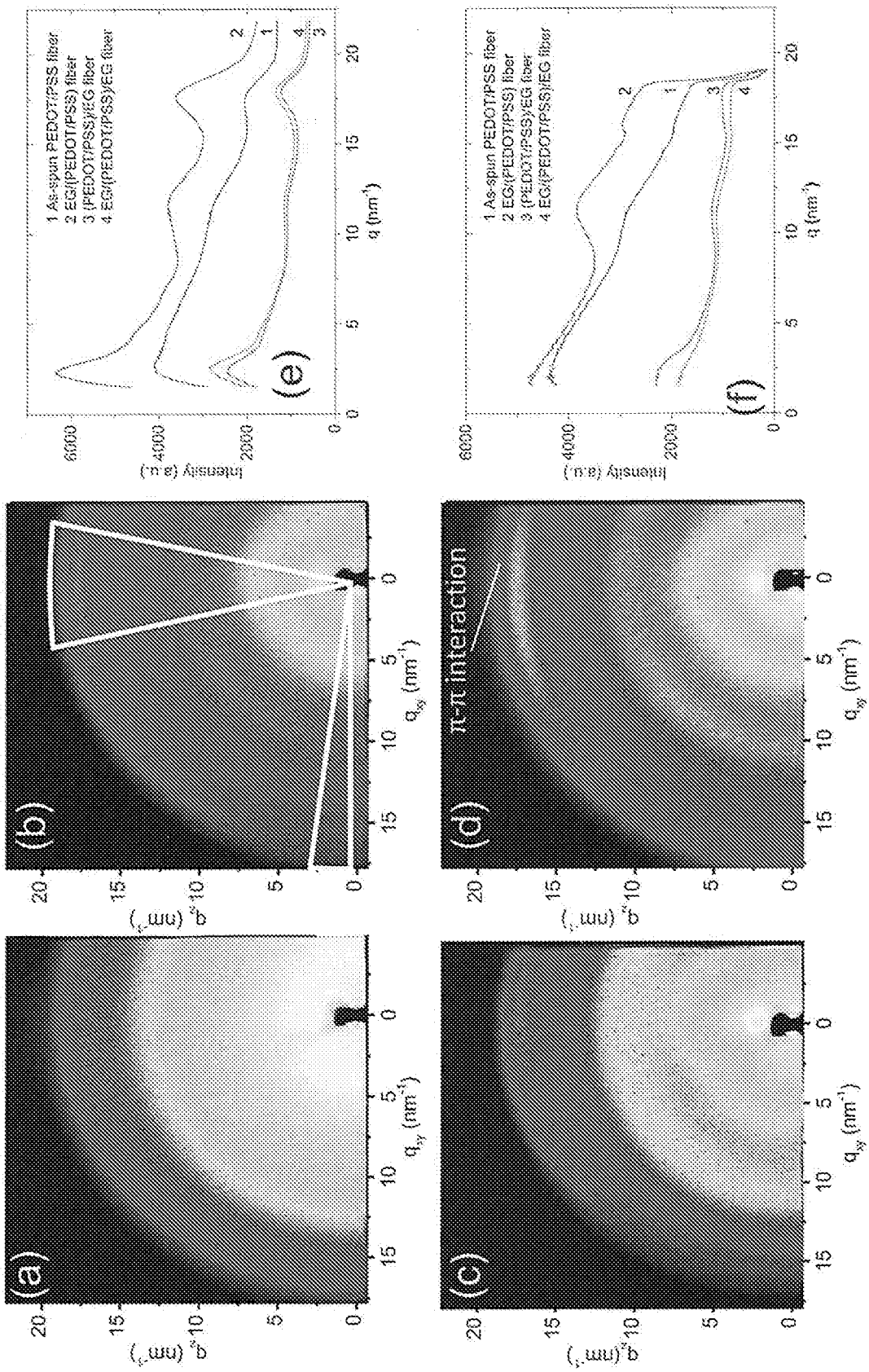
(a)
(b)
(c)
(d)
(e)
(f)
π-π interaction
1 As-spun PEDOT/PSS fiber
2 EG/(PEDOT/PSS) fiber
3 (PEDOT/PSS)/EG fiber
4 EG/(PEDOT/PSS)/EG fiber
Intensity (a.u.)
q (nm⁻¹)
q_xy (nm⁻¹)
q_z (nm⁻¹)

FIGURE 5

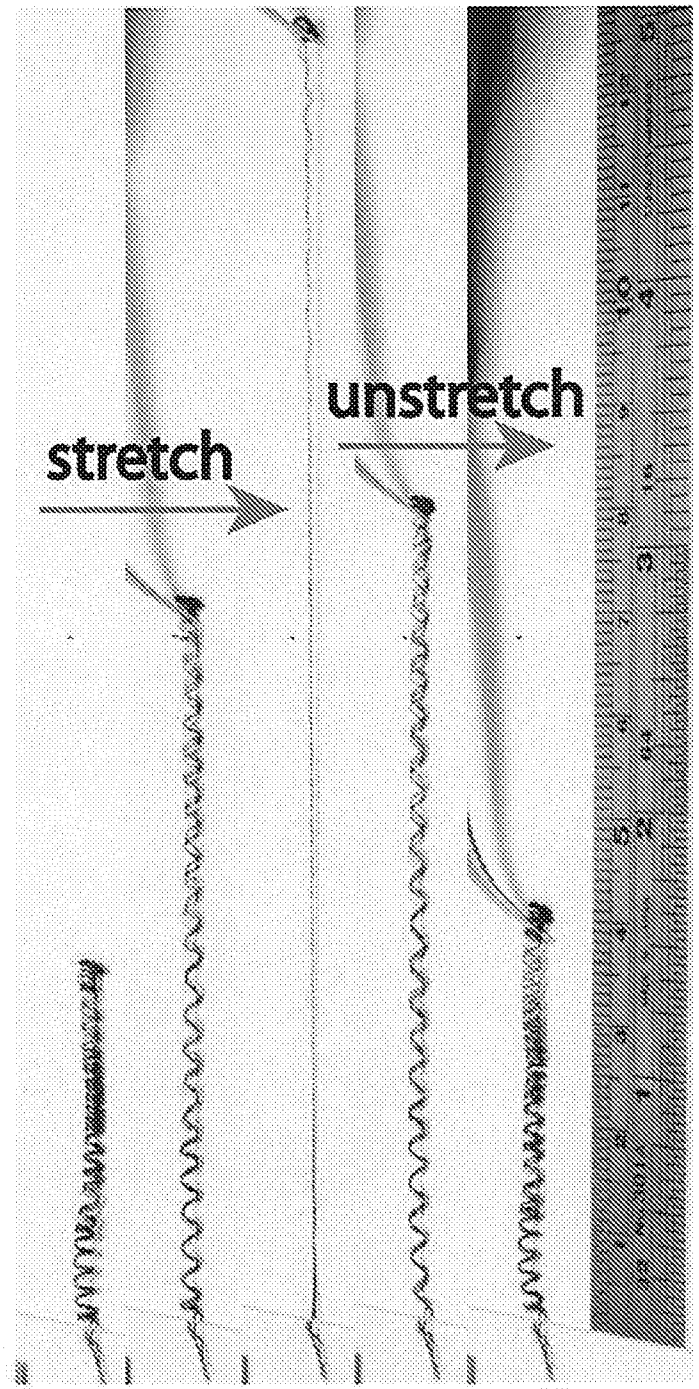

FIGURE 6

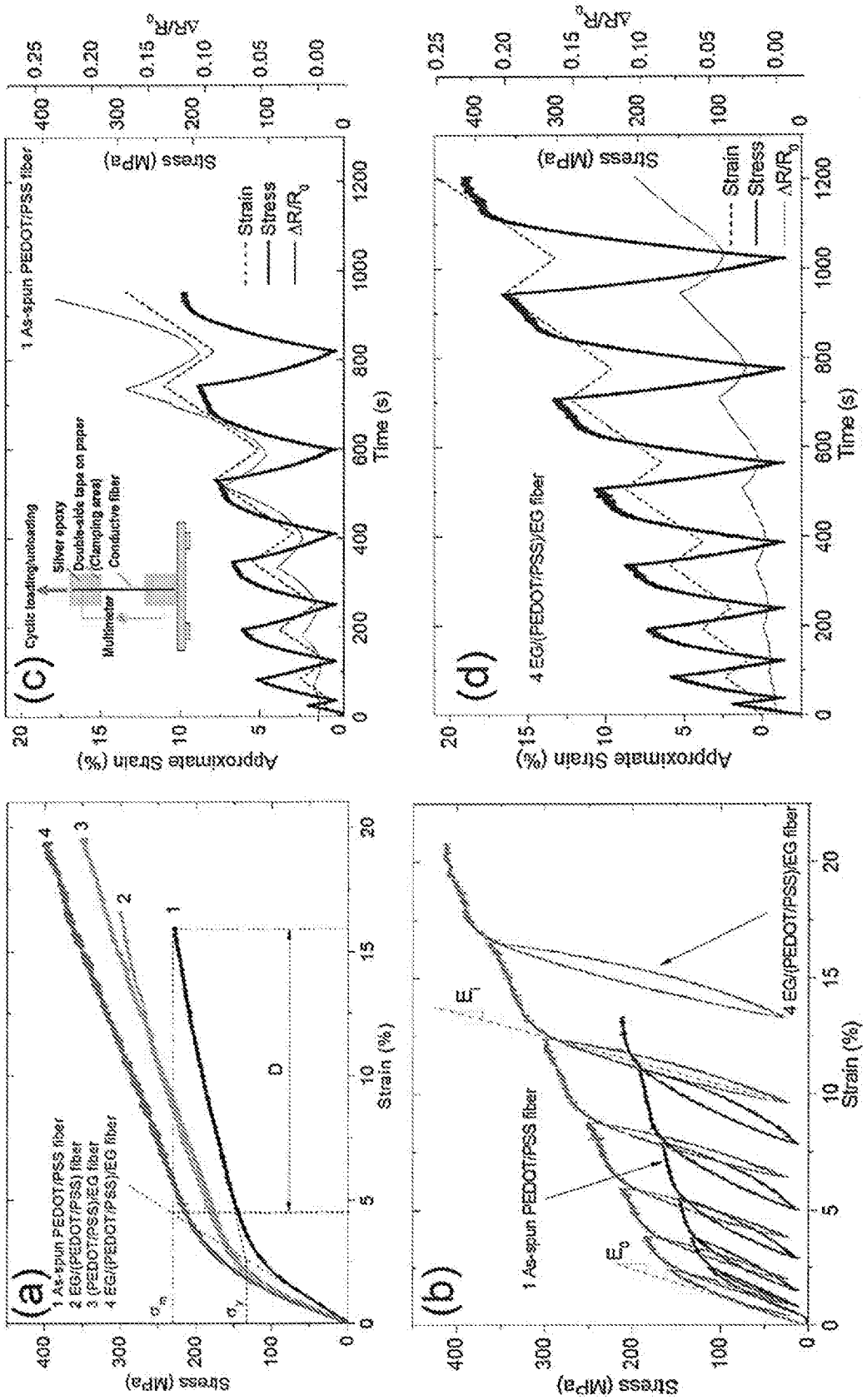
(a)
1 As-spun PEDOT/PSS fiber
2 EG/(PEDOT/PSS) fiber
3 (PEDOT/PSS)/EG fiber
4 EG/(PEDOT/PSS)/EG fiber
Stress (MPa)
Strain (%)
D
(b)
1 As-spun PEDOT/PSS fiber
4 EG/(PEDOT/PSS)/EG fiber
Stress (MPa)
Strain (%)
(c)
1 As-spun PEDOT/PSS fiber
Cyclic loading/unloading
Silver epoxy
Double-side tape on paper (Clamping area)
Conductive fiber
Multimeter
Strain
Stress
ΔR/R0
Approximate Strain (%)
Stress (MPa)
Time (s)
(d)
4 EG/(PEDOT/PSS)/EG fiber
Strain
Stress
ΔR/R0
Approximate Strain (%)
Stress (MPa)
Time (s)

FIGURE 7

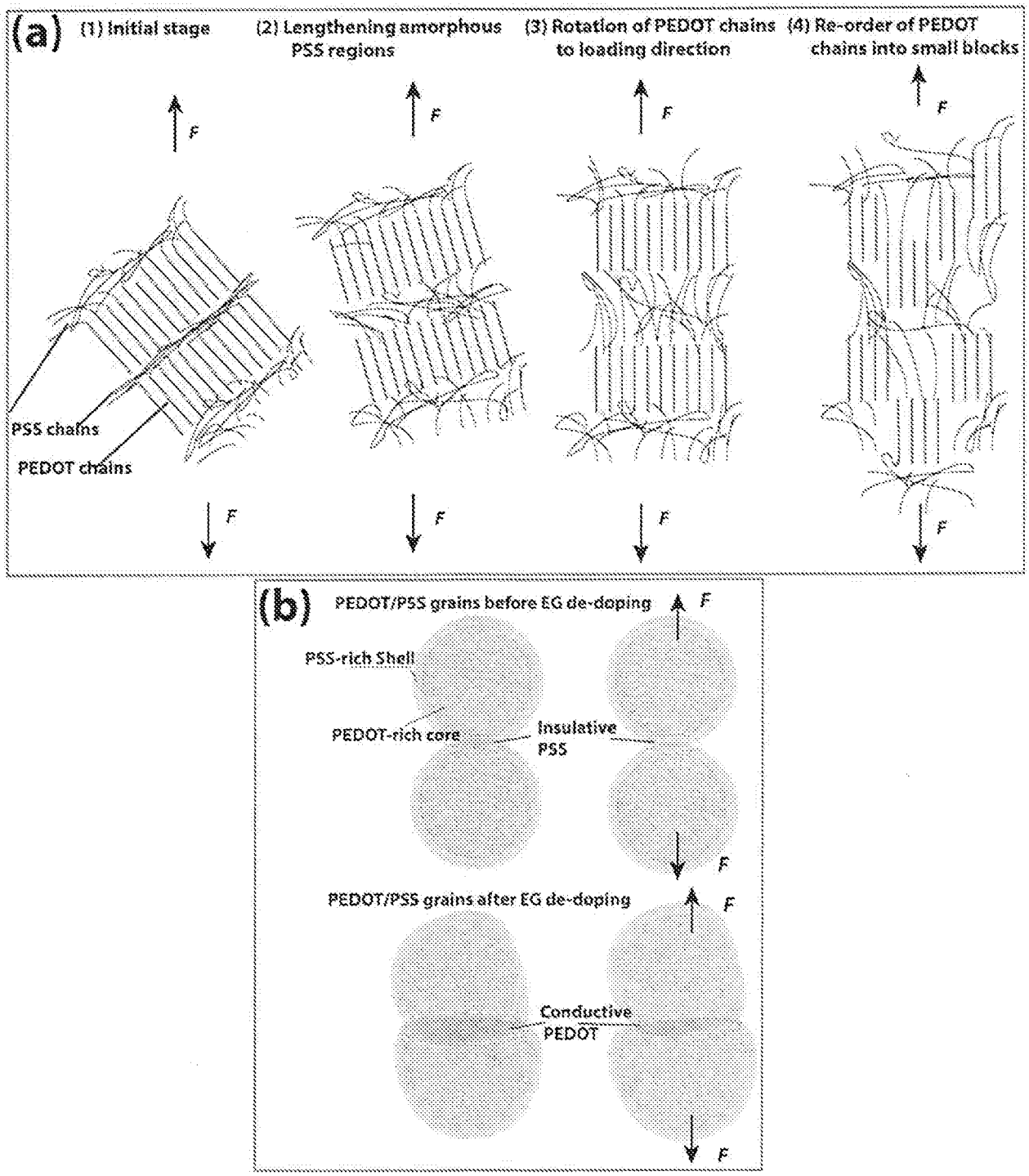
(a)
(1) Initial stage
(2) Lengthening amorphous PSS regions
(3) Rotation of PEDOT chains to loading direction
(4) Re-order of PEDOT chains into small blocks
F
PSS chains
PEDOT chains
(b)
PEDOT/PSS grains before EG de-doping
PSS-rich Shell
PEDOT-rich core
Insulative PSS
PEDOT/PSS grains after EG de-doping
Conductive PEDOT

FIGURE 8

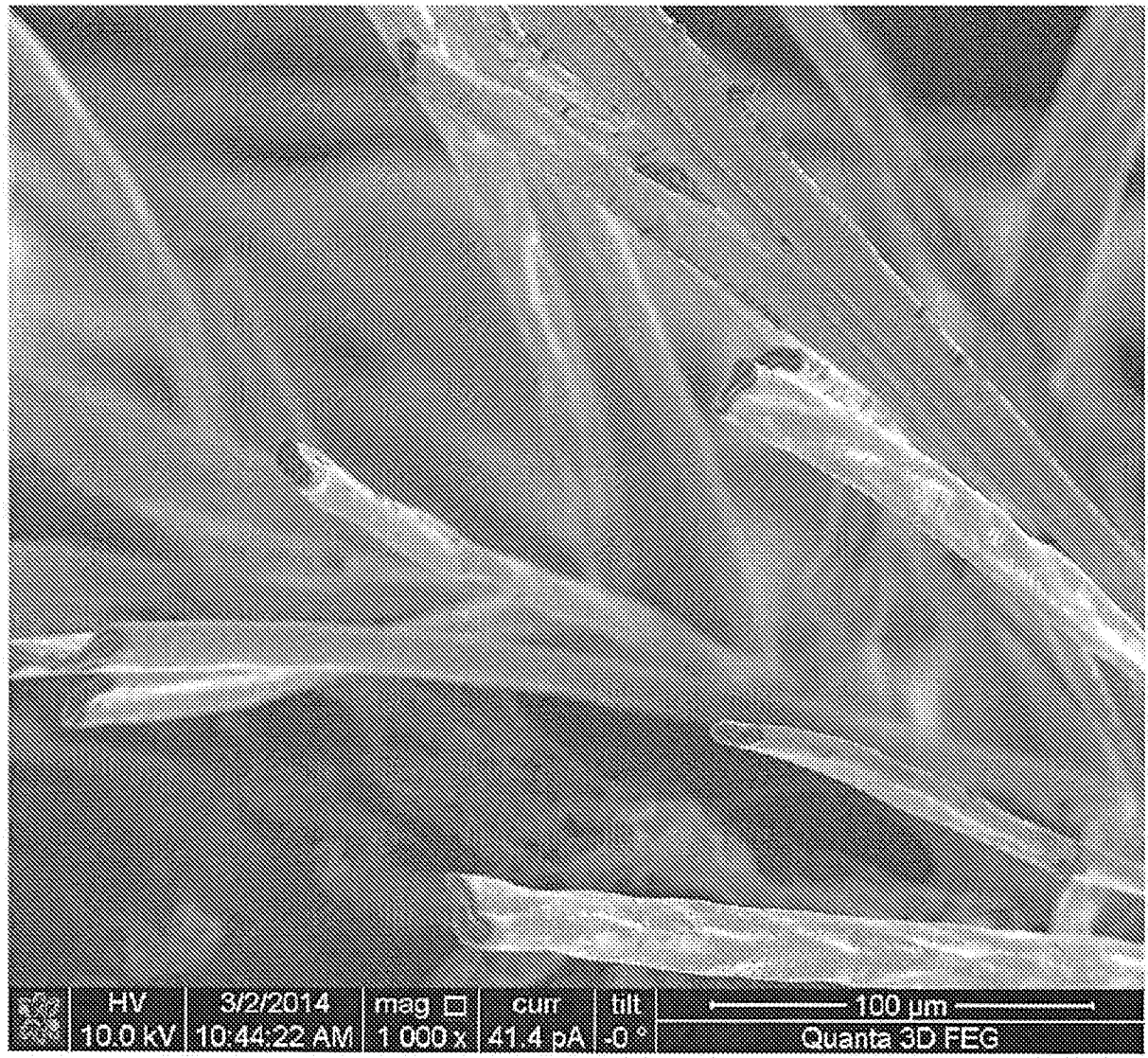
HV
10.0 kV
3/2/2014
10:44:22 AM
mag
1 000 x
curr
41.4 pA
tilt
-0 °
100 µm
Quanta 3D FEG

FIGURE 9

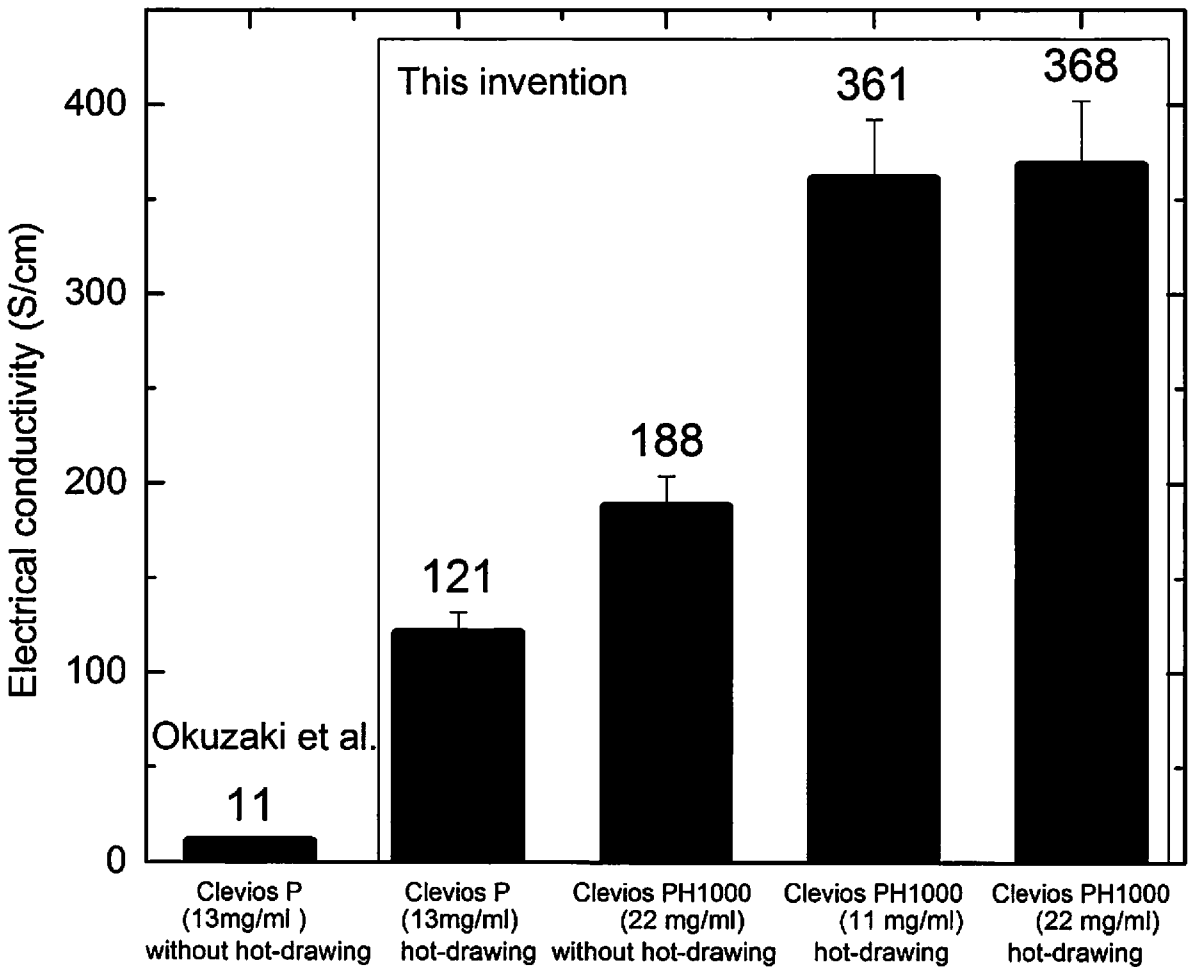
Electrical conductivity (S/cm)
0
100
200
300
400
This invention
Okuzaki et al.
11
121
188
361
368
Clevios P (13mg/ml) without hot-drawing
Clevios P (13mg/ml) hot-drawing
Clevios PH1000 (22 mg/ml) without hot-drawing
Clevios PH1000 (11 mg/ml) hot-drawing
Clevios PH1000 (22 mg/ml) hot-drawing

FIGURE 10

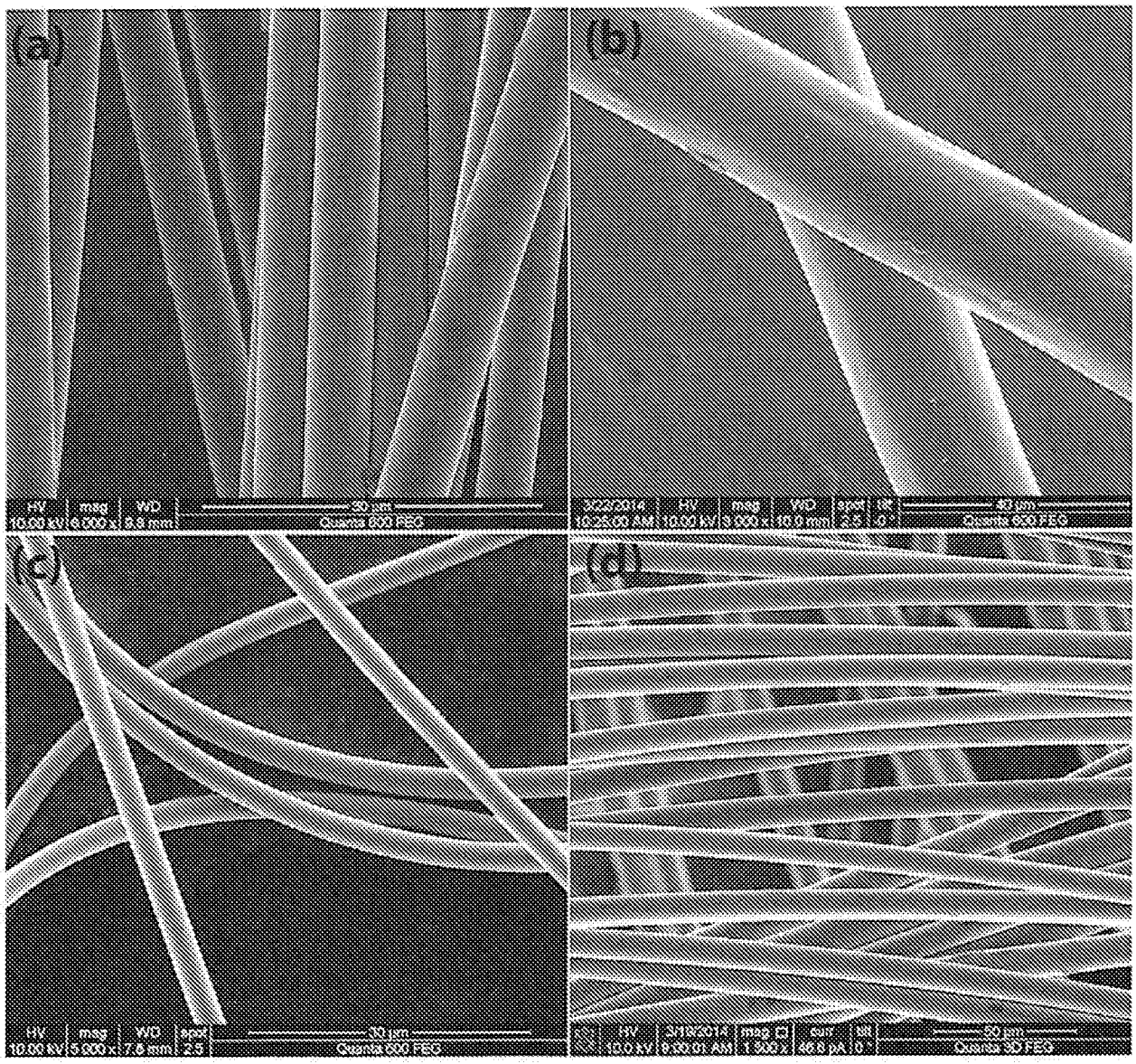

FIGURE 11

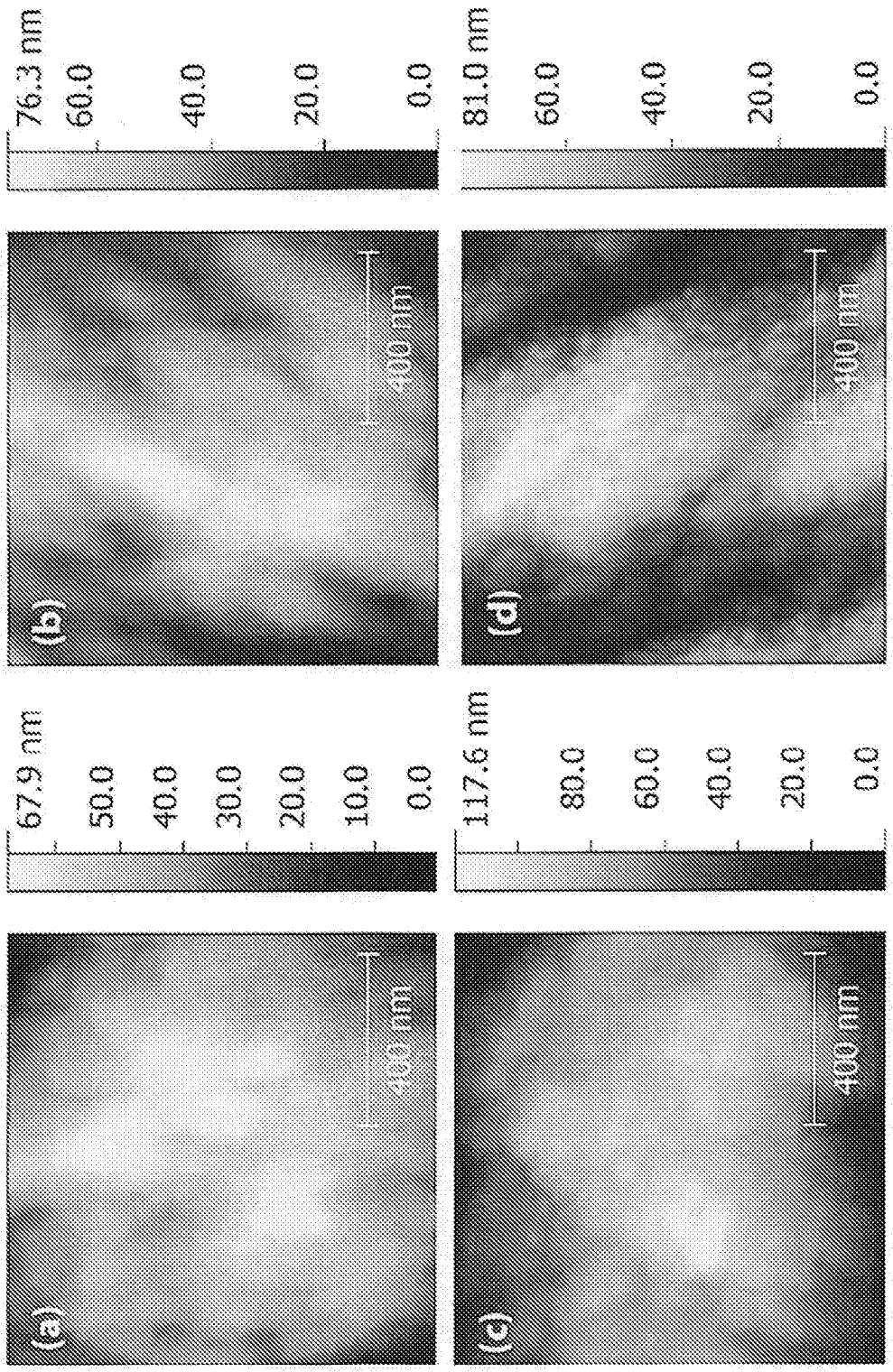
(a)
400 nm
67.9 nm
50.0
40.0
30.0
20.0
10.0
0.0
(b)
400 nm
76.3 nm
60.0
40.0
20.0
0.0
(c)
400 nm
117.6 nm
80.0
60.0
40.0
20.0
0.0
(d)
400 nm
81.0 nm
60.0
40.0
20.0
0.0

FIGURE 12

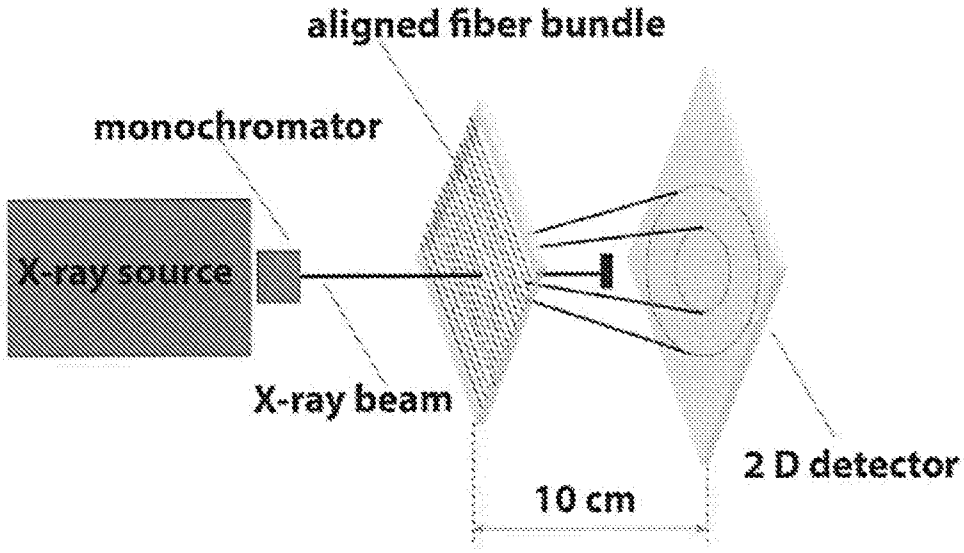
aligned fiber bundle
monochromator
X-ray source
X-ray beam
2 D detector
10 cm

FIGURE 13

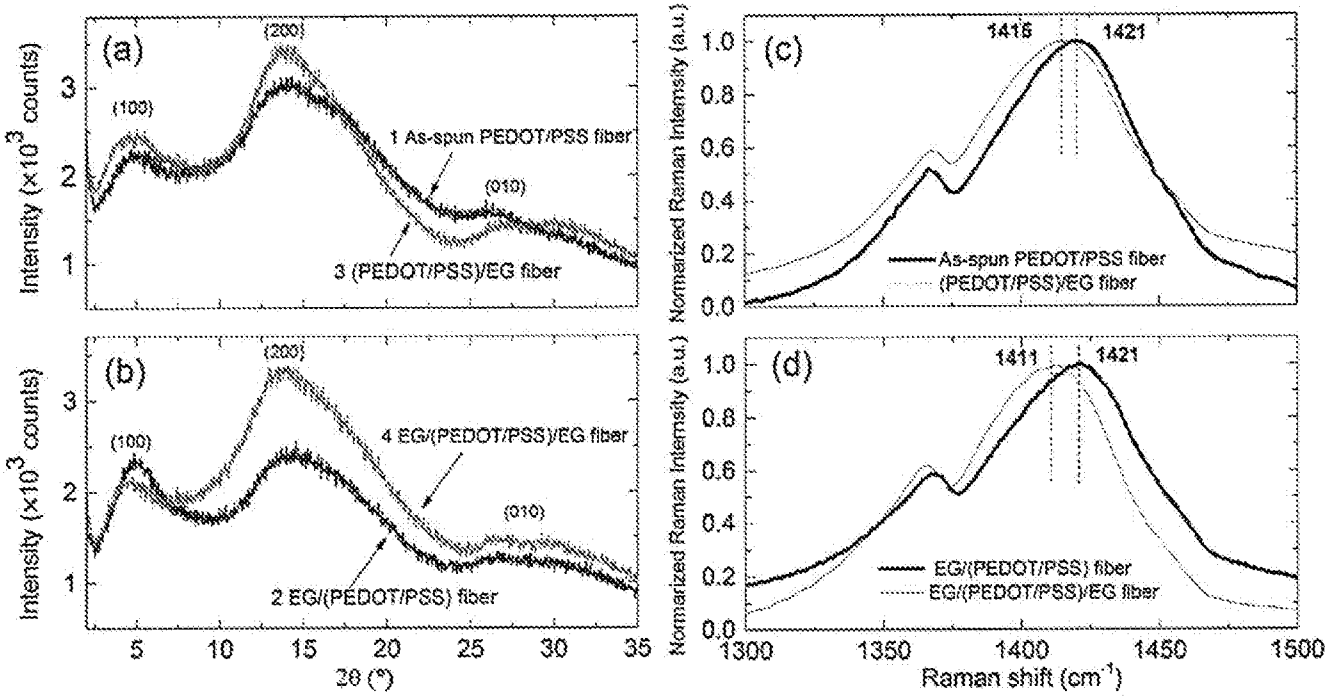
(a)
(200)
(100)
(010)
1 As-spun PEDOT/PSS fiber
3 (PEDOT/PSS)/EG fiber
Intensity (×10^3 counts)
(b)
(200)
(100)
(010)
4 EG/(PEDOT/PSS)/EG fiber
2 EG/(PEDOT/PSS) fiber
Intensity (×10^3 counts)
2θ (°)
(c)
1416
1421
As-spun PEDOT/PSS fiber
(PEDOT/PSS)/EG fiber
Normarized Raman Intensity (a.u.)
(d)
1411
1421
EG/(PEDOT/PSS) fiber
EG/(PEDOT/PSS)/EG fiber
Normarized Raman Intensity (a.u.)
Raman shift (cm^-1)

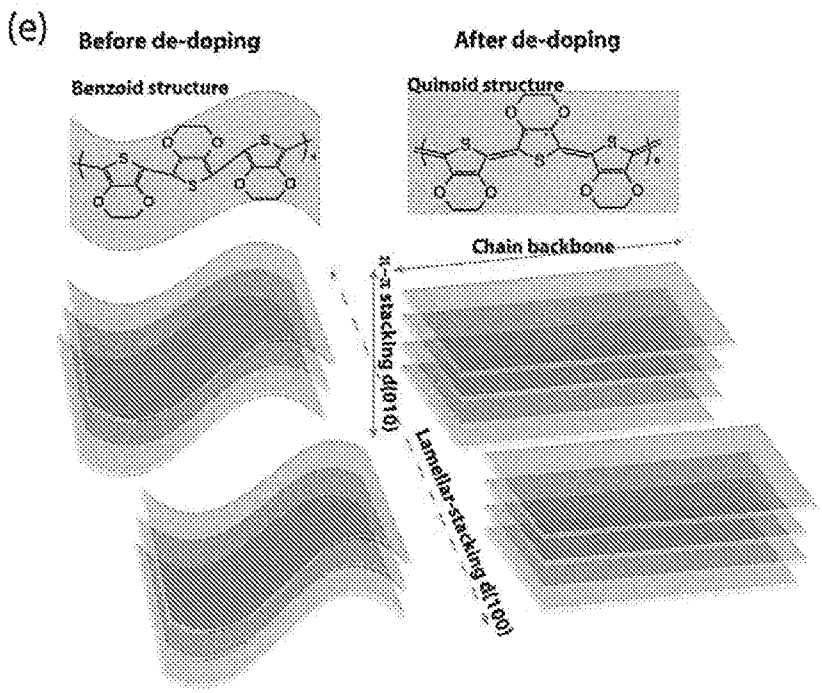
(e)
Before de-doping
After de-doping
Benzoid structure
Quinoid structure
Chain backbone
π–π stacking d(010)
Lamellar-stacking d(100)

FIGURE 14

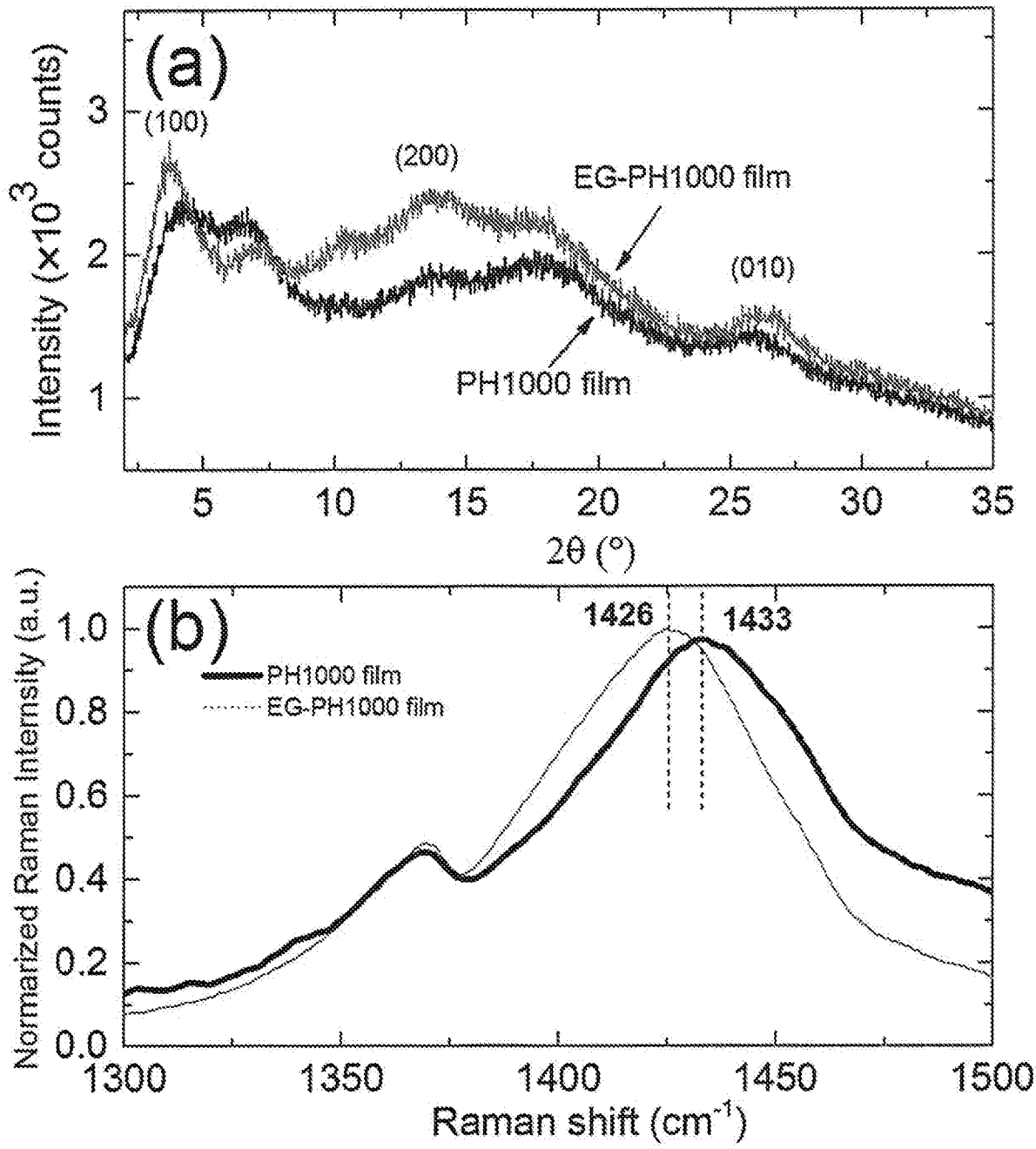
(a)
(100)
(200)
EG-PH1000 film
(010)
PH1000 film
Intensity (×10^3 counts)
2θ (°)
(b)
1426
1433
PH1000 film
EG-PH1000 film
Normarized Raman Intensity (a.u.)
Raman shift (cm^-1)

FIGURE 15

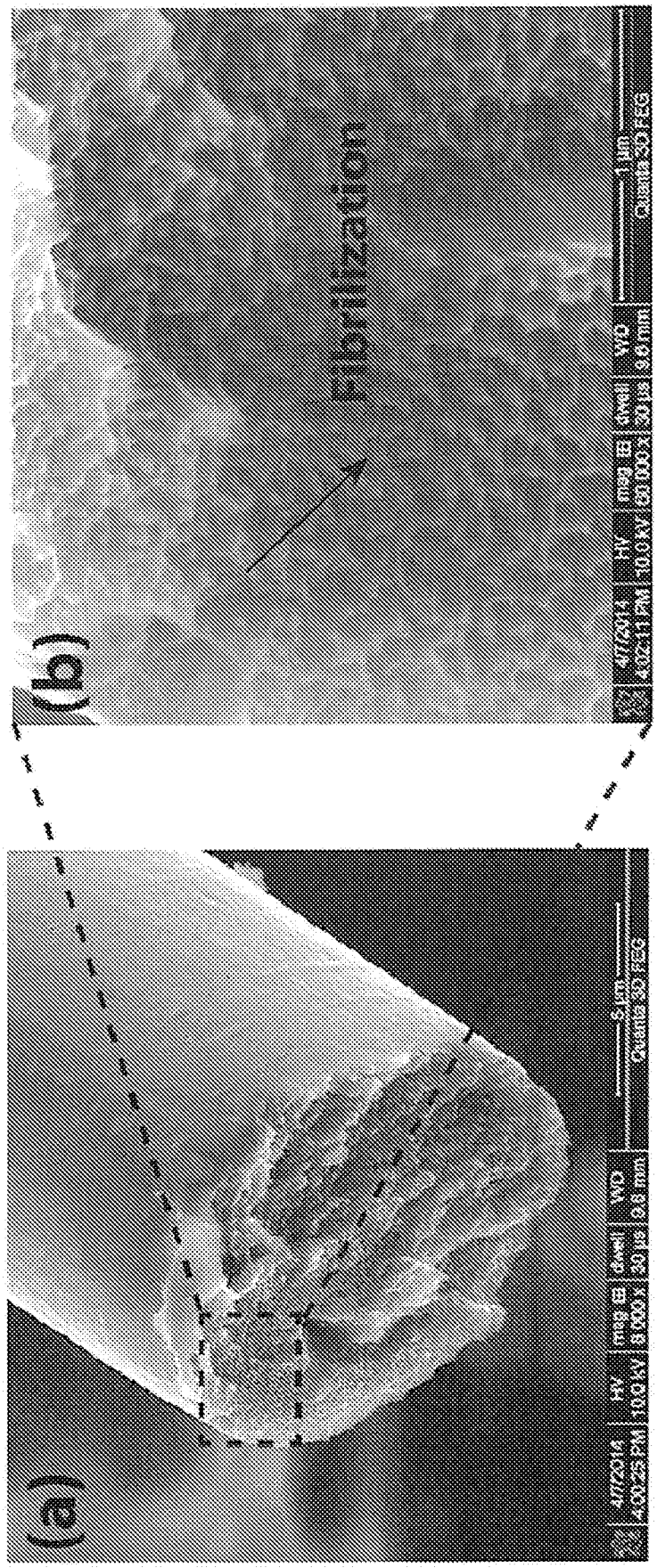

FIGURE 16

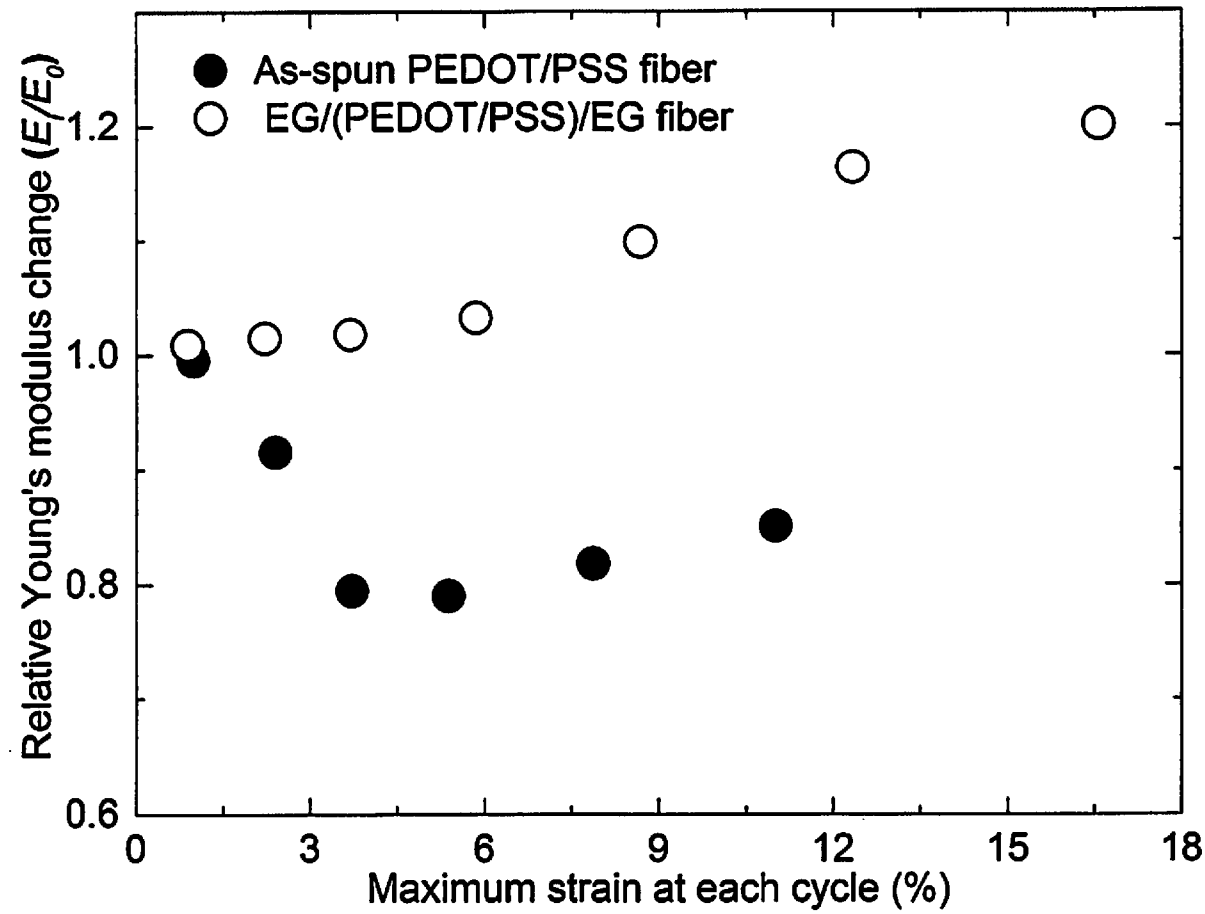
As-spun PEDOT/PSS fiber
EG/(PEDOT/PSS)/EG fiber
Relative Young's modulus change (E/E_0)
1.2
1.0
0.8
0.6
0
3
6
9
12
15
18
Maximum strain at each cycle (%)

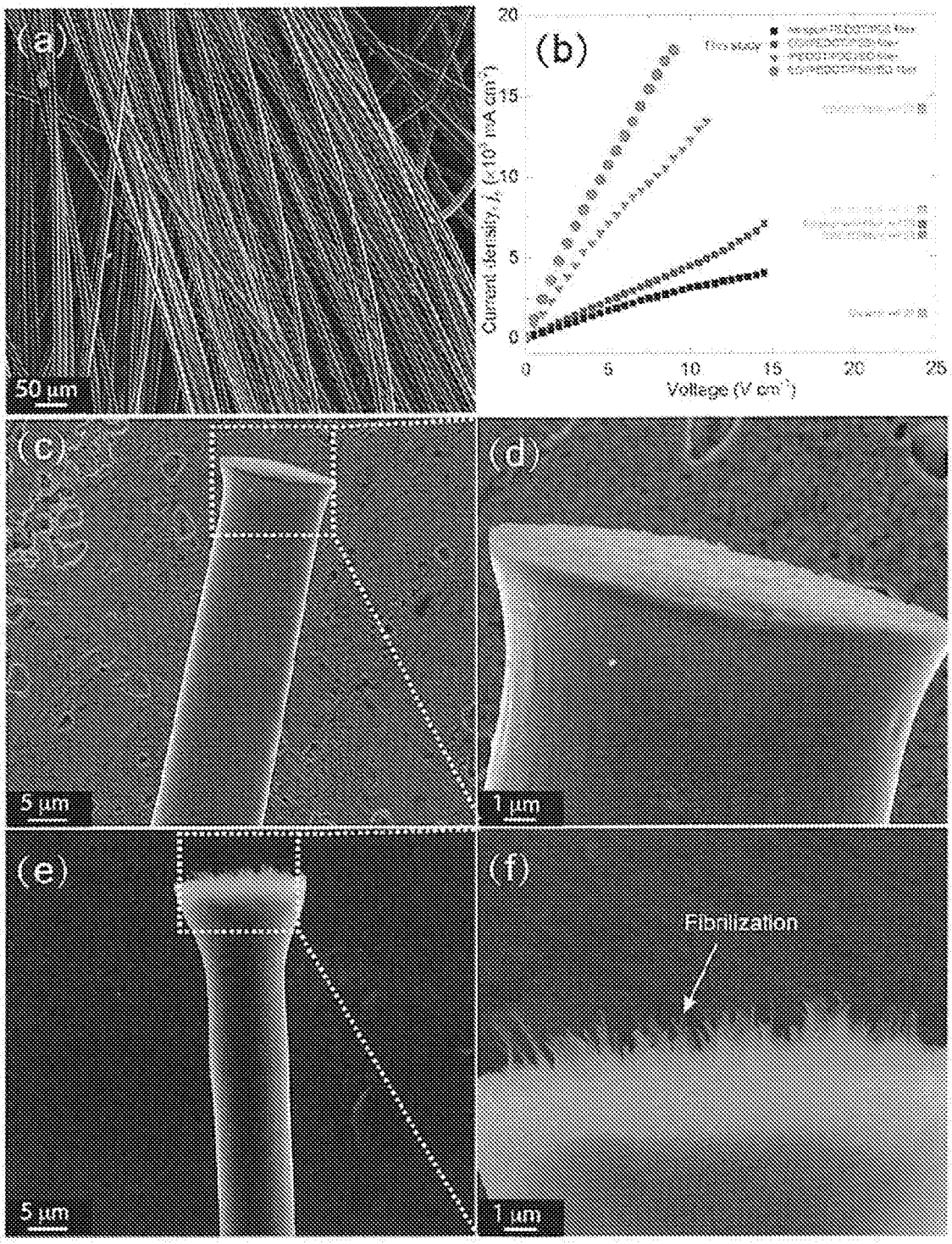
(a)
50 µm
(b)
Current density, J_c ($\times 10^3$ mA cm^{-2})
Voltage (V cm^{-1})
0
5
10
15
20
25
(c)
5 µm
(d)
1 µm
(e)
5 µm
(f)
Fibrilization
1 µm

FIGURE 17

FIGURE 18

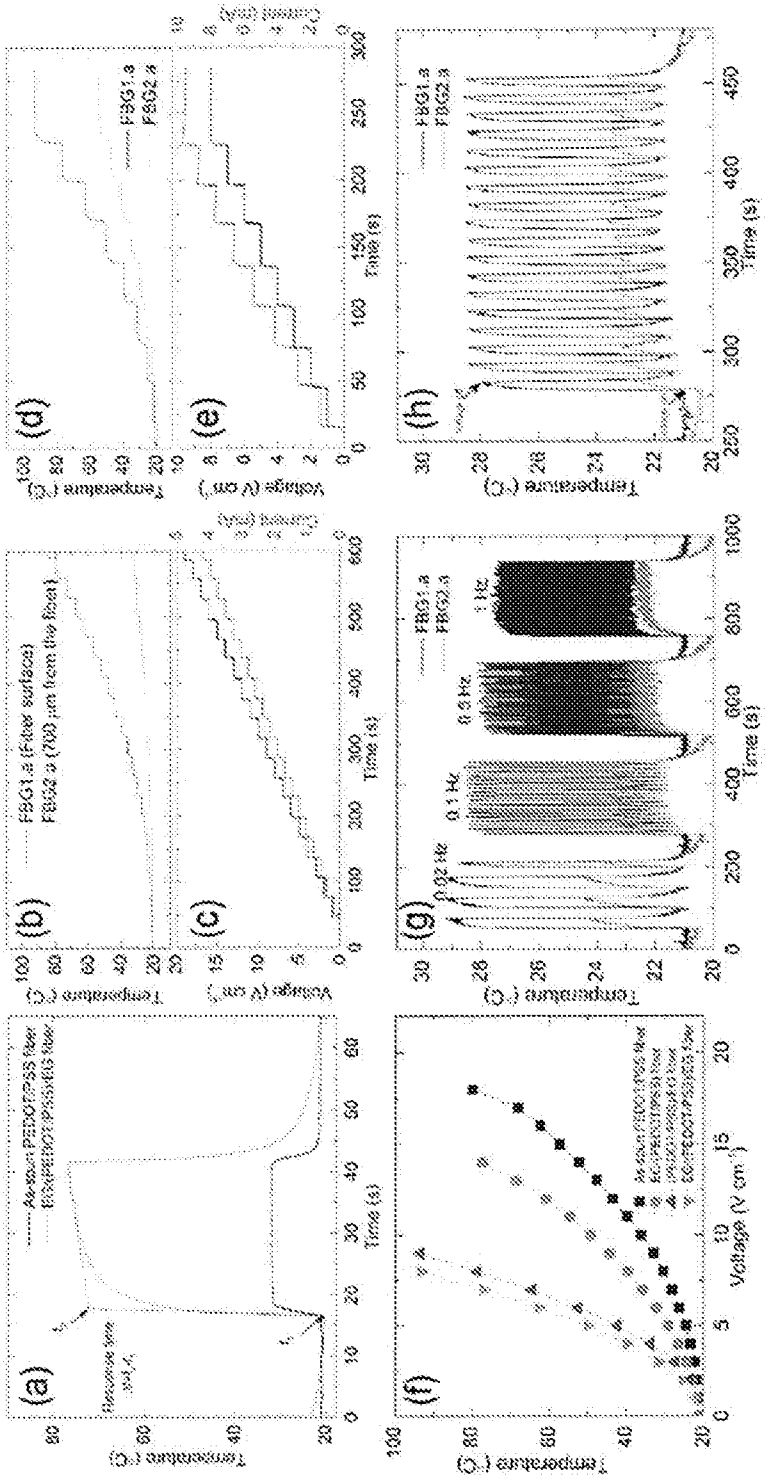
(a)
(b)
(c)
(d)
(e)
(f)
(g)
(h)
Temperature (°C)
Voltage (V cm⁻¹)
Time (s)
FBG1.a
FBG2.a
0.02 Hz
0.1 Hz
0.5 Hz
1 Hz

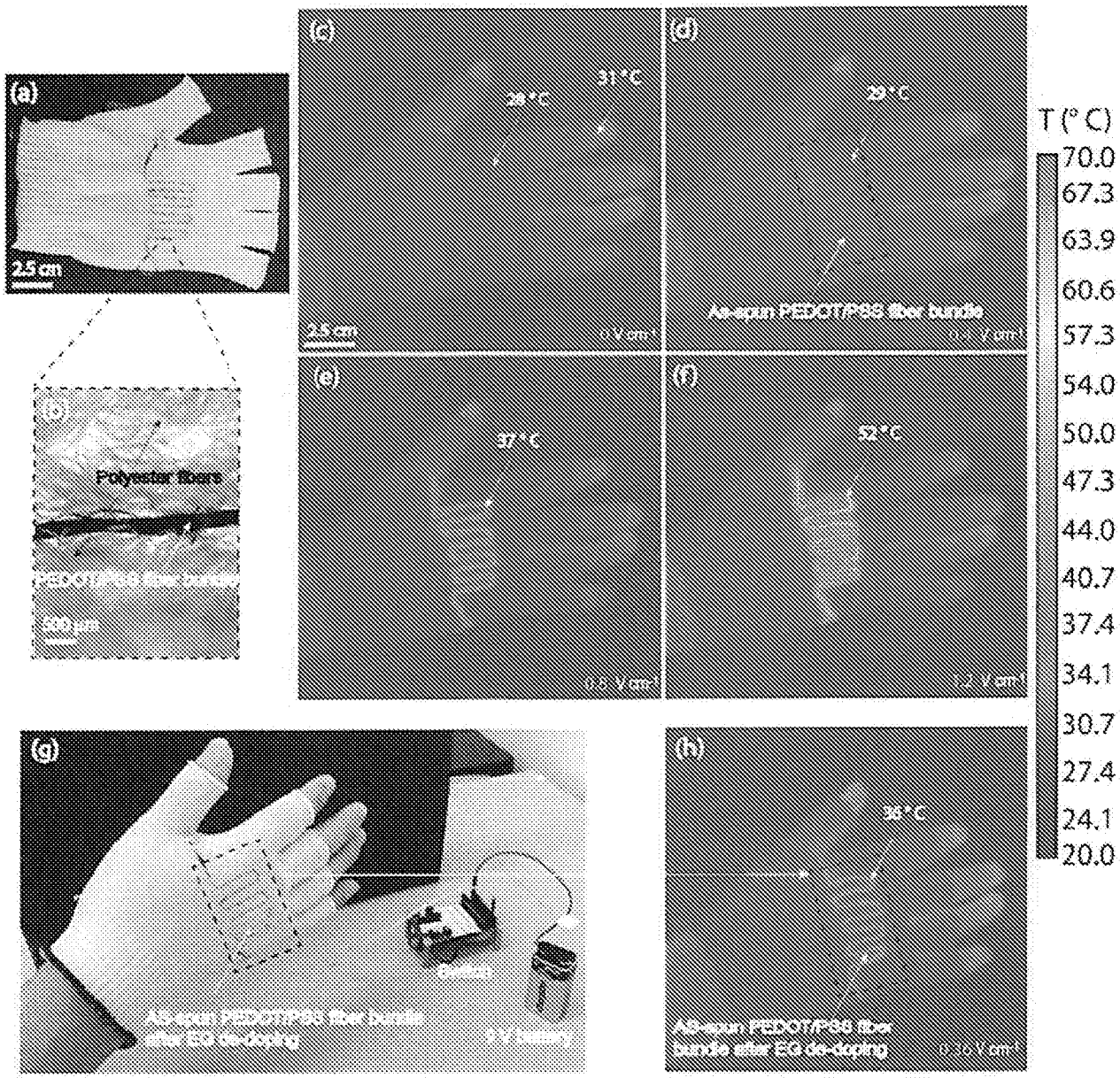
(a)
2.5 cm
(b)
Polyester fibers
PEDOT/PSS fiber bundle
200 μm
(c)
28 °C
31 °C
2.5 cm
0 V cm⁻¹
(d)
29 °C
As-spun PEDOT/PSS fiber bundle
0.4 V cm⁻¹
(e)
37 °C
0.8 V cm⁻¹
(f)
52 °C
1.2 V cm⁻¹
T (° C)
70.0
67.3
63.9
60.6
57.3
54.0
50.0
47.3
44.0
40.7
37.4
34.1
30.7
27.4
24.1
20.0
(g)
Electrodes
As-spun PEDOT/PSS fiber bundle after EG de-doping
0 V (bottom)
(h)
28 °C
As-spun PEDOT/PSS fiber bundle after EG de-doping
0.16 V cm⁻¹

FIGURE 19

FIGURE 20

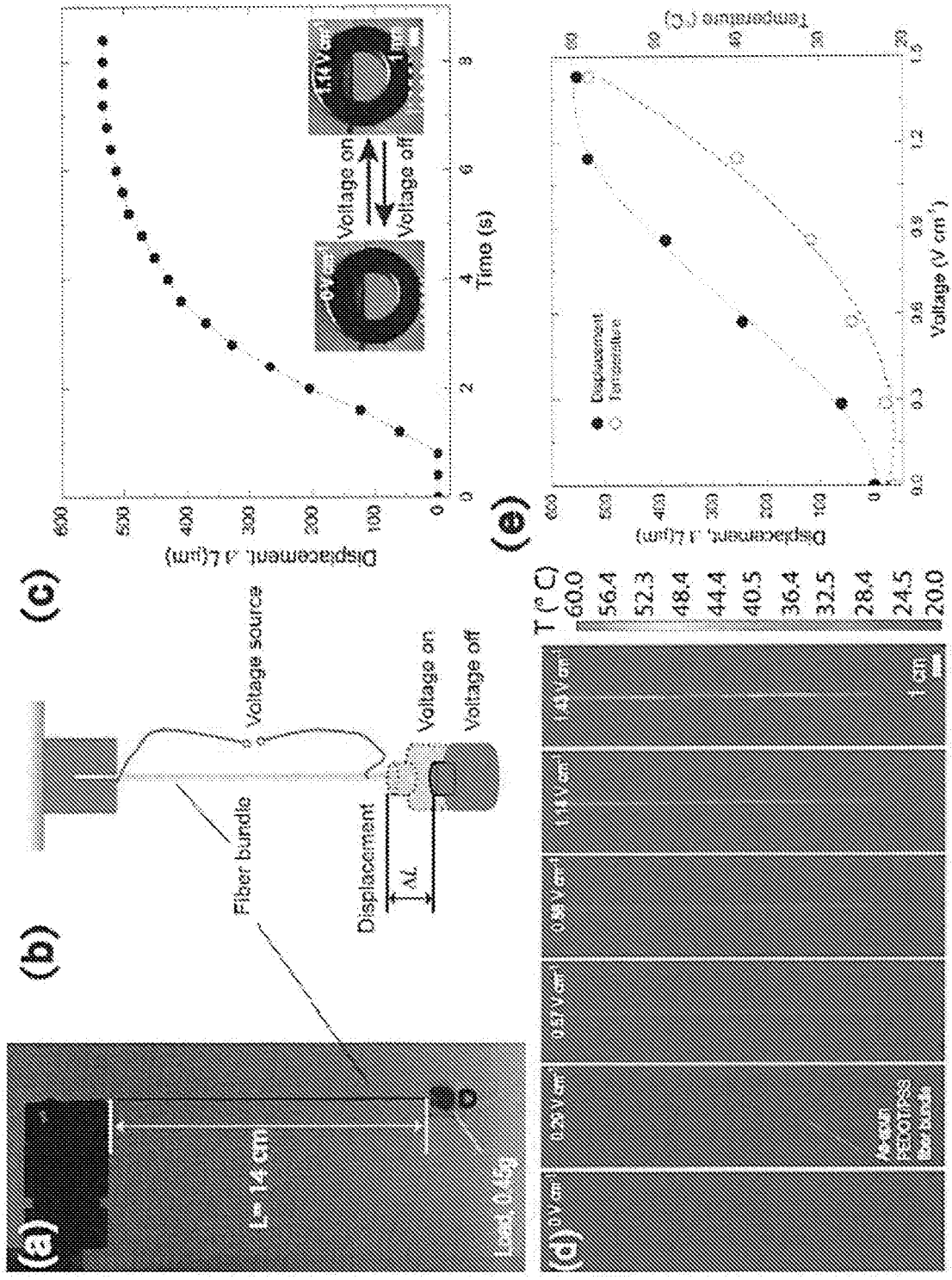
(a)
L = 14 cm
Laser NIR
(b)
Fiber bundle
Voltage source
Displacement
Δl
Voltage on
Voltage off
(c)
Displacement, Δ l (μm)
Time (s)
Voltage on
Voltage off
(e)
Displacement
Temperature
Displacement, Δ l (μm)
Temperature (°C)
Voltage (V cm⁻¹)
T (°C)
60.0
56.4
52.3
48.4
44.4
40.5
36.4
32.5
28.4
24.5
20.0
(d)
0 V cm⁻¹
0.71 V cm⁻¹
0.91 V cm⁻¹
1.06 V cm⁻¹
1.11 V cm⁻¹
1.21 V cm⁻¹
1 cm

FIGURE 21

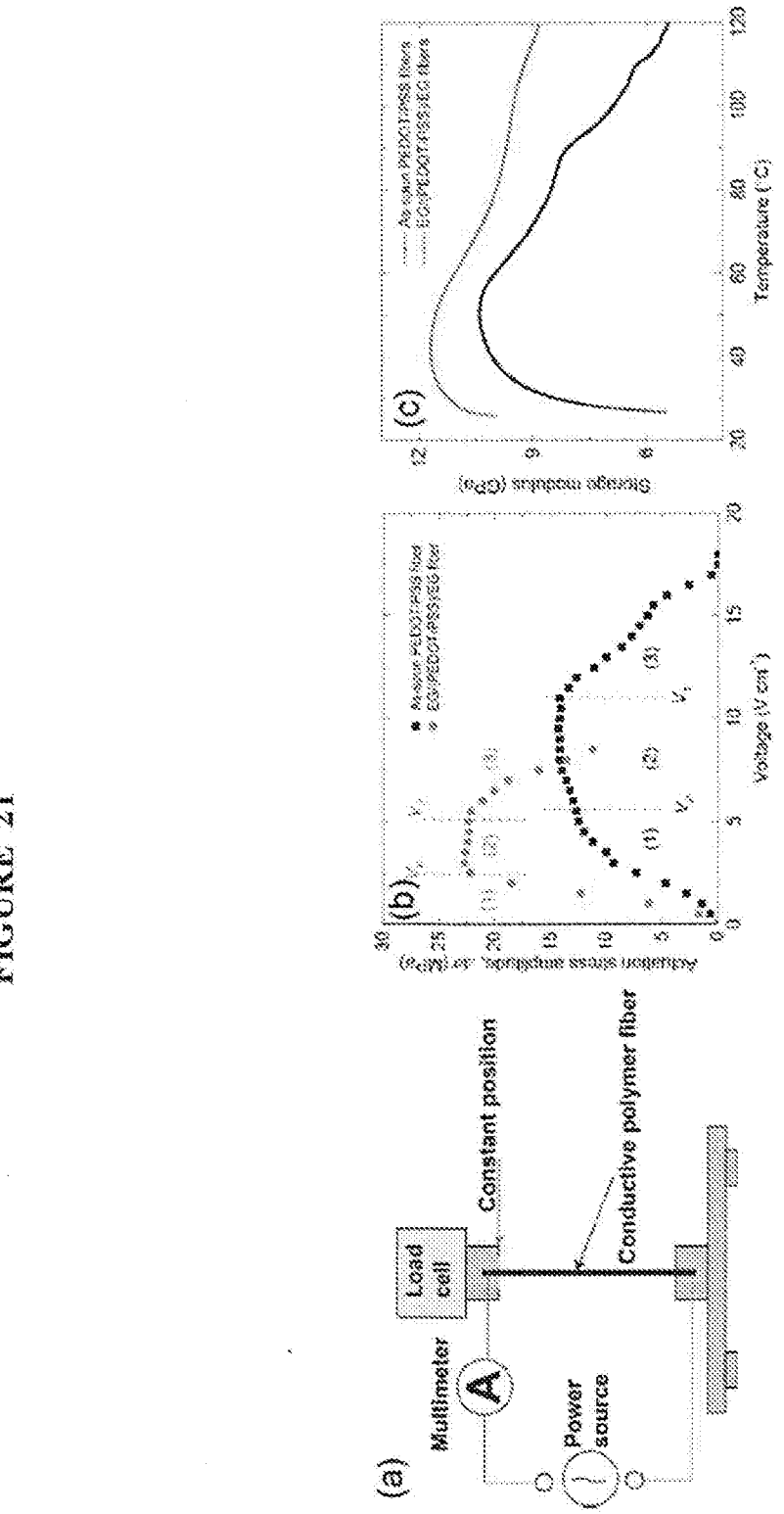
(a)
Multimeter
A
Load cell
Constant position
Conductive polymer fiber
Power source
(b)
(c)
Temperature (°C)

FIGURE 22

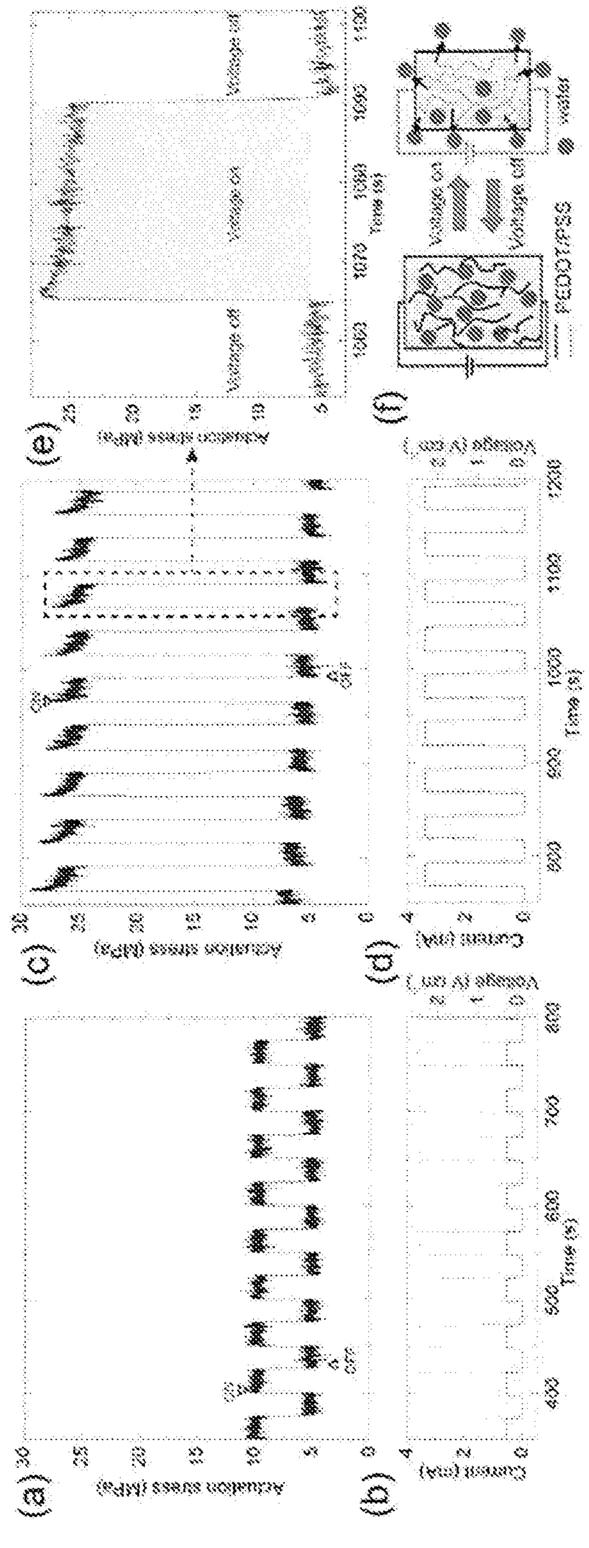
(a)
(b)
(c)
(d)
(e)
(f)
Actuation stress (MPa)
Current (mA)
Voltage (V on)
Time (s)
Voltage on
Voltage off
PEDOT:PSS
water

FIGURE 23

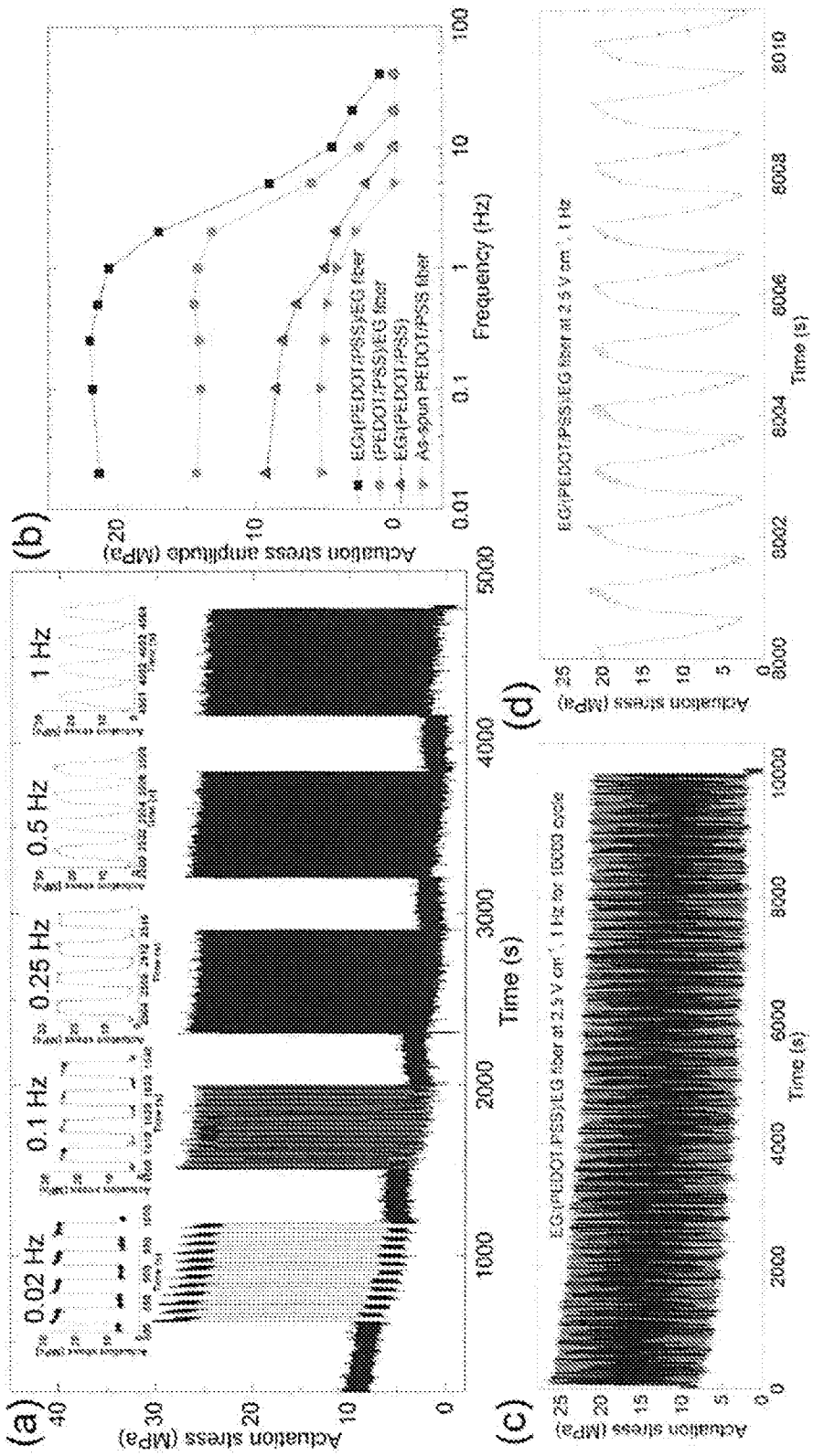
(a)
Actuation stress (MPa)
Time (s)
0.02 Hz
0.1 Hz
0.25 Hz
0.5 Hz
1 Hz
(b)
Actuation stress amplitude (MPa)
Frequency (Hz)
EG/PEDOT:PSS/EG fiber
(PEDOT:PSS/EG fiber
EG/PEDOT:PSS)
As-spun PEDOT:PSS fiber
(c)
EG/PEDOT:PSS/EG fiber at 2.5 V cm⁻¹, 1 Hz for 10000 cycle
Actuation stress (MPa)
Time (s)
(d)
EG/PEDOT:PSS/EG fiber at 2.5 V cm⁻¹, 1 Hz
Actuation stress (MPa)
Time (s)

FIGURE 24

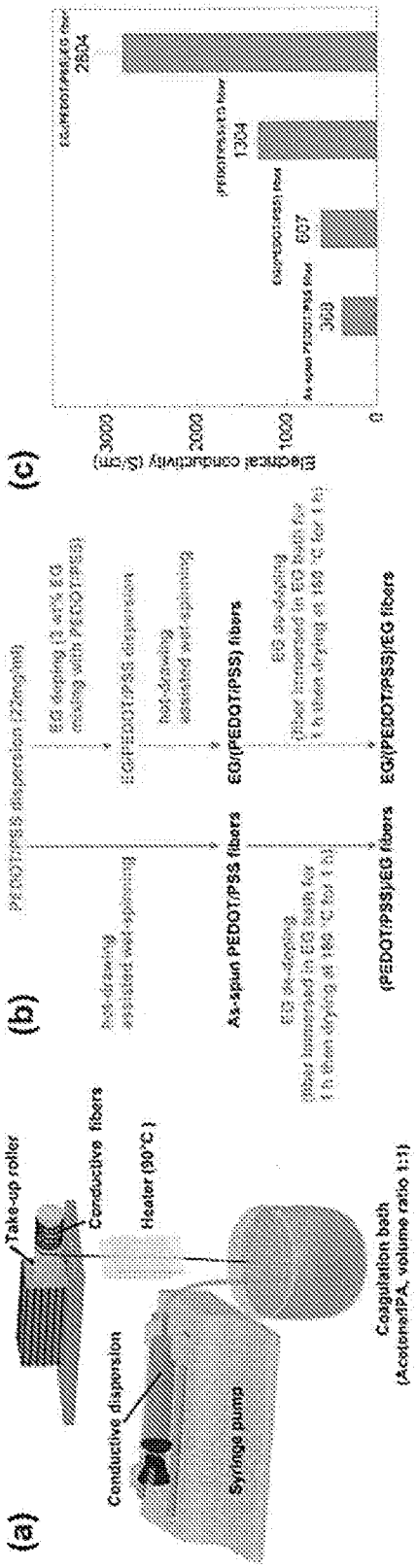
(a)
Take-up roller
Conductive fibers
Heater (90°C)
Conductive dispersion
Syringe pump
Coagulation bath
(Acetone/IPA, volume ratio 1:1)
(b)
PEDOT:PSS dispersion (2 steps)
EG doping (5 wt% EG
mixing with PEDOT:PSS)
Wet-drawing
assisted wet-spinning
EG/PEDOT:PSS dispersion
Wet-drawing
assisted wet-spinning
As-spun PEDOT:PSS fibers
EG/(PEDOT:PSS) fibers
EG re-doping
(fiber immersed in EG bath for
1 h then drying at 165 °C for 1 h)
EG re-doping
(fiber immersed in EG bath for
1 h then drying at 165 °C for 1 h)
(PEDOT:PSS)/EG fibers
EG/(PEDOT:PSS)/EG fibers
(c)
Electrical conductivity (S/cm)
3000
2000
1000
0
369
637
1304
2824

FIGURE 25

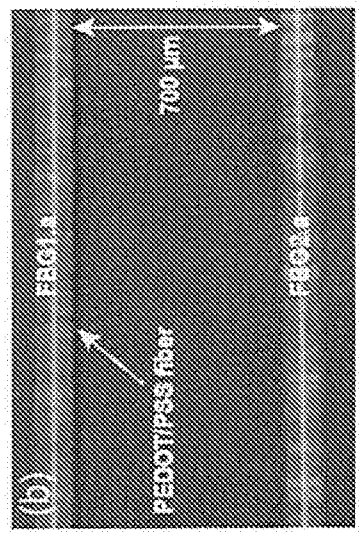
(b)
FBG1.a
700 µm
FBG2.a

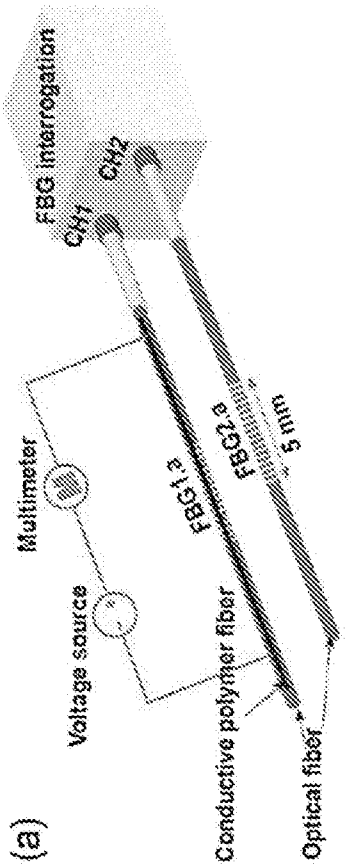
FBG interrogation
Ch1
Ch2
Multimeter
Voltage source
FBG1.a
FBG2.a
5 mm
Conductive polymer fiber
Optical fiber
(a)

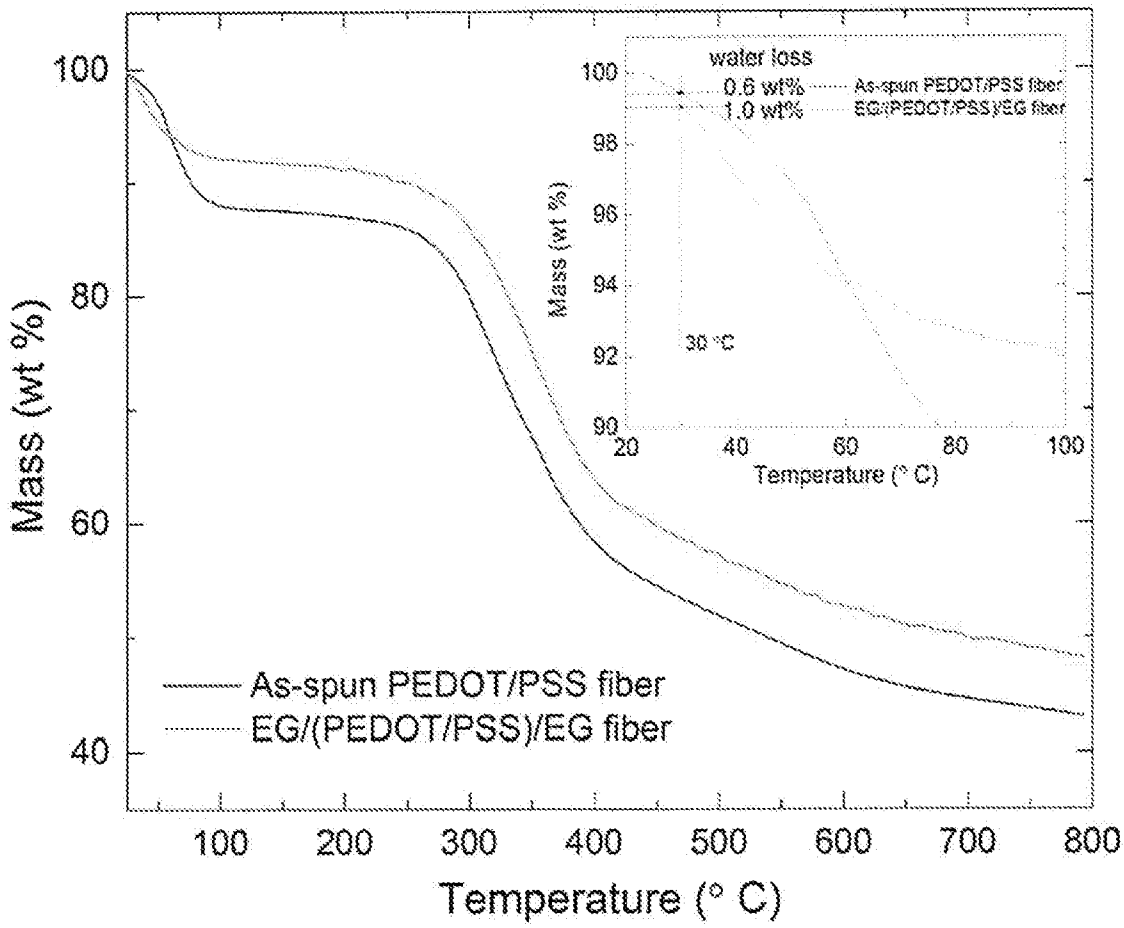
Mass (wt %)
Temperature (° C)
As-spun PEDOT/PSS fiber
EG/(PEDOT/PSS)/EG fiber
water loss
0.6 wt%
1.0 wt%
30 °C

FIGURE 26

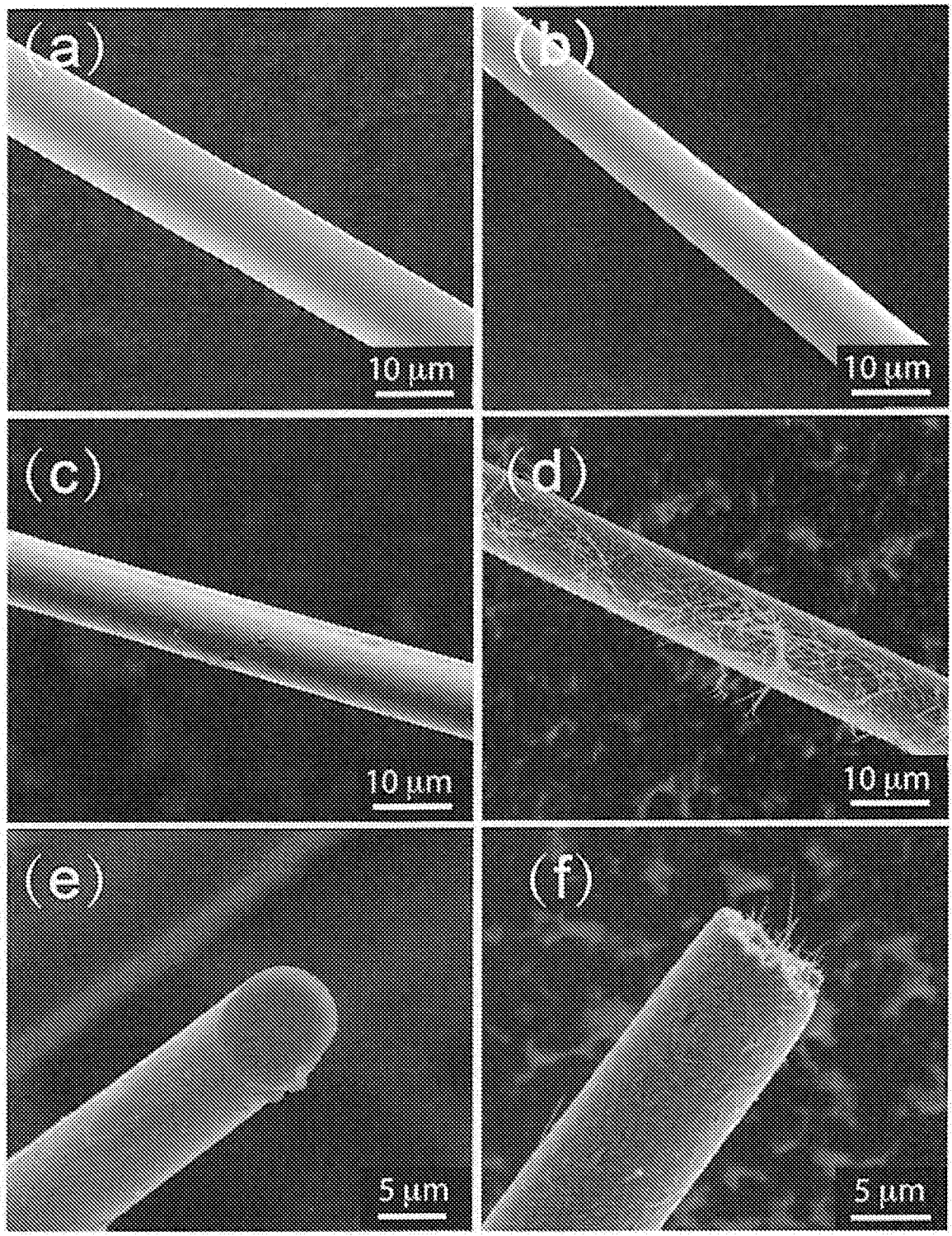

FIGURE 27

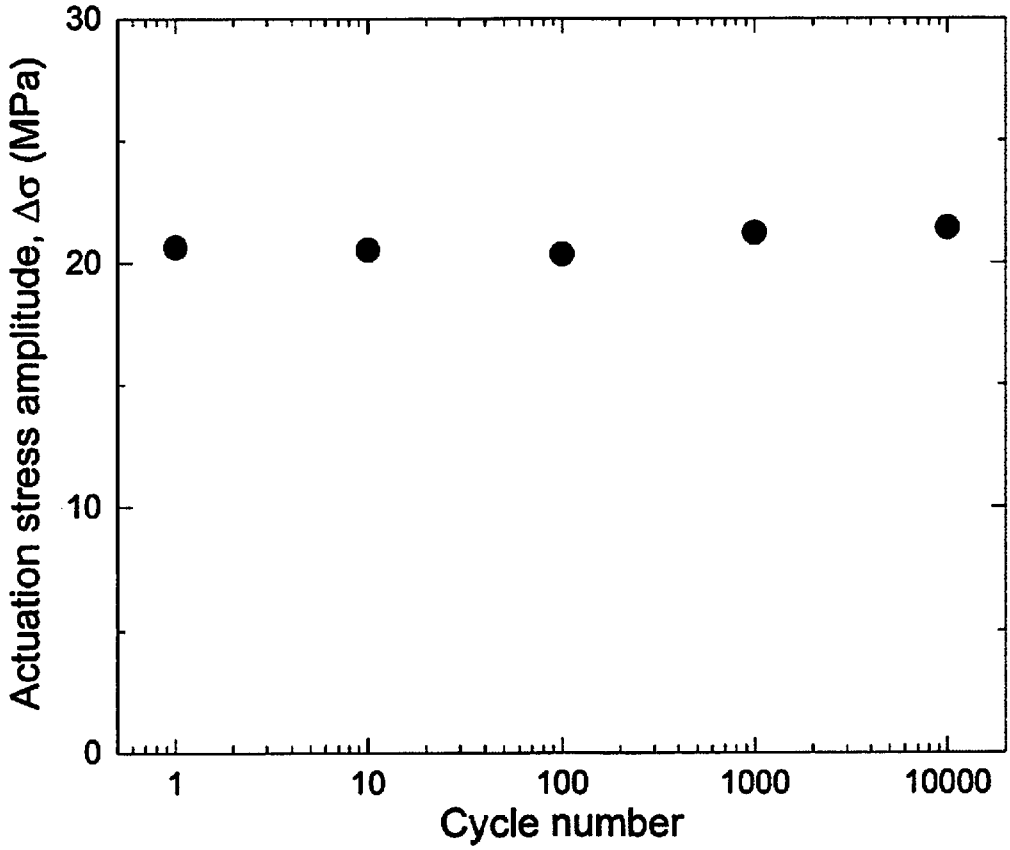
30
20
10
0
Actuation stress amplitude, Δσ (MPa)
1
10
100
1000
10000
Cycle number

FIGURE 28